MODEL FOR FRACTURING FLUID FLOWBACK AND CHARACTERIZATION OF FLOWBACK MECHANISMS

A Dissertation

by

BO SONG

Submitted to the Office of Graduate and Professional Studies of
Texas A&M University
in partial fulfillment of the requirements for the degree of

DOCTOR OF PHILOSOPHY

Chair of Committee,	Christine A. Ehlig-Economides
Committee Members,	Peter P. Valko
	David S. Schechter
	Yunfeng Sun
Head of Department,	Daniel A. Hill

December 2014

Major Subject: Petroleum Engineering

ABSTRACT

A large volume of fracturing fluid that may include slick water and various sorts of additives is injected into shale formations along with proppant to create hydraulic fractures which define a stimulated shale volume a shale gas well will actually drain. While in hydraulic fractures in conventional reservoirs most of the injected fracturing fluid flows back quickly, field observations have reported that load recovery from shale gas wells occurs over a long period, and in some shale formations only a small fraction of total injected fluid is recovered.

An unresolved question is whether unrecovered injected fluids are detrimental to well performance. This study emphasizes three main aspects: the location of injected water after fracturing treatment; the mechanisms of water retention underground; and the mechanisms behind the observed flowback behavior.

To locate the injected fracturing fluid we cataloged the possible fracture types including the main propped fracture and secondary fractures that may or may not be filled with injected fluid or proppant or even hydraulically connected. The investigation of factors impacting water retention will consider formation properties and fracture configurations of the cataloged locations for injected water and will evaluate the degree to which each factor plays. Finally, we will model long term flowback and formation flow behavior and mechanisms in order to quantify fundamental implications of retained water on well performance and expected ultimate recovery.

The significance of this research work lies on understanding how flowback behavior impacts the gas production performance of shale gas wells in both short term and long term view. Whether the unrecovered water blocks the gas flow path to the well or behaves as proppant to keep the fractures open and enhance the conductivity of an induced fracture system should be understood before the fracturing treatment design and flowback scheme determination. More specifically, an aggressive flowback schedule might reduce the effective stimulated shale volume and/or the gas production rate. Therefore, understanding where the injected water is located, how water is distributed underground, how water flows with gas and what controls water flowback are critical to understand the beneficial or detrimental effects of flowback and load recovery on shale gas well production.

DEDICATION

To my advisor, committee members and my family

ACKNOWLEDGEMENTS

I would like to thank my committee chair, Dr. Christine. A. Ehlig-Economides, and my committee members, Dr. Peter. P. Valko, Dr. David. S. Schechter and Dr. Yuefeng Sun for their guidance and supports throughout the course of this research.

Thanks also go to my friends and colleagues and the department faculty and staff in Petroleum Engineering Department for making my time at Texas A&M University a great experience.

Finally, thanks to my mother and father for their encouragement and to my wife Meixi. Lu and my daughter Christine. Song for their patience and love. Thanks to God for the graces and blessing.

NOMENCLATURE

a	Mole fraction of vaporized water correlation coefficient
b	Mole fraction of vaporized water correlation exponent
B_g	Formation volume factor of gaseous phase fluid, rf/scf
B_{gg}	Formation volume factor of gas composite in gaseous phase fluid, rf/scf
B_l	Formation volume factor of liquid phase fluid, rf/scf
B_w	Formation volume factor of water, rf/scf
c_f	Formation compressibility, 1/psi
c_g	Gas compressibility, 1/psi
c_l	Liquid compressibility, 1/psi
c_w	Water compressibility, 1/psi
f	Function of the mole fraction of vaporized water in gaseous phase
g	Function of the mole fraction of gas in gaseous phase
h	Mole fraction of vaporized water in gaseous phase correlation function
IZ	Invasion zone
k	Absolute permeability, md
k_{rg}	Relative permeability to gas or gaseous phase fluid
k_{rl}	Relative permeability to gas or liquid phase fluid
k_{rw}	Relative permeability to water
LR	Load recovery, fraction
M_g	Molar mass of gaseous phase fluid, lbm/mole

M_{gg}	Molar mass of gas composite in gaseous phase, lbm/mole
M_{wg}	Molar mass of vaporized water in gaseous phase, lbm/mole
M_w	Molar mass of water, lbm/mole
p	Pressure, psi
p_g	Gaseous phase fluid pressure, psi
p_c	Capillary pressure, psi
p_l	Liquid phase fluid pressure, psi
PF	Primary fracture
q_g	Gaseous fluid flow rate, Scf/d
q_{gg}	Gas flow rate, Scf/d
q_l	Liquid flow rate, Stb/d
q_w	Water flow rate, Stb/d
Q_g	Cumulative gas production, Scf
r_d	Effective drainage radius, ft
r_w	Wellbore radius, ft
s	Skin factor
S_g	Gaseous fluid saturation, fraction
S_l	Liquid saturation, fraction
S_w	Water saturation, fraction
SF	Second fracture
t	Time, day
T	Average formation temperature, F˚

v	Fluid flow velocity, ft/s
V	Volume, ft^3
WGR	Water gas ratio, Stb/Scf
y_{wg}	Mole fraction of vaporized water in gaseous phase, fraction
y_{gg}	Mole fraction of gas in gaseous phase, fraction
Δt	Time step, days
ΔV	Volume of grid block, ft^3
Δx	Grid block dimension in x direction, ft
Δy	Grid block dimension in y direction, ft
Δz	Grid block dimension in z direction, ft
ϕ	Porosity, fraction
γ_g	Gaseous fluid specific gravity, fraction
γ_w	Water specific gravity, fraction
μ_g	Gaseous phase fluid viscosity, cp
μ_{gg}	Viscosity of gas composite in gaseous phase fluid, cp
μ_l	Liquid phase fluid viscosity, cp
μ_w	Water viscosity, cp
θ	Dip angle of the formation, ˚
ρ_g	Density of gaseous phase fluid, lbm/mole
ρ_{gg}	Density of gas composite in gaseous phase, lbm/mole
ρ_l	Density of liquid fluid, lbm/ft^3

TABLE OF CONTENTS

Page

LIST OF FIGURES

Page

LIST OF TABLES

Page

CHAPTER I

INTRODUCTION

This section introduces briefly the background of shale gas development, provides an extensive literature review of studies related to fracturing fluid flowback, and explains the research objectives.

1.1 Background

The multi-fracture horizontal well technology has been applying to shale gas development for many years and great successes have been achieved through this revolutionary technique along the history of oil and gas industry. To create a number of hydraulic fractures in horizontal wells, a large volume of fracturing fluid must be injected into the formation by fracture treatment. Different from the fracturing fluid system applied on conventional reservoirs which is usually referred as "cross-linked" system, the fluid system for unconventional reservoirs utilizes water with friction reducer and low concentration of linear gel. Palisch, Vincent and Handren (2008) indicated that the fracturing treatment by water-fracturing usually places a certain mass of proppant in low slurry concentration with a high injection rate so a large volume of slick water is required. Additionally, biocide is usually added into the fluid system as well (Aften, Paktinat and O'neil 2011). Though some discussion such as the proppant transportation and settling by slick water (Dayan, Stracener and Clark 2009) and the impacts of geomechanical parameters on slick water's performance of carrying on

proppant (Das and Achalpurkar 2013) and so on, slick water is still considered as the main component of the fracturing fluid system for unconventional gas reservoirs. Comparing with cross-linked fluids, slick water used as a fracturing fluid has several advantages, including low cost, a higher possibility of creating complex fracture networks, less formation damage, and ease of cleanup (Cheng 2010).

1.2 Literature Review

We basically reviewed the literatures referring to 3 main aspects, including the location of injected fluid, injected fluid retention and the modeling work and mechanism study on flow back behavior.

1.2.1 Locations of Injected Fluid

After hydraulic fracturing treatment the injected fluid will be distributed in the formation. The fracturing fluid will create hydraulic fractures which open against the minimum horizontal stress; some induced fracture branches might be also created if the fracture fluid broke the rock during the main fracture propagation; existing micro-fractures might be reopened by the injected fracturing fluid with a high net pressure; fracturing fluid might be leaked off or adsorbed into formation matrix by imbibition mechanism, and etc. All these possibilities provide storage space for injected fracturing fluid. Panga et al (2007) indicated that in gas reservoirs water block usually occurs near wellbore and fracture face; Penny et al (2006) found that about 60% to 90% of injected fluid around the near fracture zone in Barnett Shale gas wells; King (2010), Warpinski et

al (2008), and Cipolla et al (2008) discussed on the creation of fracture network or fracture complexity in some shale gas plays and the existing natural fractures or induced fractures which might be orthogonal to the main fractures are considered as a possible location of injected fluid; Ehlig-Economides and Economides (2012) described the distribution of the "water" in shale gas well stimulated reservoir volume, and indicated the water can be located in either propped hydraulic fractures or in unpropped natural fractures and Apiwathanasorn and Ehlig-Economides (2012) confirmed the evidence of reopened micro-fractures in production data analysis of hydraulically fractured shale gas wells in Barnett Shale; Fan, Thompson and Robinson (2010) argued that the thinking of most of injected fluid is imbibed into shale matrix conflicts with the observed high gas production performance so they believed that the water mainly stays in fracture system, either complex fracture network or planar fractures; Odusina et al (2011) ran the experiment to study the imbibition of water into the shale core and they found the imbibition effect is mainly due to micro-fractures but not matrix; Wang et al (2010) also ran the core test which also showed that fractures rather than matrix really affect imbibition; Alkouh and Watternbarger (2013) study the ratio of lost water in the formation by adjusting 20% flowback efficiency and indicated 50% of the total injected fluid is lost to some locations which cannot effectively communicate with the flow path to the well.

1.2.2 Injected Fluid Retention

The reasons for low injected fluid recovery efficiency have been researched for years. There are several factors which may induce that a large portion of total injected water to remain underground, and this causes the so called "load recovery" ranges from 10% to 40% (Chekani et al 2010). The essence of low load recovery is that the injected fluid is maintained by some resistance which the draining force cannot overcome to make effective fluid flow or some forces holding the water in place.

Holditch (1979) studied factors impacting the flow back performance in gas wells. He claimed that capillary pressure, the change in capillary pressure and relative permeability are important to liquid flow back. Additionally, he also emphasized that if the pressure drawdown is not large enough to overcome the capillary pressure the water may block the gas production. Another possible explanation to the poor flow back is the damage in rock permeability as he indicated in his conclusions as well. Similarly, Penny et al (2006), Mahadevan and Sharma (2003) also claim that the introduction of fracturing fluid into the formation may cause a reduction to absolute permeability of the formation, especially near the wellbore and fracture face, an increment in liquid phase saturation which results in the decrement in gas relative permeability. Also, the high capillary pressure due to the small pore size in unconventional reservoirs was discussed by the authors. Penny et al (2006) distinguished the capillary pressure in different media by indicating that the capillary pressure in main hydraulic fracture is negligible while that in natural fractures system and matrix could be as high as thousands of psi. Alkouh et al (2013) integrated this consideration in their simulation model to explain the low load

recovery and claimed that the high capillary pressure can result in high water holdup in natural fractures.

Relative permeability is another potential factor inducing the water retention in the formation since many researchers are concerning that the relative permeability in unconventional formations may be quite different from that in conventional reservoirs. Shanley et al (2004) provided a concept of permeability jail in tight gas reservoir relative permeability profile which differs from conventional one and Blasingame (2008) emphasized these characteristics in fluid flow in unconventional reservoirs.

Imbibition is a factor of many arguments, especially when it is referred to matrix imbibition. Definitely, if the formation imbibes the water, imbibition will be one of the mechanisms of holding the water in the formation. However, the matrix of shale formations is usually considered non-water wetting since it is the source generating the hydrocarbon. Some research works were carried out to figure out whether the imbibition will really happen and if so whether it is by natural fractures or matrix part of the shale. Wang et al (2012) tested the core sample from Bakken Shale in North Dakota and found the shale is oil-wetting or intermediate wetting. Dutta et al (2012) studied the fracturing fluid migration due to spontaneous imbibition in fractured tight formations by X-ray computed tomography. By visualizing the water saturation of the core used in the experiments, the authors concluded that even the matrix is water wetting only a very controlled imbibition is allowed through rock matrix due to the low pore volume and low permeability. Also they claimed that the loss of injected water in the tight formations relates to the combination of permeability, capillarity and heterogeneity.

Makhanov, Dehghanpour and Kuru (2012) studied the spontaneous imbibition in Horn River Shale by experiments. They found that the shale rock can imbibe the water and the imbibition rate is faster in bedding direction than perpendicular to bedding direction. However, those research in which the imbibition of water was demonstrated did not specify whether the imbibition was into the micro-fractures or into the matrix. However, from the experiment of Odusina et al (2011) and Wang et al (2010), the imbibition is relied on the fractures but not matrix. Roychaudhuri et al (2011) concluded the imbibition from the perspective of shale rock mineral components: less clay and more total organic content induce less imbibition since non-wetting matters repel water. Above all, the imbibition in shale formation is a quite complex issue due to the complex heterogeneous wettability system.

Fracture network or complexity is also considered as a reason for water retention. Besides the relatively lower conductivity, the high capillary pressure of micro-fractures in the network, the complex geometry and tortuous of the fracture path also make the flowback more difficult. Warpinski et al (2008) indicated that portions of the fracture network may never efficiently cleanup due to the low pressure drop and fracture network conductivity which are not sufficient to remove the water from the far reaches of the network. He also claimed that fast cleanup process with a high percentage of load recovery may actually be an indicator that a "simple" fracture is generated rather than "complex" fracture network.

Liquid loading in fractures or wellbore is another reason contributing the observation of low load recovery. Turner et al (1969) indicated that if the gas flow

velocity is not large enough water loading will occur in the wellbore of gas wells. Zhou and Yuan (2009) discussed the mechanism of liquid-droplet concentration for describing the liquid loading in gas wells. Parmar et al (2013) indicated that liquid loading in fractures can occur and it may impact gas flow dramatically. The effective stimulated reservoir volume will be reduced if heavy liquid loading happens in fractures even the pressure drop overcomes the capillary pressure. Additionally, main drainage against gravity direction will make load recovery low. Alkouh and Watternbarger (2013) indicated that increment in hydraulic fracture width will induce liquid loading effect while the effect does not exist in natural fractures due to the small width.

1.2.3 Flowback Analysis

Understanding flowback dynamics may help the design of the well and production strategy to improve the gas production performance of shale gas wells.

As early as 2003, Mahadevan and Sharma (2003) claimed that the cleanup of water blocking occurs in two flow regimes: displacement and the following vaporization. Zhang (2013) applied this diagnostic method to investigate the flowback behavior of shale gas wells in Barnett Shale and Horn River Shale. She found that flow back in Horn River Shale gas wells is due to both mechanisms while in Barnett Shale gas wells is only due to displacement. Vaporization of liquid phase in flowing gas may result in ultra-low water saturation, abnormally high capillary pressure and increasing salinity (Newsham et al, 2003). Rushing et al (2008) studied the factors affecting water dissolubility in gas and claimed that temperature, pressure, and gas composition matter.

Sage and Lacey (1955) conducted laboratory measurement to correlate the vaporization ability to in-situ temperature and pressure conditions.

Some researchers worked on modeling the flowback behavior. Alkouh and Watternbarger (2013) built up a simulation model and emphasized the importance of flowback data to PDA. They emphasized the hybrid permeability profile should be used to model the flow back data. Clarkson (2012) developed a method to evaluate hydraulic fracture properties with early flowback data and he analogized the physics of the flowback to the 2-phase flow in natural fracture system (cleats) in coalbed methane reservoirs. Ezulike, Dehghanpour and Hawkes (2013) developed a flowback analytical model (FAM) by extending the existing linear dual-porosity flow model (DPM) to understand flow back as a transient 2-phase displacement process.

Munoz et al (2009) claimed that the initial post-frac well performance related mainly to flowback from near wellbore fracture part while long-term post-frac well performance mainly corresponded to cleanup at the fracture tip. Crafton (2010) simulated the flowback and observed that the flow back behavior is related to the filling up phase in natural fracture system. He claimed that if the natural fracture system is initially gas filled or gas-energized fluid, the highly compressible gas bubble with high pressure will purge the fractures from the toe toward the heel in the form of a water bank. Once the fracture is sufficiently voided the gas enters at the toe and flow to heel. This scenario is insensitive to the flowback rate and natural fracture intensity only seems to impact on the volume to store and conduct the pressurized gas. On the other hand, he claimed that liquid-filled fracture has poor liquid voidage due to the low compressibility

and higher viscosity. Higher pressure drawdown is required to result in a gas cone into the fracture from the reservoir at the heel of the fracture. The conductivity is crucial to this sort of system and flowback is sensitive to rates since gas enters the fractures at the heel.

Ehlig-Economides et al (2012) indicated that the water production of a shale gas well might be impacted by the fracturing treatment in a nearby well and they had some observation of this effect in Horn River Shale wells. Zhang (2013) identified a number of Barnett shale gas wells that produced water from nearby well fracturing operations.

Crafton and Gunderson (2007) and Crafton (2008) indicated that flowback impacts the production performance of gas wells significantly. A high flowback rate might be detrimental to gas production performance because it may cause the proppant flowback and fracture collapse. Munoz et al (2009) claimed that wellbore cleanup affects the initial gas production performance post-frac while fracture tip cleanup affects more the long-term gas production performance. Cheng (2010) showed that shut-in also had an impact on flowback and gas production. Through simulation of a Marcellus shale gas well, he found that long extended post-frac shut-in will induce an increase in the gas production before shut-in extrapolation and the water production will be lower than the before shut-in extrapolation. He concluded that capillary pressure could further enforce the water to be sucked in the matrix during shut-in. Ehlig-Economides and Economides (2011) proposed that the injected water may behave as proppant to keep unpropped fractures open. This consideration explains some observation that in some shale gas wells low load recovery corresponded to higher gas production performance.

1.3 Study Objectives

A recent study by Zhang (2013) indicates that actual data on load recovery in shale gas wells is rare. Data from Barnett and Horn River shale wells showed load recovery values approaching and even exceeding 50%, but the flowback duration can continue for many years. The objective of this research is to determine whether the retained injection fluid improves or impairs the well performance.

This chapter provided the basic background of this study and specified the specific objective based on the research interest and literature review.

CHAPTER II

CATALOG OF INJECTED FLUID LOCATIONS

We reviewed previous studies on the locations of injected fracturing fluid in gas wells, the mechanisms of injected fluid retention and flowback behavior analysis in the literature. In this chapter we catalog possible locations of injected fracturing fluid and characterize the storage and flow capacity properties for each possible medium in which the injected fracturing fluid might be stored. The understanding of the distribution of injected fracturing fluid provides a solid base for the further study on the flowback dynamics.

2.1 Injected Fracturing Fluid Location Catalog

A large volume of fracturing fluid is injected into underground to create hydraulic fractures, which effectively increase the contact area between the formation and the well. As the hydraulic fracture propagates, the injected fluid does not not only fill up the voidage of main hydraulic fracture, but also possibly reopens the existing natural fractures, induces micro-fractures and invades into the matrix of the formation.

Figure 1 shows fracturing fluid system selection strategy according to the rock type in terms of the brittleness. In shale gas formations, especially very brittle ones, slick water of low viscosity is injected with low proppant concentration under a high pumping rate. The reasons for applying slick water system include higher possibility of creating fracture complexity, low cost, easy cleaning up and low formation damage.

However, if there are natural fractures in place and the fracturing fluid can reopen the natural fractures by the high treatment net pressure, some portion of the injected fracturing fluid will be stored in the reopened natural fractures; additionally, during the hydraulic fracture propagation, it is possible that some induced branching fractures may occur and the fracturing fluid will be stored in this type of fractures; Injected fluid may also invade into the formation matrix due to some mechanisms such as the high pressure gradient though in some tight formations such as tight sand and gas shale the matrix is considered to be too tight to result in high leak off.

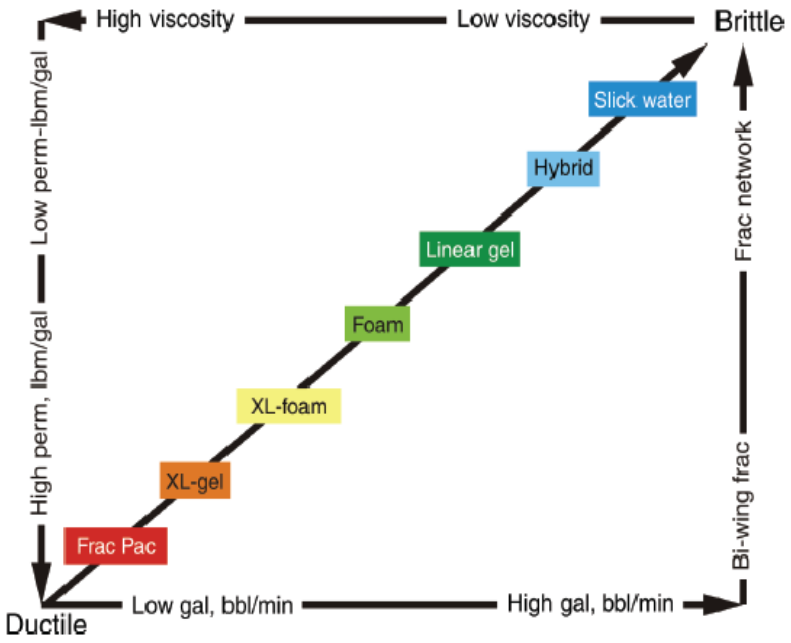

Figure 1. Fracturing fluid system selection strategy (Das and Achalpurkar, 2013)

Table 1 catalogs the possible locations for injected fracturing fluid storage. The media storing the injected fracturing fluid can be cataloged into two main series: the

fracture system and the shale matrix. Fracture system contains primary and secondary fractures. Primary fracture basically indicates the main hydraulic fracture, which is created by the hydraulic fracturing treatment. Primary fracture is usually propped by the proppant of either high or low permeability and after treatment pumping it is purely filled up by the injected fracturing fluid. Secondary fractures can be reopened fractures or induced branching fractures. They are usually unpropped because the fracture width is usually too small for the proppant particles to enter, but they are not always injected fracturing fluid saturated after fracturing treatment. If the reopened natural fractures or induced micro-fractures are hydraulically connected with primary fractures, injected fracturing fluid can enter the cracks without carrying proppant. However, injected fracturing fluid cannot access some secondary fractures, such as the ones yielded by shear slippage during the fracturing treatment procedure, and this type of secondary fractures are saturated by gas and original water and cannot be considered as the storage medium for injected fracturing fluid.

Shale matrix, even very tight, can still be a possible location for injected fracturing fluid. Unlike the leak off happening in conventional reservoirs, the invasion of injected fracturing fluid into shale matrix is more likely controlled by other mechanisms. Spontaneous imbibition has been challenged by the original non-water wettability of shale matrix, though observations from laboratory experiment confirm that the water can be absorbed into the shale core. An argument on the wettability that gaseous phase is always non-wetting phase makes the imbibition consideration reasonable. The clay content in shale matrix most of which are water-swelling will absorb the injected

fracturing fluid. What's more, the high treatment pressure may force the injected fracturing fluid to invade into the matrix if the pressure gradient between the fracture and matrix pore space is large enough. As long as the injected fracturing fluid invades into the matrix, the fluid saturation in the invaded part will be contributed by original gas and water in place and the invading fracturing fluid.

Table 1. Injected fluid location catalog

System	**Fracture system**		**Matrix**	
Storage Medium	**primary fracture**	**secondary fracture**	**Invaded matrix**	**original matrix**
Origin	Hydraulic fracturing treatment	Reopened natural fracture or induced branching fracture	Injected fluid invasion	Original
Propping status	Propped	Unpropped	N/A	N/A
Saturated fluid	Liquid: Fracturing fluid	Liquid: Fracturing fluid gas	Liquid: Fracturing fluid Liquid: Original water Gas	Liquid: Original water Gas
Injected fluid storage	Yes			No
Drainage status	Inside or outside of well drainage (Not applied to isolated well)			

Another point deserving concerns is that some part of the total injected fracturing fluid volume might be located outside the well drainage. This phenomenon was observed from Horn River shale gas wells study (Zhang, 2013). Figure 2 shows a 16 wells pad drilled in Evia and Muskwa members in Horn River Shale play. The water gas ratio of Well A, B, C, D, E and Zero increased when the fracturing treatment was in process in another well pad on the northeast side, as Figure 3 indicates. The increment in the water gas ratio in the above wells indicated that the injected fracturing fluid pumped through

the nearby well pad flew into the drainage of those wells mentioned above and was produced. As long as the injected fracturing fluid escapes the drainage of the very well via which it is injected into the formation, it might be never flowed back through the jame well. For isolated well this case is not to be necessarily taken into account while it is a concern when well pad is applied to the development, especially the fractures created from adjacent wells are overlapped and hydraulically connected.

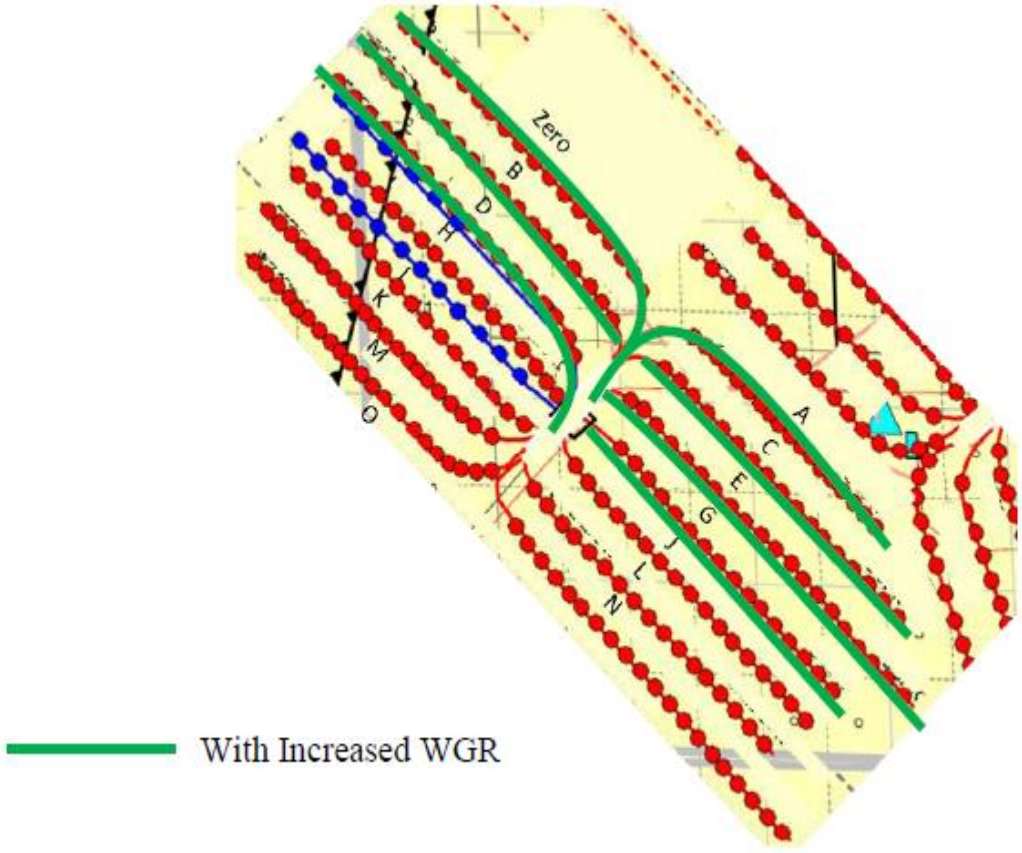

Figure 2. Well pad map in Horn River Shale (Zhang, 2013)

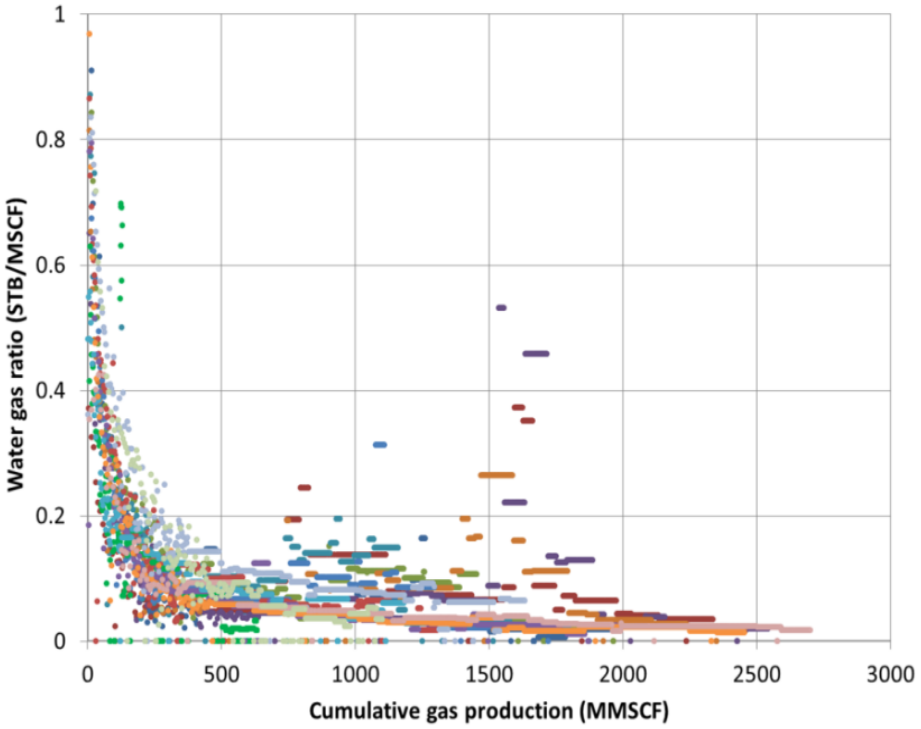

Figure 3. Increased water gas ratio during long-term gas production period (Adopted from Zhang, 2013)

We divided the media in shale gas formation after fracturing treatment into 4 types: Primary fracture (PF), which mainly refers to the propped hydraulic fractures filled up by injected fluid; Secondary fracture (SF), which refers to all unpropped micro-fractures or cracks and can be saturated by injected fluid or gas; Invasion zone (IZ), which is the matrix damaged by fracturing fluid invasion; Non-damage zone which means the formation with original properties and fluid saturation. The first three media are considered as the potential locations for injected fluid storage, but we should pay attention that all the media for injected fracturing fluid storage should be inside the drainage range of the well through which the fluid is injected.

2.1 Characteristics of the Media of Injected Fracturing Fluid Storage

Table 2 shows the description of the characteristics of each injected fracturing fluid storage medium.

Table 2. Injected fracturing fluid storage medium characteristics description

System / Characteristics	Fracture system		Matrix	
	primary fracture	**secondary fracture**	**Invaded matrix**	**original matrix**
Flow capacity	high or low permeability proppant pack	low conductivity due to the lack of proppant	Damage to permeability	Original matrix permeability
Relative permeability	Typical high relative permeability	Various low relative permeability profiles	Various low relative permeability profiles	It doesn't matter if $S_w<=S_{wir}$
Capillary pressure	Usually negligible	Medium to high capillary pressure profiles	High capillary pressure profiles	It doesn't matter if $S_w<=S_{wir}$
Gravity segregation	May happen	Unlikely to happen	Unlikely to happen	It doesn't matter if $S_w<=S_{wir}$

The conductivity of primary fracture is usually high and it depends on the permeability of the proppant pack and the width of the fracture. In the actual fracturing treatment different types of proppant might be used for different purpose. For example, the early stage proppant could be 100 mesh which cleans up the fracturing perforations and late stage proppant could be 40/70 mesh which establishes the conductivity of the primary fracture (Ahmed and Ehlig-Economides 2013). But in any case the primary fracture has higher conductivity since it is propped by the proppant.

Both the relative permeability of liquid phase and that of gas phase in primary fracture are usually high. The well connected porous flow path and the large pore space

diminish the interference between gaseous and liquid phase flow. In some extreme cases, the relative permeability profile in primary fracture could be as high as that in pipe flow.

Capillary pressure is not usually taken into account in propped primary fracture because the pore space is too large to induce high capillary pressure effect which may yield obvious imbibition or considerable drainage resistance (Alkouh and Wattenbarger 2013).

Gravity effect may take place in primary fracture (Parmar et al 2013). If the primary fracture height is large, liquid phase fluid may accumulate at the bottom of the primary fracture when the draining pressure gradient for upward flow to the well is not sufficient large to overcome the gravity.

The properties of secondary fractures are quite different from those of primary fractures since usually secondary fractures are not propped. The width of the secondary fractures is usually small and sometimes they are even not visible. That makes the conductivity of secondary fracture much smaller than that of primary fractures (Hill et al 2013).

Several sorts of relative permeability profiles in secondary fractures are discussed by the previous researchers. Alkouh and Wattenbarger (2013) summarized four types of relative permeability profiles which are possibly appropriate for secondary fractures. Figure 4 shows the four types of the relative permeability profiles including conventional, unconventional (lower relative permeability), permeability jail and hybrid permeability jail (Blasingame 2008). Compared to the conventional one, the other three profiles all have both lower water and gas relative permeability curves. The permeability

jail and hybrid permeability jail profiles contain a water saturation range within which neither water nor gas phase can effectively flow.

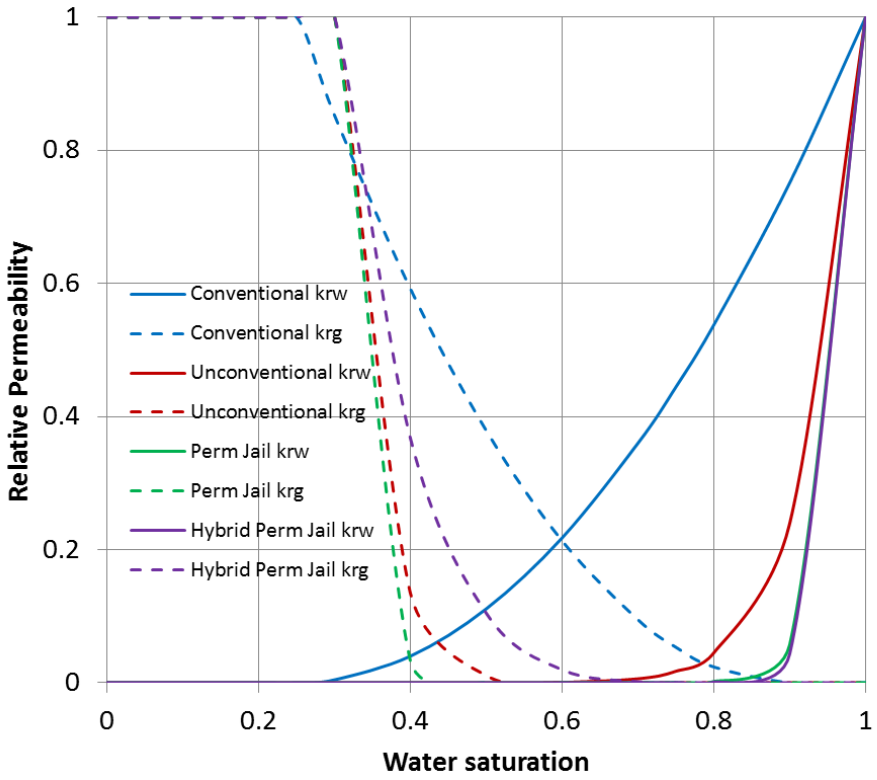

Figure 4. Four types of relative permeability profiles for secondary fracture system (Adopted from Alkouh and Wattenbarger 2013)

Capillary pressure in secondary fractures could be as high as thousands of psi due to the small width of the secondary fractures (Pegals et al 2012). For flowback modeling purpose, the capillary pressure is the resistance for gas flow to drain the injected fracturing fluid located in the secondary fractures.

Gravity effect is unlikely to be obvious in secondary fracture system because secondary fractures are usually very narrow (Alkouh and Watternbarger 2013).

Additionally, secondary fracture can be connected with the primary fracture from the top to the bottom so even there is an accumulation of water at the bottom of secondary fracture it is still able to be flowed to the primary fracture by the pressure gradient between the secondary fracture and primary fracture.

In the invasion matrix zone, permeability is usually damaged by the injected fracturing fluid invasion. The invasion of injected fracturing fluid into the shale matrix may yield a change in the structure and morphology of porous flow path, and the swelling effect induced by the chemical reaction between the injected fracturing fluid and the clay minerals such as kaolinite, illite and chlorite, will compress the pore space in shale matrix which originally is very small. The permeability reduction in the invasion zone may prevent the shale matrix from providing sufficient gas flow strength to clean up the liquid in the fracture system.

Alike secondary fracture system the relative permeability for both liquid and gas phase might be very low in the invasion zone and capillary pressure might be even higher to several thousand psi (Penny et al 2006). But the gravity segregation is unlikely to occur in the invasion zone because of the extremely low permeability in vertical direction.

In the non-damage matrix zone, if there is not mobile water in place, relative permeability or capillary pressure are not usually considered. Single gas phase flow may maintain the relative permeability of gas at a high value. Moreover, if the water saturation is always maintained at the irreducible water saturation, capillary pressure effect will never appear since the water saturation is not high enough for the gas flow

(Cheng 2010). Immobile water would not induce gravity effect in the non-damage zone anyway.

In this chapter we cataloged all possible locations for injected fracturing fluid storage after hydraulic fracturing treatment in shale gas wells, including propped primary fracture, unpropped secondary fracture and invaded matrix zone surrounding fracture faces. We also characterized the storage and flow properties of each storage medium, such as fracture conductivity, relative permeability and capillary pressure and so on. Understanding the distribution of injected fracturing fluid provides a foundation for construction of the flowback model. How the properties impact flowback and load recovery is investigated by numerically simulation modeling in the next chapter.

CHAPTER III

INJECTED FRACTURING FLUID RETENTION

The catalog of injected fracturing fluid locations and the characterization of the properties of each possible storage medium provides a basic idea for construction of models to model the flowback process. In this chapter we classified 4 scenarios for flowback models and set up numerical simulation models for each scenario using the commercial simulator CMG. Through the simulation work we investigate how the properties of the possible injected fracturing fluid storage media induce injected water retention, and evaluate their impact on load recovery.

3.1 Factors Impacting Fracturing Fluid Flowback

The water retention in gas is the result of competition between the flowback draining force and resistance. To specify the factors affecting load recovery the mechanisms of flowback and injected fracturing fluid retention should be revealed. Figure 5 shows an illustration of the flowback of injected fracturing fluid from primary fracture as example. Here we include the capillary pressure for completion.

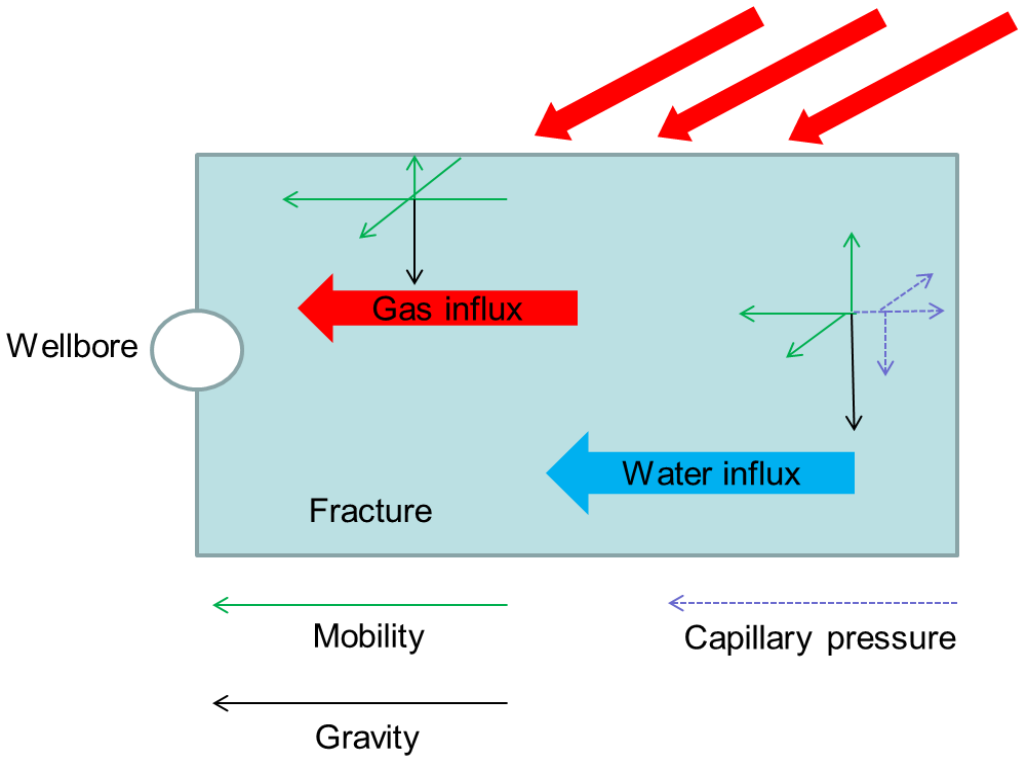

Figure 5. Illustration of injected fracturing fluid flowback from primary fracture

Equation 1 is the fundamental flow equation for fluid flow in porous media, the Darcy's law. We analyzed the draining force and resistances to injected fracturing fluid flowback by examining the terms in Eq. 1.

$$v_i = \frac{kk_{ri}(s_w)}{\mu_i(p)} \nabla(p - p_c(s_w) - \rho_i g \Delta z),\ \text{i} = \text{gas or water} \qquad (1)$$

The draining force of injected fracturing fluid flowback mainly includes two mechanisms: flow of the injected fracturing fluid and the gas expansion drainage. Whenever the pressure gradient is established in the porous medium where the injected

fracturing fluid is located, the potential of injected fracturing fluid flow occurs. Though whether the injected fracturing fluid really happens and how it flows depends on other factors such as the permeability, relative permeability, and fluid viscosity. The pressure gradient provides a drive force to flow the injected fracturing fluid from the current location to the wellbore. In a gas well, gas inflow into the injected fracturing fluid storage media will provide an additional draining force to the injected fracturing fluid by expansion. The entry of gas inflow requires a pressure gradient from the matrix to fracture system, and once gas flows from a higher pressure location into a lower pressure location, gas will expand due to the high compressibility and low pressure environment so that will compel the slightly compressible fracturing fluid to flow toward to the location of much lower pressure.

There are three main resistances to injected fracturing fluid flow back: Gas blocking effect, capillary pressure (imbibition) and liquid loading. Gas has much less viscosity than the injected fracturing fluid so that, with the same pressure gradient, gas flow is much faster than the fracturing fluid. The faster gas flow may establish quick high gas saturation which yields high gas relative permeability and low relative permeability for fracturing fluid so that the mobility difference between gas and fracturing fluid will be enlarged. Once the gas flow dominated the path to the wellbore, fracturing fluid may not flow effectively or rather the flowback of injected fracturing fluid is blocked by gas. This is the gas blocking effect which can make injected fracturing fluid retained in the media. For a two phase system of both liquid and gas, if the gas is non-wetting phase the flowback is a drainage process. The capillary pressure is

a resistance for gas flow to displace injected fracturing fluid and it can be also a force for injected fracturing fluid to be imbibed into the secondary or matrix. Liquid loading or rather gravity segregation effect is induced by the density difference between gas and liquid phase. If the pressure gradient for injected fracturing fluid flow upward is overwhelmed by the gravity, the injected fracturing fluid will be accumulated at the bottom of the storage media.

3.2 Simulation Model for the Study on Factors Impacting Load Recovery

This section specifies fours simulation model scenarios to take different injected fracturing fluid distribution possibilities into account. The based model of each scenario is described in details and sensitivity studies on the factors which potentially impact load recovery are cataloged.

3.2.1 Injected Fracturing Fluid Distribution Scenarios

According to the catalog of possible injected fracturing fluid locations we classified four scenarios of injected fracturing fluid distribution. In Scenario 1 injected fracturing fluid is only located in Primary fracture; in Scenario 2 the injected fracturing fluid is located in both primary fracture and secondary fractures which are orthogonal to the primary fracture; in Scenario 3 the injected fracturing fluid is located in the primary fracture and the invasion zone surrounding the primary fracture face; in Scenario 4 the fracturing fluid is located in primary fracture, secondary fractures and the invasion zone

surrounding the whole fracture system. Figure 6 illustrates the 3-dimension scheme of the four injected fracturing fluid distribution scenarios.

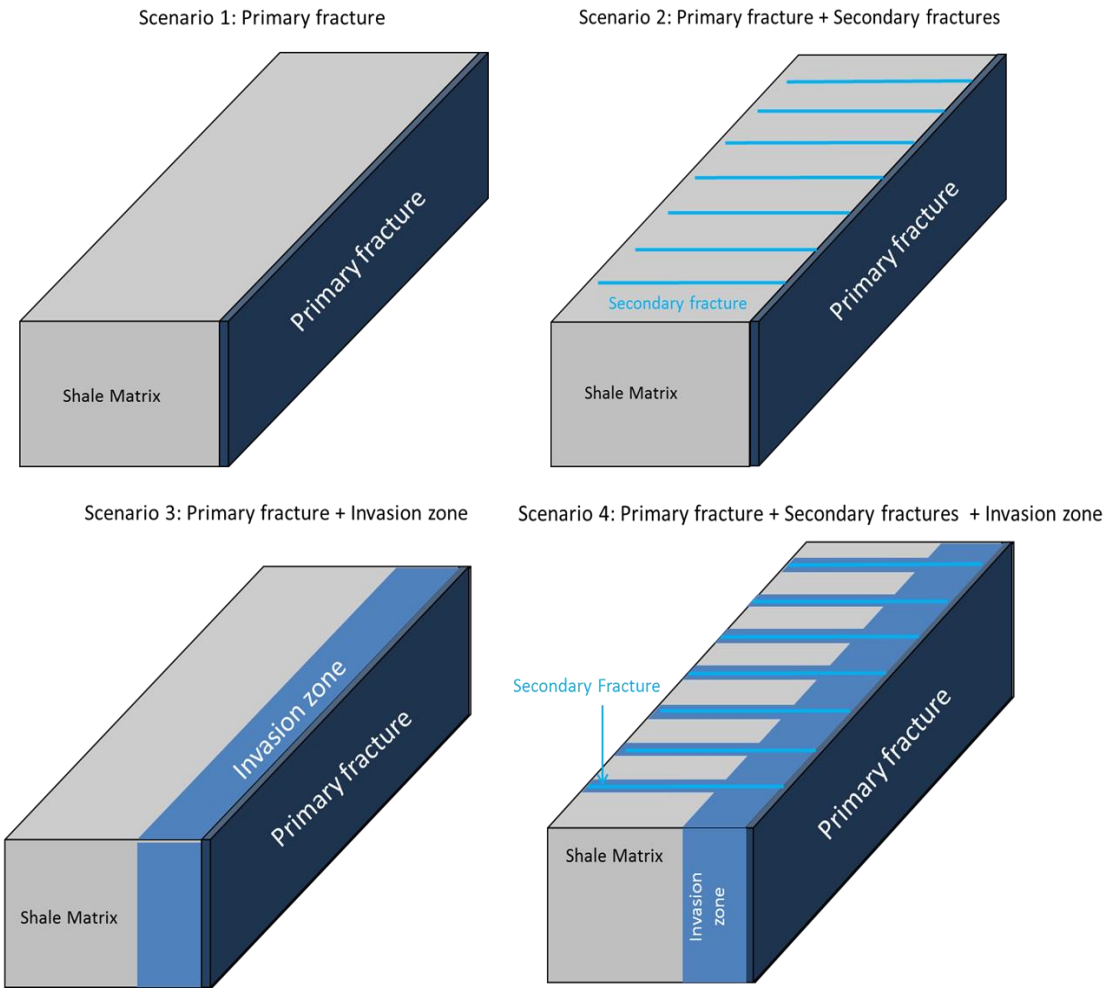

Figure 6. 3D scheme of four injected fracturing fluid distribution scenarios

3.2.2 Base Simulation Model Description of Each Scenario

The simulation model is accounting for one quarter of a single primary fracture drainage element due to the symmetric feature of the whole model. Figure 7 shows the illustration of the extent the model actually simulates.

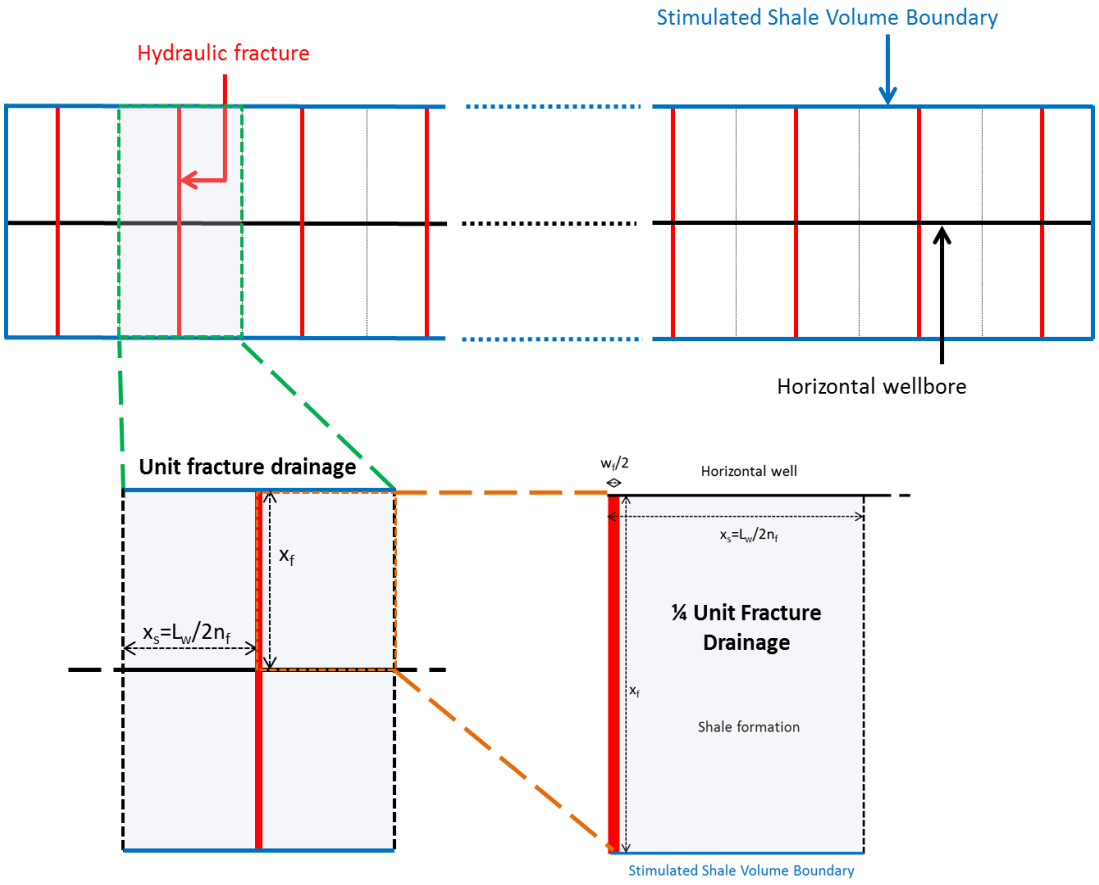

Figure 7. Illustration of single simulation element

The full scale base model of Scenario 1 includes a horizontal well of 6000 ft length with 30 primary fracture evenly distributed along the horizontal wellbore. The detailed information is listed in Table 3. If we only treat the water in place in primary

fracture space the total injected fracturing fluid volume is 904 bbl and that of single simulation element is 7.53 bbl.

Table 3. Full scale simulation model of Scenario 1 description

Shale formation properties		
Shale formation top depth	3500	ft
Shale formation thickness	90	ft
Shale matrix porosity	0.08	fraction
Shale matrix permeability	1.00E-04	md
Shale formation average temperature	200	F deg
Shale formation initial pressure	4500	psia
Initial water saturation	0.25	fraction
Formation compressibility		1/psi
Fluid properties		
Hydrocarbon composite	CH_4	N/A
Gas specific gravity	0.65	fraction
Water formation volume factor	1	rb/stb
Water compressibility	3.00E-06	1/psi
Water viscosity	1	cp
Well and Primary fracture properties		
Horizontal well length	6000	ft
Primary fracture half length	200	ft
Primary fracture height	90	ft
Primary fracture width	0.24	inch
Primary fracture conductivity	2	md-ft
Proppant pack porosity	0.47	fraction
Primary fracture spacing	200	ft
The number of primary fractures	30	1

The commercial simulator Computer Modeling Group (SMG) is applied to carry out the simulation modeling work. Figure 8 shows the 3D model built in CMG simulator. To model one perforation cluster from the horizontal well, we set a vertical well with the perforation at the center of the fracture, which is also the center of the formation since

the primary fracture is assumed to fully penetrate the shale formation in vertical direction. Well is flowing with 500 psia BHP.

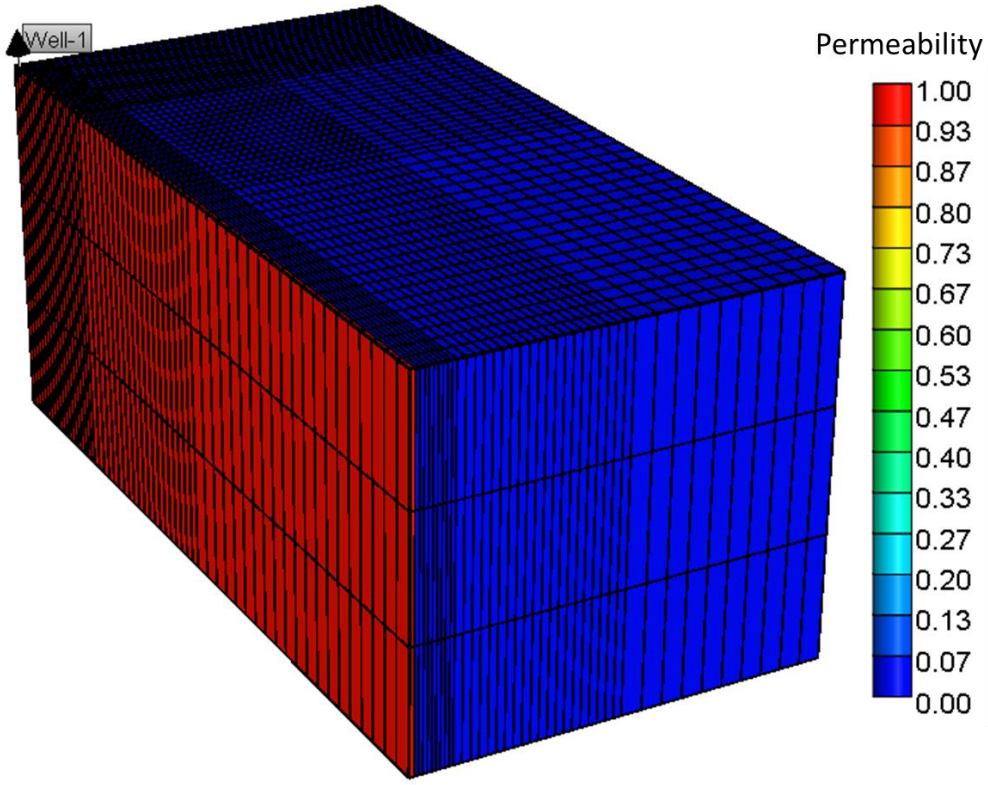

Figure 8. 3D numerical simulation model of Scenario 1

The base models of Scenario 2, Scenario 3 and Scenario 4 are all built based on that of Scenario 1. Table 4 listed the parameters applied in the based models of the four scenarios. Table 5 summarizes the injected fracturing fluid volume and its distribution in various media for each scenario. In all simulation, we treat the injected fracturing fluid as water approximately since the main component of the fracturing fluid system for shale gas wells is slick water.

Table 4. Base model simulation inputs of four scenarios

For 1/2 Single PF drainage		*SCN 1*		*SCN 2*		*SCN 3*		*SCN 4*	
Primary Fracture	length	200	ft	200	ft	200	ft	200	ft
	width in sim.	1	ft	1	ft	1	ft	1	ft
	height	90	ft	90	ft	90	ft	90	ft
	porosity in sim.	0.00235	frac.	0.00235	frac.	0.00235	frac.	0.00235	frac.
	permeability sim.	1	md	1	md	1	md	1	md
	conductivity	1	md-ft	1	md-ft	1	md-ft	1	md-ft
	initial water saturation	1	frac.	1	frac.	1	frac.	1	frac.
Single Secondary Fracture	length	N/A	ft	100	ft	N/A	ft	100	ft
	width in sim.	N/A	ft	1	ft	N/A	ft	1	ft
	height	N/A	ft	90	ft	N/A	ft	90	ft
	porosity in sim.	N/A	frac.	1	frac.	N/A	frac.	1	frac.
	permeability sim.	N/A	md	0.01	md	N/A	md	0.01	md
	conductivity	N/A	md-ft	0.01	md-ft	N/A	md-ft	0.01	md-ft
	initial water saturation	N/A	frac.	1	frac.	N/A	frac.	1	frac.
	spacing	N/A	ft	20	ft	N/A	ft	20	ft
Invasion Zone Surrounding Primary Fracture	length	N/A	ft	N/A	ft	200	ft	190	ft
	width	N/A	ft	N/A	ft	1	ft	1	ft
	height	N/A	ft	N/A	ft	90	ft	90	ft
	porosity	N/A	frac.	N/A	frac.	0.08	frac.	0.08	frac.
	permeability	N/A	md	N/A	md	0.0001	md	0.0001	md
	initial water saturation	N/A	frac.	N/A	frac.	0.253264	frac.	0.253264	frac.
Invasion Zone Surrounding Single Secondary Fracture	length	N/A	ft	N/A	ft	N/A	ft	98	ft
	width	N/A	ft	N/A	ft	N/A	ft	2	ft
	height	N/A	ft	N/A	ft	N/A	ft	90	ft
	porosity	N/A	frac.	N/A	frac.	N/A	frac.	0.08	frac.
	permeability	N/A	md	N/A	md	N/A	md	0.0001	md
	initial water saturation	N/A	frac.	N/A	frac.	N/A	frac.	0.250165	frac.

Table 5. Total injected fracturing fluid volume summary

Injection volume location (Single simulation element)	*SCN 1*		*SCN 2*		*SCN 3*		*SCN 4*	
Primary fracture	7.533393	bbl	7.533393	bbl	7.533393	bbl	7.533393	bbl
Secondary fractures	0	bbl	16.02689	bbl	0	bbl	16.02689	bbl
Invasion zone surrounding PF	0	bbl	0	bbl	0.837042	bbl	0.837042	bbl
Invasion zone surrounding SF	0	bbl	0	bbl	0	bbl	0.82863	bbl
Total injection volume	7.533393	bbl	23.56028	bbl	8.370435	bbl	25.22596	bbl

3.2.3 Sensitivity Study Specification

Multiple parameter sensitivity studies are performed to investigate the impacts of the factors of primary fracture, secondary fracture and invasion zone on load recovery. Table 6 specified the range of each parameter for sensitivity study.

Table 6. Parameter range for sensitivity study in each medium

Primary fracture				
Parameter	***Base***	***Min.***	***Max.***	***Note***
Conductivity, md-ft	1	0.1	1000	
Height, ft	90	3	180	
Relative permeability	k_r_PF_1	k_r_PF_1	k_r_PF_5	kr_PF_1 is the highest
Secondary fracture				
Parameter	***Base***	***Min.***	***Max.***	***Note***
Conductivity, md-ft	0.01	0.001	0.1	
Height, ft	90	3	180	
Relative permeability	k_r_SF_1	k_r_SF_1	k_r_SF_5	kr_SF_1 is the highest
Capillary pressure	P_c_SF_1	P_c_SF_1	P_c_SF_5	Pc_SF_1 is the lowest
Spacing, ft	20	5	40	
Invasion zone				
Parameter	***Base***	***Min.***	***Max.***	***Note***
Permeability, md	1.00E-04	1.00E-05	1.00E-03	
Height, ft	90	3	180	
Relative permeability	k_r_IZ_1	k_r_IZ_1	k_r_IZ_5	kr_IZ_1 is the highest
Capillary pressure	P_c_IZ_1	P_c_IZ_1	P_c_IZ_5	Pc_IZ_1 is the lowest
Invasion depth (PF), ft	1	1	5	
Invasion depth (SF), ft	0.1	0.1	0.5	

Figure 9 shows the relative permeability profiles for primary fracture; Figure. 10 and Figure 11 show the relative permeability profiles and capillary pressure profiles for secondary fracture; Figure 12 and Figure 13 show the relative permeability profiles and capillary pressure profiles for invasion zone.

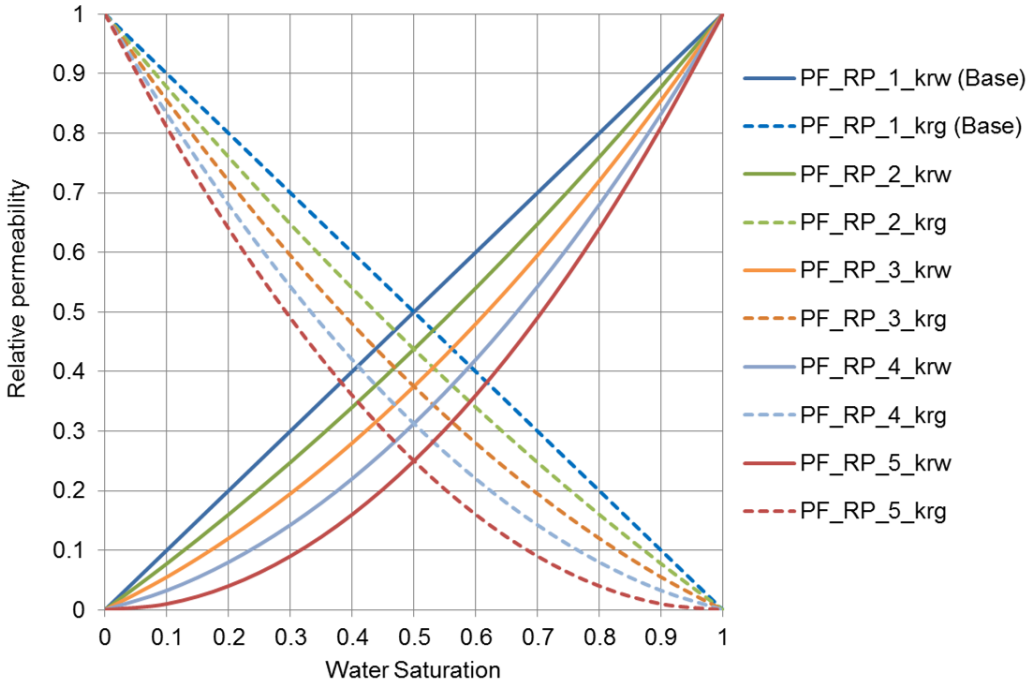

Figure 9. Relative permeability profiles for primary fracture

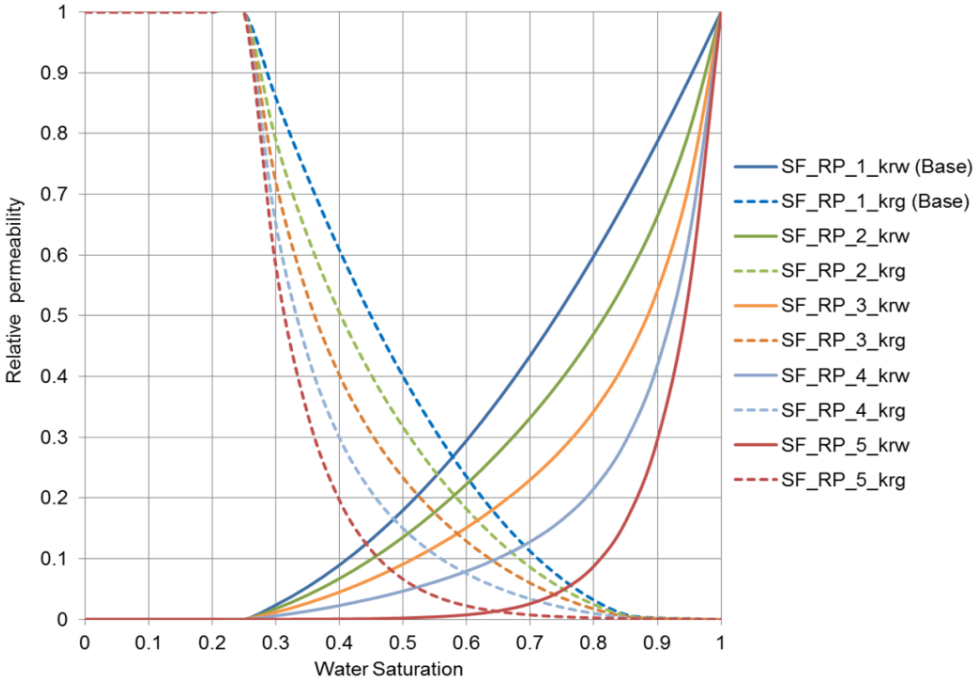

Figure 10. Relative permeability profiles for secondary fracture

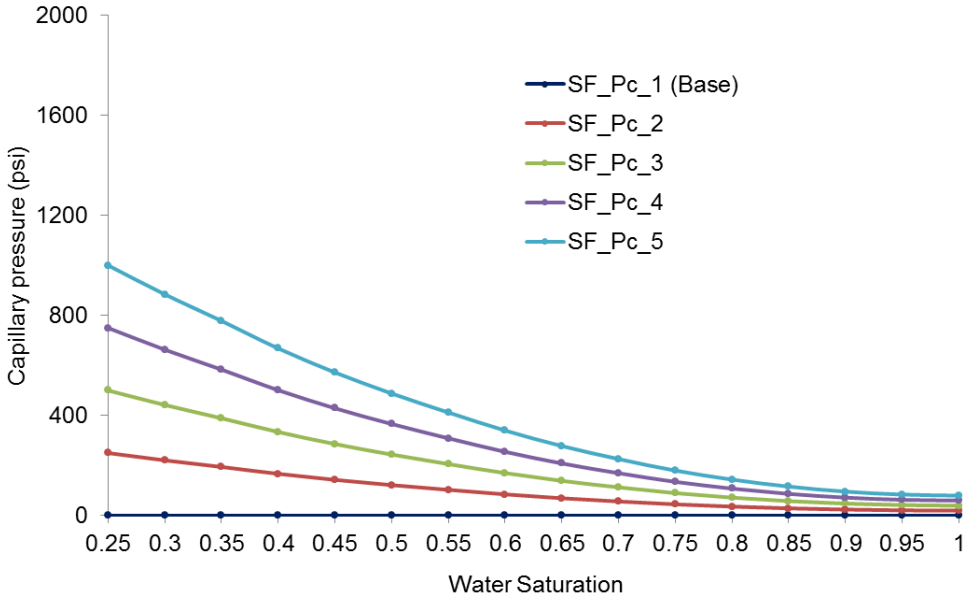

Figure 11. Capillary pressure profiles for secondary fracture

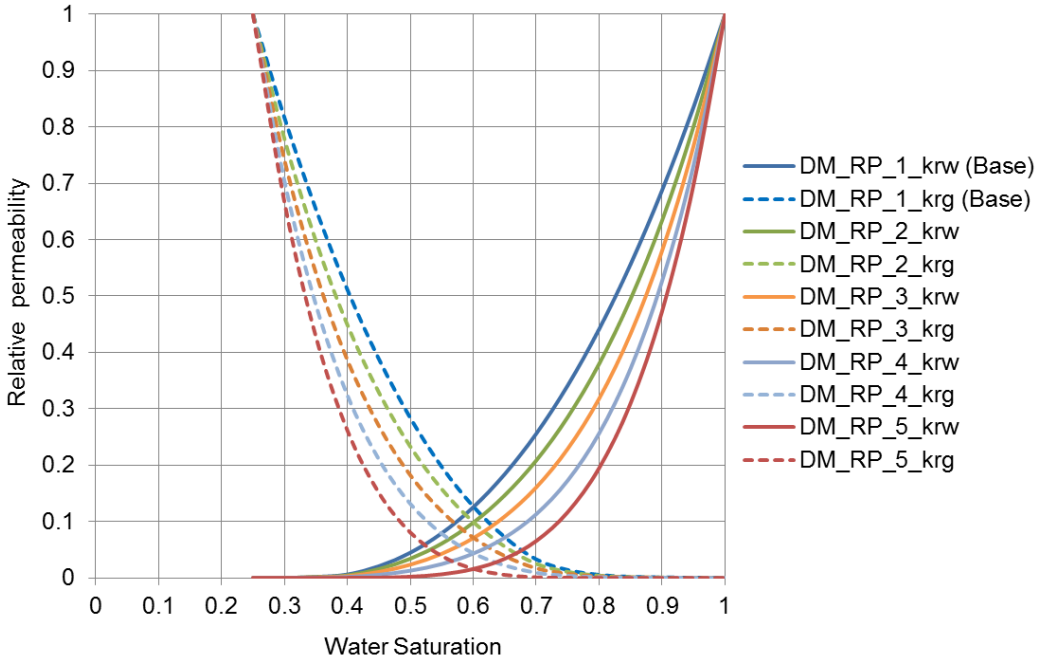

Figure 12. Relative permeability profiles for invasion zone

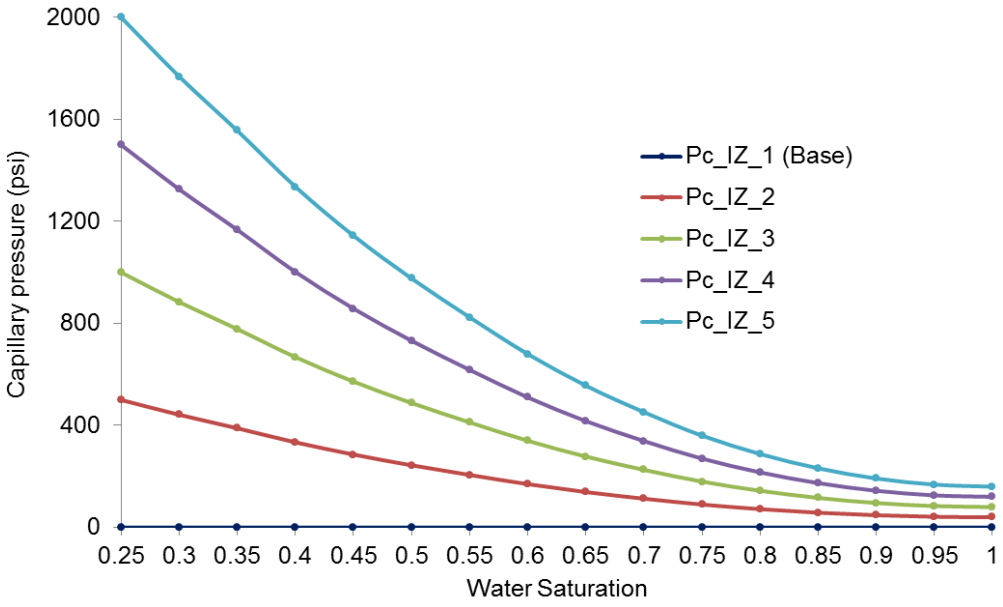

Figure 13. Capillary pressure profiles for invasion zone

3.3 Simulation Result Interpretation

For each scenario, we investigated the impacts of the factors which potentially affect flowback on load recovery with the plots of load recovery and the factors of interest. Furthermore, we explained the observation from the perspective of flowback and injected fracturing fluid retention mechanism.

3.3.1 Scenario 1: Primary Fracture

Figure 14 shows the plot of load recovery versus primary conductivity sensing relative permeability profiles for different fracture heights in 2D coordinate. According to Figure 14, it is not true that the higher conductivity of primary fracture always facilitate flowback for Scenario 1. As Figure 14 shows a medium range of conductivity

helps increase load recovery. Lower conductivity yields lower load recovery because the mobility of the water is too low, Even the occurrence of gas blocking takes longer time; While the very high conductivity yields lower load recovery because the gas blocking is too fast so there is not sufficient time for more water to flow back.

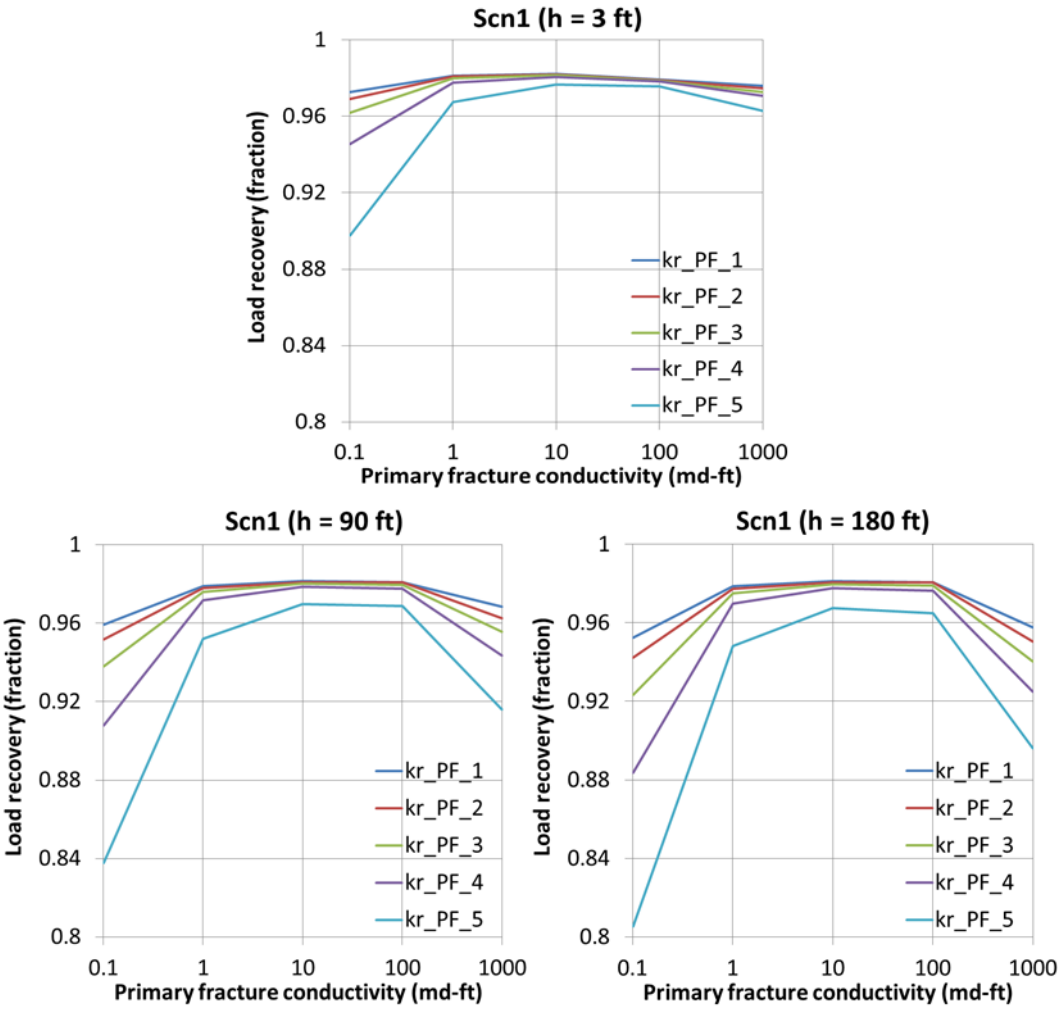

Figure 14. Impacts of primary fracture properties on load recovery study: Scenario 1, LR vs. F_c-PF sensing k_r-PF (Varying h)

Figure 15 shows the conductivity of primary fracturing impacts load recovery in Scenario 1. For a given 90 ft height and primary fracture relative permeability profile, gas blocking is established at different time depending on the primary fracture conductivity. The turning point at which the slope the cumulative water production curve is approximately the time when gas domination starts because after that water production is small so that the cumulative water production curve is gradually flattened. As Figure 16 indicates, it takes about 2 months, 4 days, and less than 1 day for gas blocking to occur corresponding to 0.1 md-ft, 10 md-ft and 1000 md-ft primary fracture conductivity. When primary fracture conductivity is 1000 md-ft, the cumulative water production before gas blocking is increasing sharply but this trend is quickly switched to a very flat trend due to the quick gas domination; while when primary fracture conductivity is 0.1 md-ft, though gas blocking occurrence is much delayed the cumulative water production before gas blocking is increasing much more slowly.

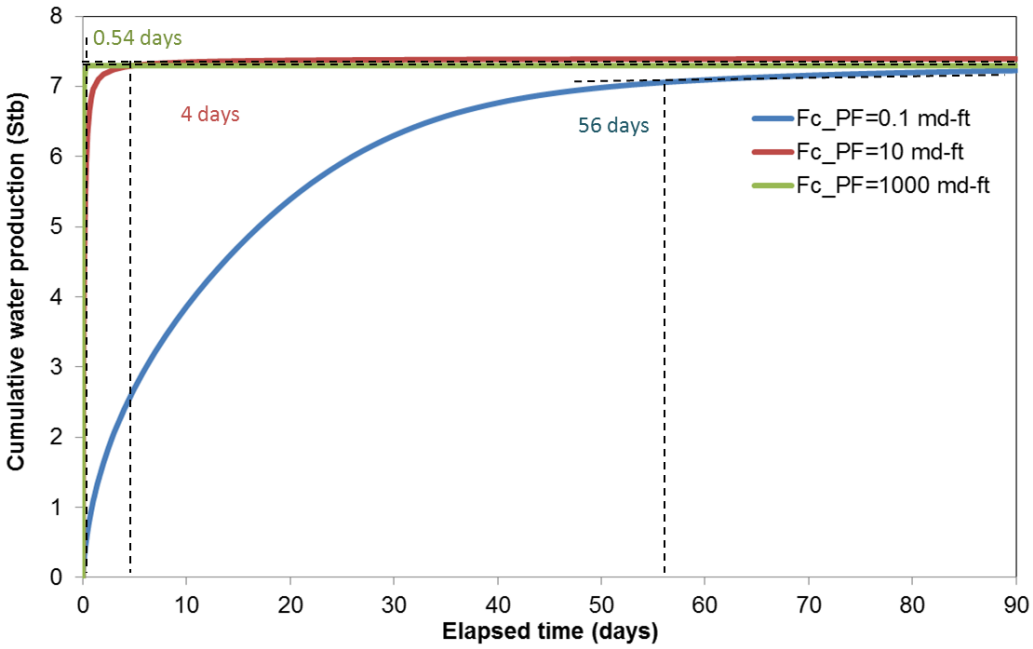

Figure 15. Cumulative water production comparison: Scenario 1, h = 90 ft, k_r-PF -1

Figure 16 shows the water saturation profile in the primary fracture at 10 days for the 3 conductivity values mentioned above. At 10 days, in the case of F_c-PF = 10 md-ft and 1000 md-ft most of the water in the primary fracture has been flowed back while much of the water is still in the primary fracture space in the case of F_c-PF = 0.1 md-ft and the water saturation is increasing as the distance does further from the well perforation. However, the unrecovered water is settled down right below the well perforation when F_c-PF = 1000 md-ft. Therefore, again for low primary fracture conductivity the retention is mainly at the location far away from well because the fracturing fluid has not even been flowed though gas blocking has not been established; for high conductivity the retention is accumulated at nearby well perforation location and it is because the fast water flowback due to the high primary fracture conductivity is

blocked by even faster gas domination at the well perforation, and most of the unrecovered water is likely accumulated right below the well perforation.

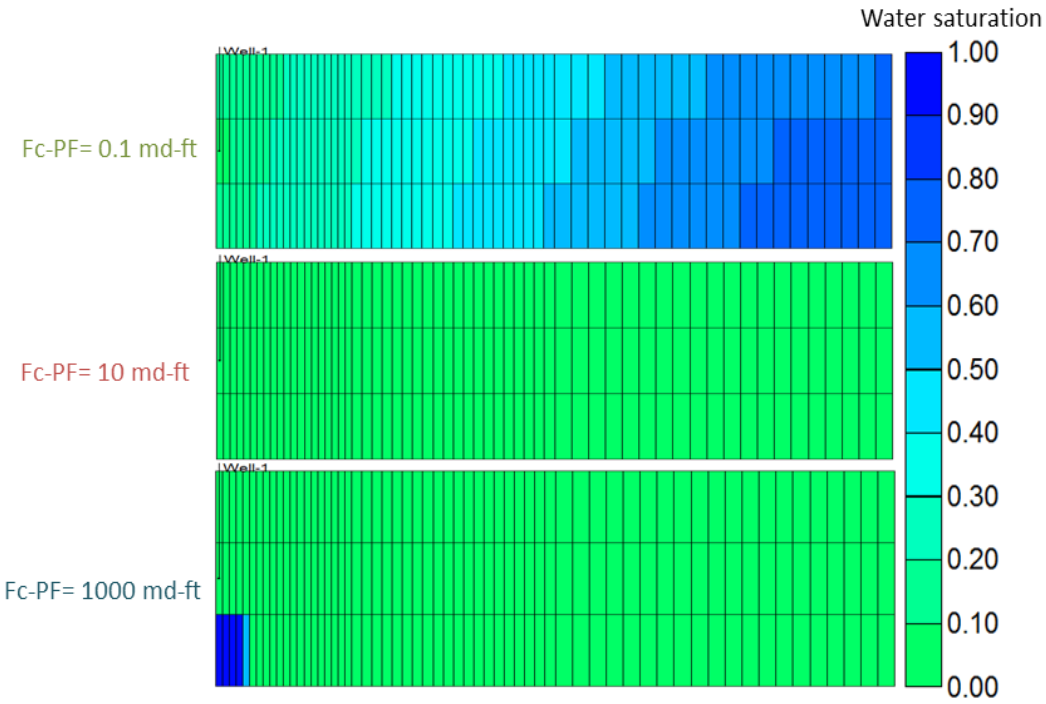

Figure 16. Primary fracture water saturation profile comparison at 10 days: Scenario 1, h = 90 ft, k_r-PF -1

Liquid loading is likely to happen in primary fracture of larger height, especially when the conductivity is too high or too low and relative permeability is low. To illustrate the liquid loading effect we compared the water saturation profile of primary fracture at 3 month for three different heights: 3 ft, 90 ft and 180 ft with 1000 md-ft primary fracture conductivity and kr_PF_5 because with these conditions liquid loading effect won't be much eliminated by the mechanisms of felicitating flowback. As Figure 17 shows, liquid loading will accumulate the unrecovered water below the well

perforation and the heavier liquid load effect is due to the larger height, the longer extension of high water saturation zone will be along primary fracture direction at the bottom. This observation is mainly because the larger height reduces the pressure gradient for upward flow.

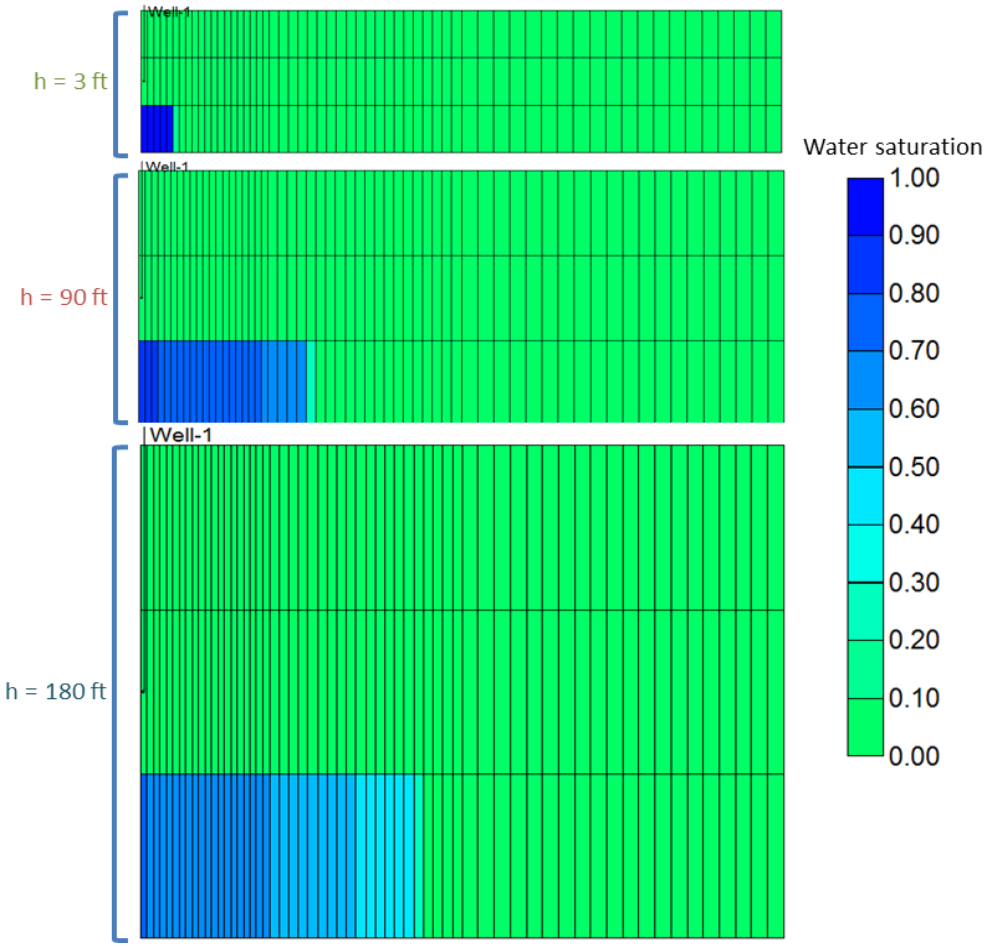

Figure 17. Primary fracture water saturation profile comparison at 90 days: Scenario 1, F_c-PF = 1000 md-ft, k_r-PF-5

Lower relative permeability results in lower load recovery, especially at "extreme" conductivity condition. We initiated with a straight line relative permeability

curve profile for primary fracture and decrease them at the same decrement rate simultaneously. The decrement in gas mobility delays the gas blocking occurrence as Figure 18 shows, however the decrement in water mobility due to the lower water relative permeability is more dominating to flowback because the reduction in water production due to the decrement in the water flow capacity cannot be made up by the extension of pre-gas blocking period. The water saturation profile comparison at 20 days (Figure 19) indicates that as relative permeability decreases more flow of injected fracturing fluid is delayed or even stagnated. Therefore, the relative permeability impacts the load recovery of Scenario 1 mainly through affecting the mobility of injected fracturing fluid since relative permeability effect on gas flow will be less due to the low viscosity of gas.

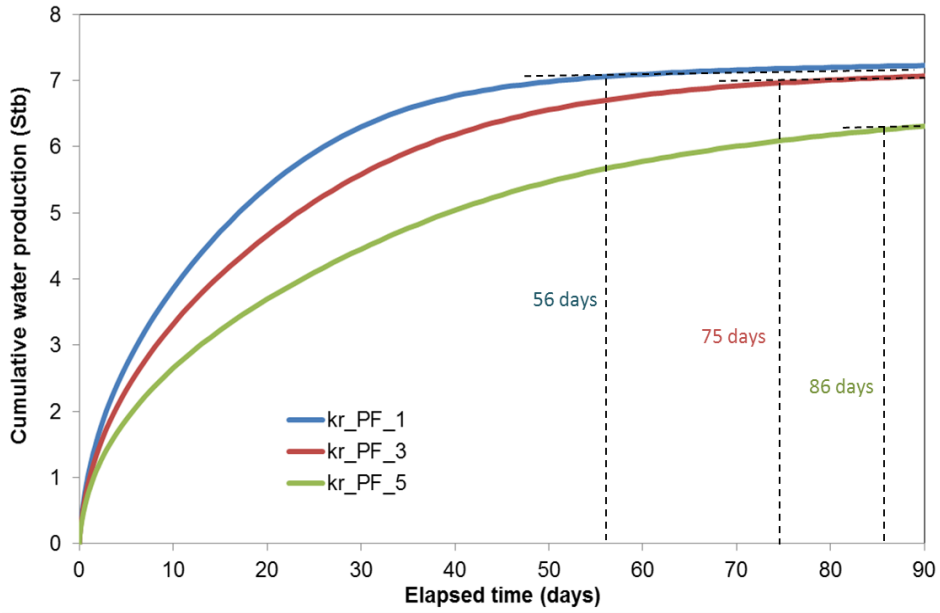

Figure 18. Cumulative water production comparison: Scenario 1, h = 90 ft, F_c-PF = 0.1 md-ft

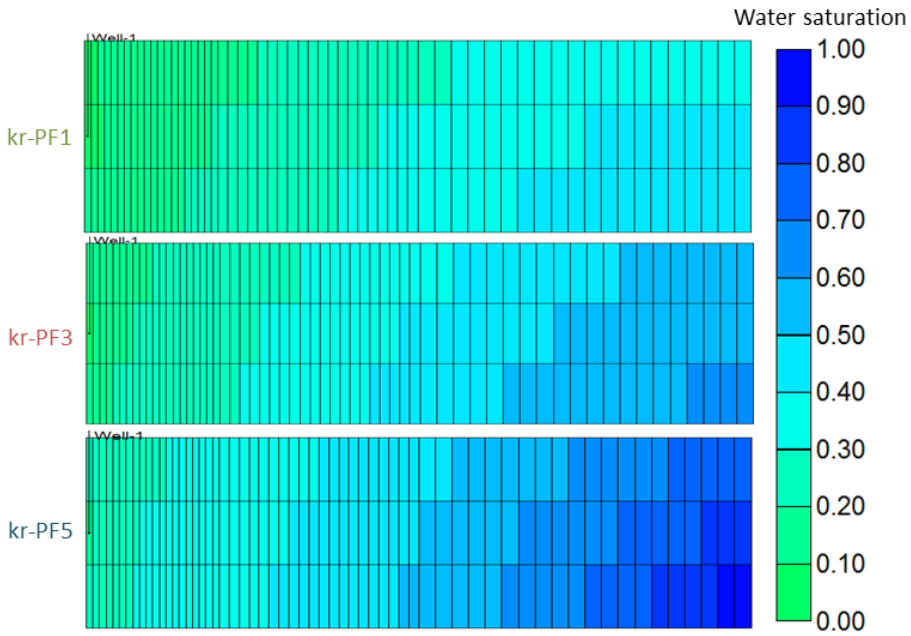

Figure 19. Primary fracture water saturation profile comparison at 20 days: Scenario 1, F_c-PF = 0.1 md-ft, h = 90 ft

As we can observe in Figure 14, the load recovery, no matter higher or lower, is generally high (usually over 80%). This basically means that the high conductivity of primary fracture will dominate the flow back capacity in Scenario 1. The larger height which might yield more liquid loading and lower relative permeability profiles may affect the mobility, but neither can prohibit the high conductivity from delivering most of the water in primary fracture back to the wellbore.

Based on the study on Scenario 1, we understand the following points:

- The general load recovery from primary fracture is very high (80% - 95%) due to the high conductivity. It is the dominating factor determining the overall load

recovery level. The impact of relative permeability is more severe at conductivity extremes.

- Extremely low conductivity reduces load recovery because the water flow capacity is low though gas blocking occurs later; the retention is at the location far away from well perforation.
- Extremely high conductivity reduces load recovery because the gas blocking is so fast that there isn't sufficient time for more water to flow back; the retention is at the location nearby well perforation.
- Liquid loading increases in primary fracture of larger height, especially when the conductivity is too high or too low and relative permeability is low. The height increment is impacting load recovery due to both the flow capacity difference between two phases in vertical direction and the density effect.

3.3.2 Scenario 2: Primary Fracture and Secondary Fracture

Figure 20 shows the 3D illustration of the model for Scenario 2, in which both primary fracture and 10 secondary fractures normal to primary fracture in this simulated drainage.

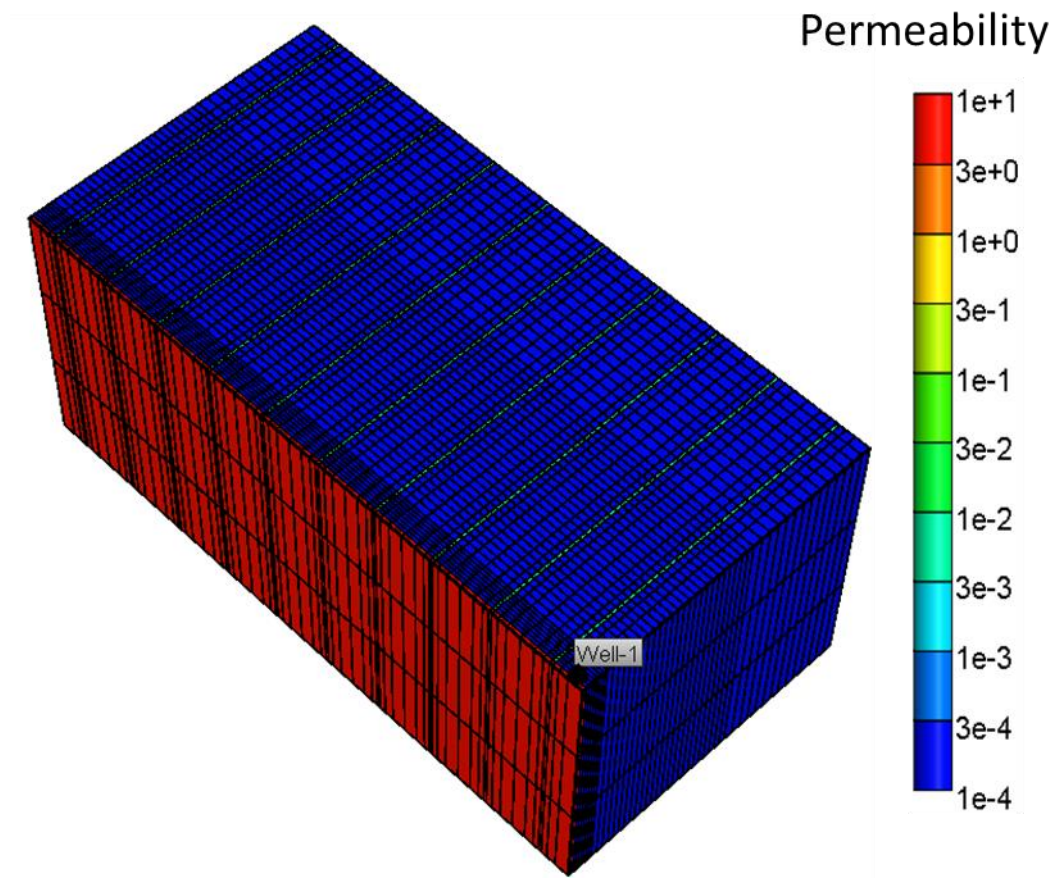

Figure 20. 3D numerical simulation model of Scenario 2

To investigate the role of secondary fracture in impacting flowback we applied a medium primary conductivity and high relative permeability to prevent the primary fracture impacts from disguising the impacts of secondary fracture. Figure 21 shows the effect of secondary fracture conductivity and height on load recovery of Scenario 2.

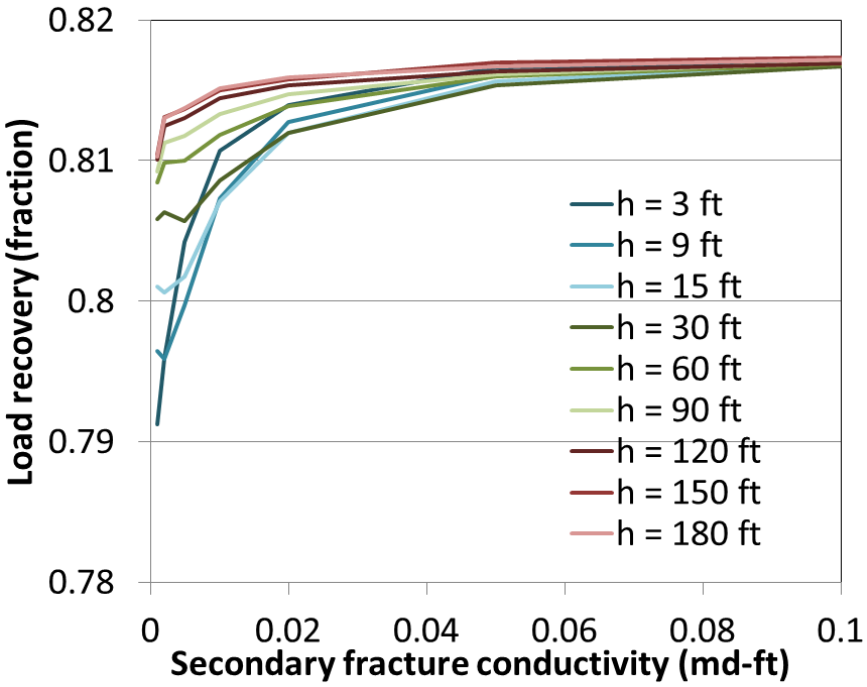

Figure 21. Impacts of secondary fracture properties on load recovery: Scenario 2, LR vs. F_c-SF sensing h (Fixing k_r-SF1, p_c-SF1)

Overall, higher secondary fracture conductivity facilitates flowback. It is not difficult to understand it because higher secondary fracture conductivity enhances the mobility of water. However, unlike in primary fracture this effect is monotonous. The reason is that the conductivity of secondary fracture cannot be high enough to possibly yield a very quick gas blocking effect in a single instant.

Another interesting observation in Scenario 2 distinguished from Scenario 1 is that smaller height results in the lower load recovery, especially at lower conductivity condition. This may indicate that as height varies, the secondary fracture does not impact on load recovery by yielding liquid loading effect in secondary fracture itself but through affecting the flow from secondary fracture to primary fracture. A possible explanation to

this phenomenon is that smaller height may accelerate the gas blocking occurrence in primary fracture. However, as we can see height actually does not impact load recovery very much if the primary fracture doesn't induce heavy liquid loading. What's more, the obvious reduction in load recovery as height decreases only happens at an unrealistic height range. Therefore, liquid loading should not be considered in secondary fractures.

Lower relative permeability yields lower load recovery but only when conductivity is small this effect is more obvious, as Figure 22 indicates. The mechanism behind this is identical to that in primary fracture. However, for any given conductivity the impact of lower relative permeability on decreasing load recovery is not quite severe until the relative permeability is down to a certain level.

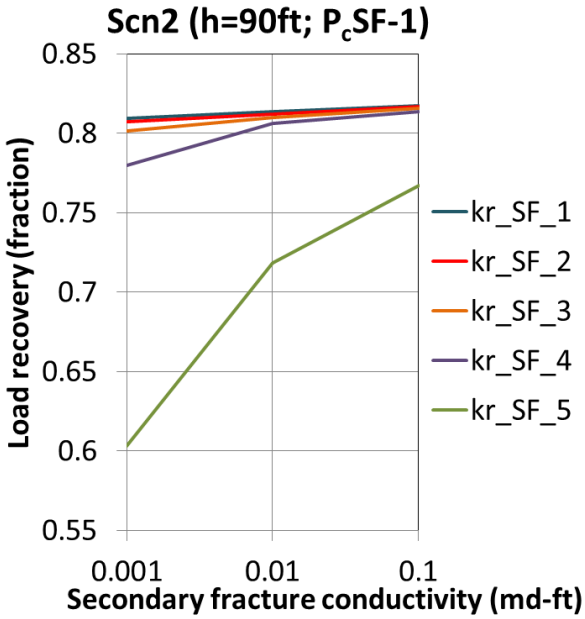

Figure 22. Impacts of secondary fracture properties on load recovery: Scenario 2, LR vs. F_c-SF sensing k_r-SF (h= 90 ft, p_c-SF1)

Similar to the relative permeability impact on the flowback performance in Scenario 1, decrease in the relative gas permeability will delay the gas blocking effect and that in relative water permeability will reduce the water mobility. As Figure 23 indicates: for any secondary relative permeability profile primary fracture is quickly cleaned up and almost all the injected fluid in primary fracture is flowed back; the smaller secondary fracture relative permeability profile will induce later occurrence of gas blocking (flattening of cumulative water production) but its reduction impact on flowing back injected fluid is more overwhelming so that the load recovery is lower.

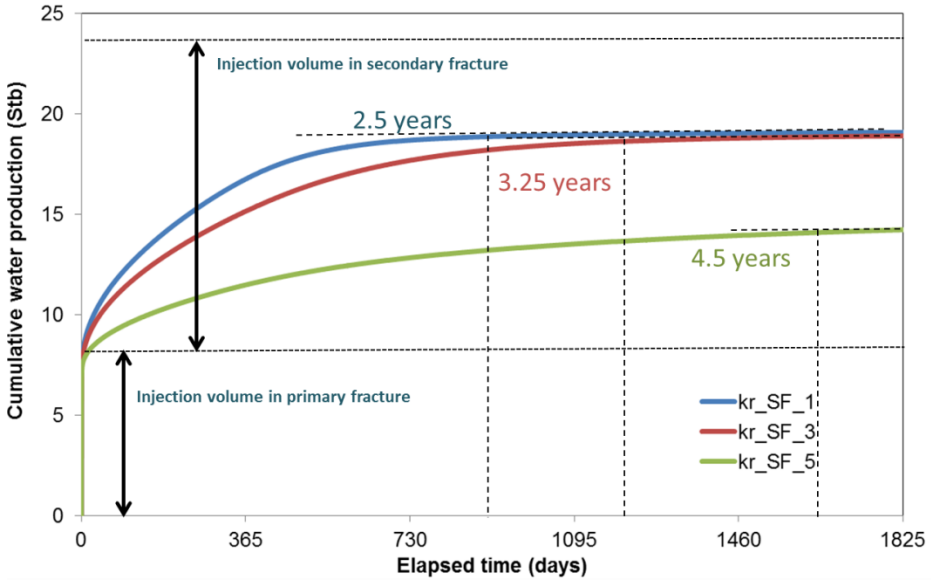

Figure 23. Cumulative water production comparison: Scenario 2, h = 90 ft, F_c-SF = 0.001 md-ft

More specifically, we can observe the location of retained injected fracturing fluid. In Scenario 2, most of unrecovered injected fracturing fluid is retained in secondary fracture space. Of course, one reason contributing to this is that the irreducible

water saturation in secondary fracture is usually higher. However, as Figure 24 indicates when the relative permeability for secondary fracture is low enough (k_r-SF5) most part of the secondary fracture space is still high in water saturation. Its value is 0.5 after 5 years flowing. Additionally in the k_r-SF5 case, some of the unrecovered water is accumulated right beneath the well perforation. The low relative permeability of the injected fracturing fluid located in secondary fractures reduces the mobility of it and this affects more than in primary fracture since generally the conductivity of secondary fracture is smaller than that of primary fracture. Once the gas saturation increases very quickly in primary fracture, the path for the injected fracturing fluid in secondary fracture to flow back toward well perforation will be blocked by high gas saturation in primary fractures.

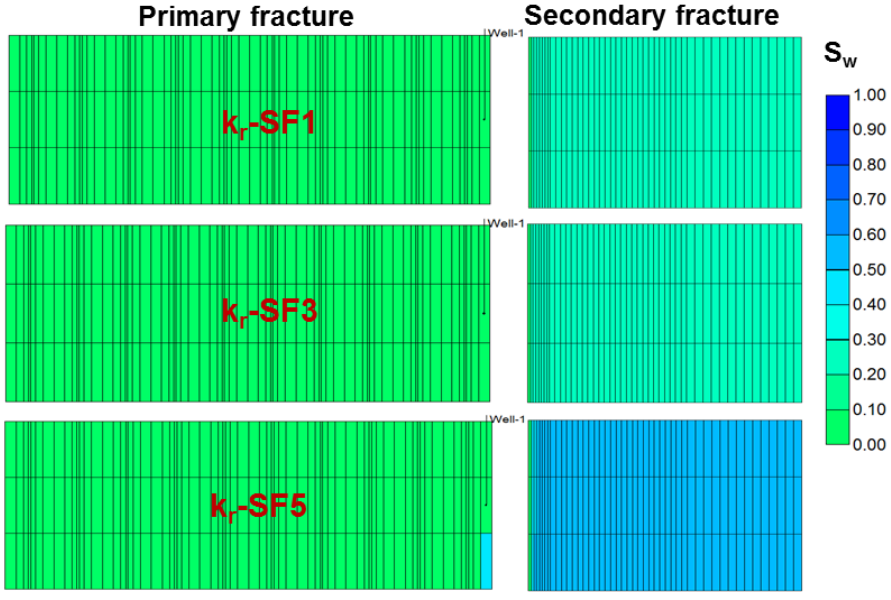

Figure 24. Primary fracture and secondary fracture water saturation at 5 years: Scenario 2, F_c-SF = 0.001 md-ft, h = 90 ft

Figure 25 provides an insight that secondary fracture conductivity and relative permeability play more important role in Scenario 2 since varying height does not result in dramatic change in load recovery computed at any given combination of secondary fracture conductivity and relative permeability profile.

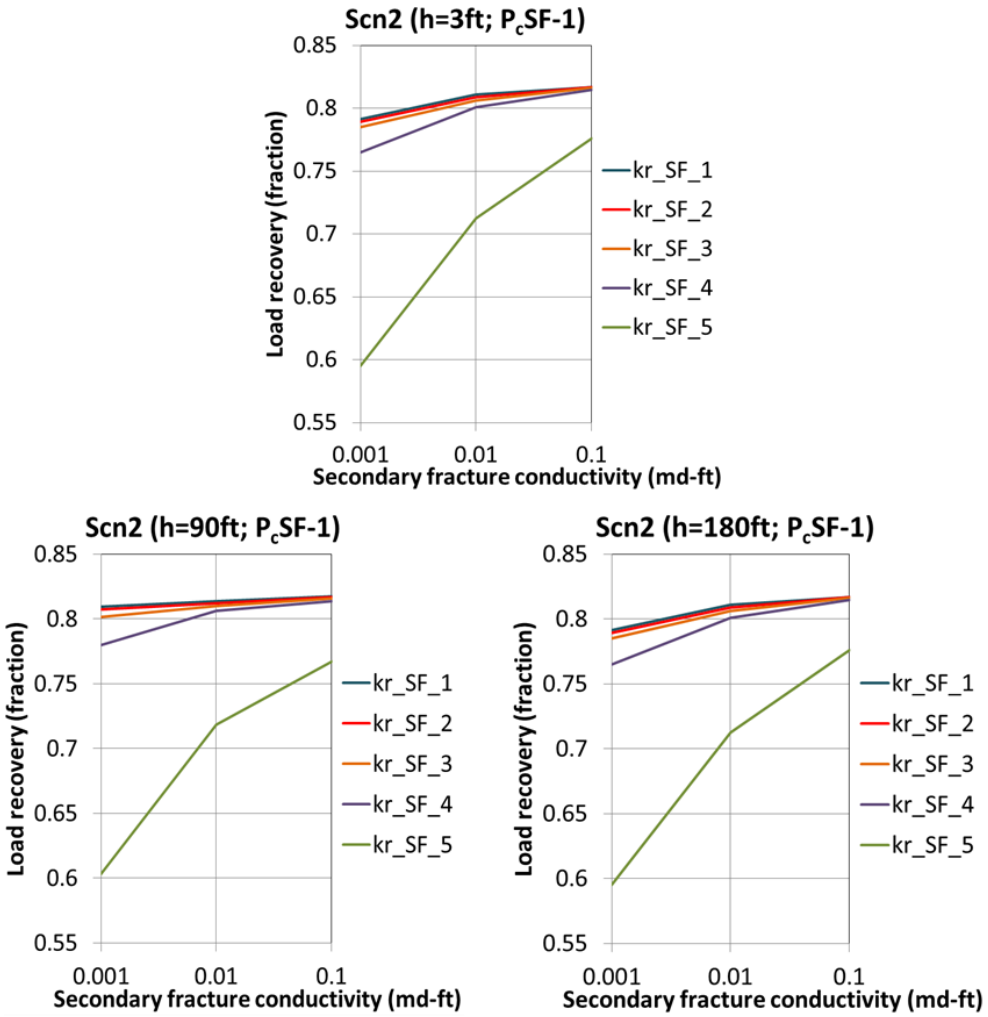

Figure 25. Impacts of secondary fracture properties on load recovery: Scenario 2, LR vs. F_c-SF sensing k_r-SF (Varying h, fixing p_c-SF1)

We applied the same strategy to investigate the impact of capillary pressure on load recovery in Scenario 2, as Figure 26 shows. Generally higher capillary pressure of secondary fracture, though decreases load recovery, doesn't influence flow back performance dramatically. This indicates that the conductivity of secondary fractures, even not as high as that of primary fracture, is sufficient to support fluid to overcome the capillary pressure in secondary fractures and flow back to wellbore.

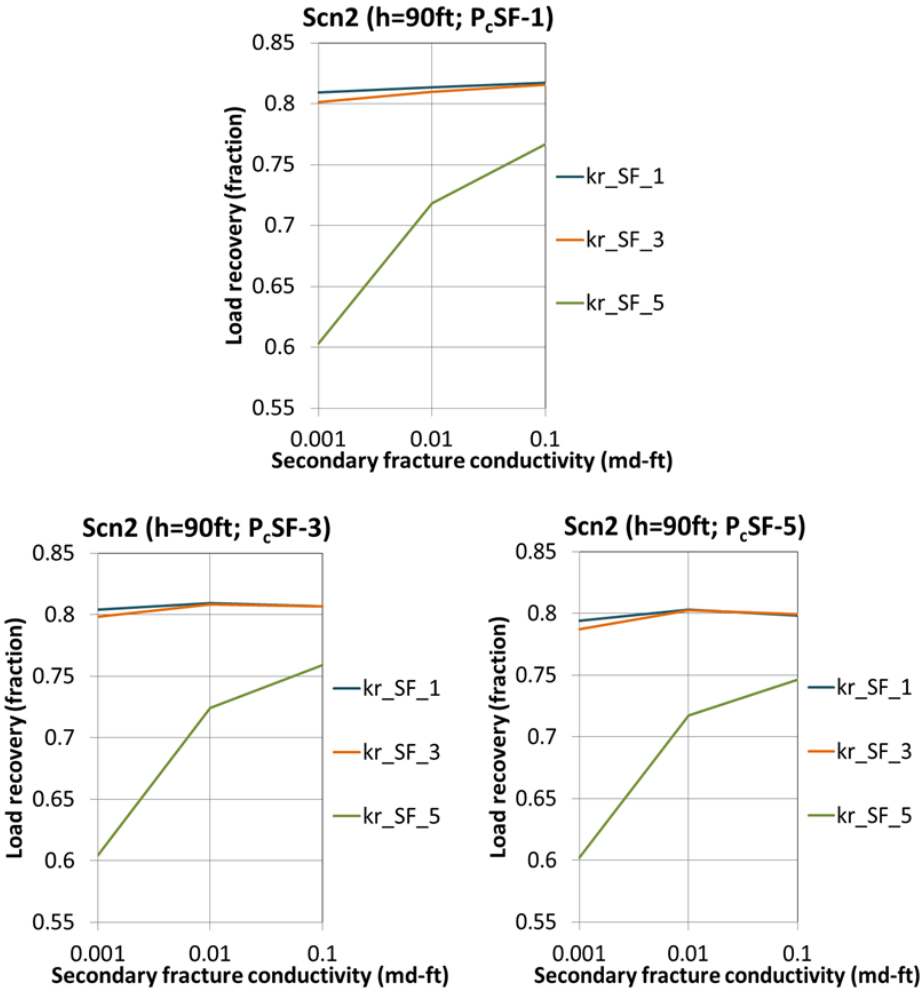

Figure 26. Impacts of secondary fracture properties on load recovery: Scenario 2, LR vs. F_c-SF sensing k_r-SF (Varying p_c-SF, fixing h=90 ft)

How the frequency (reciprocal of spacing) of secondary fracture affect load recovery depends on the total injected fluid volume in the secondary fractures. More exactly, it depends on the fraction of the injected fluid volume in secondary fracture to the total.

Two series of studies are carried out for this purpose. One is fixing the fraction of the injected fracturing fluid volume to the total injection volume and the other one is changing the ratio mentioned above.

As Figure 27 shows, if the total injected volume in secondary fracture is fixed as the spacing decreases the load recovery is lowered, but when the spacing is small enough it does not impact on load recovery much. If the total injected fluid volume is proportional to the frequency of secondary fracture the load recovery always decreases with the spacing.

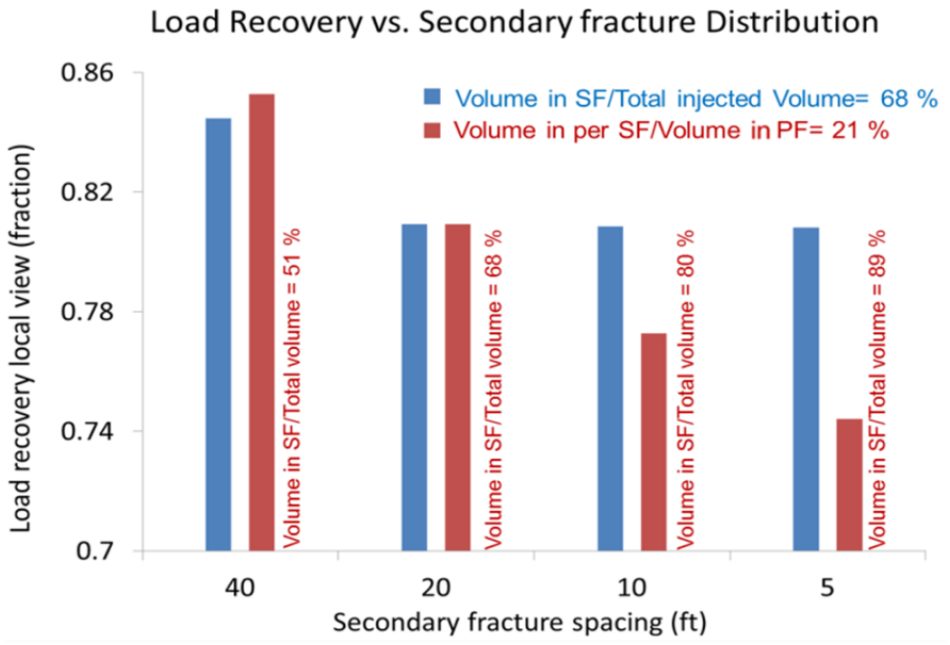

Figure 27. Impacts of secondary fracture properties on load recovery: Scenario 2, LR vs. Secondary fracture spacing

Based on the study on Scenario 2, we understand the following points:

- The occurrence of secondary fractures will lower the load recovery level of the whole system compared to the system with only a primary fracture. The more fraction of total injected volume is distributed in secondary fracture, the lower load recovery will be. This is mainly due to much lower flow capacity of the secondary fracture than primary fracture.
- Relative permeability and conductivity of secondary fracture play more dominating role of impacting flowback than capillary pressure. Even when the conductivity of secondary fractures is relatively lower, it is still sufficient to support the fluid to overcome the capillary pressure and flow back.

- The combined effect of low conductivity and low relative permeability of secondary fracture is the key of low load recovery of the primary + secondary fracture system according to field load recovery observation.
- Liquid loading does not seem to happen in secondary fractures. The height impact the load recovery of Scenario 2 through accelerating or slowing the gas blocking effect in the fracture system, but this effect is negligible for realistic height range.

3.3.3 Scenario 3: Primary Fracture and Invasion Zone

Figure 28 shows the 3D illustration of the model for Scenario 3, in which an invasion zone is surrounding the primary fracture face. In the base model of Scenario 3 the primary fracture takes 90% of the total injection volume while only 10% invades into the shale matrix. The invasion depth is 1 ft. For comparison purpose the base model of Scenario 3 applies the primary fracture properties in the based model of Scenario 1.

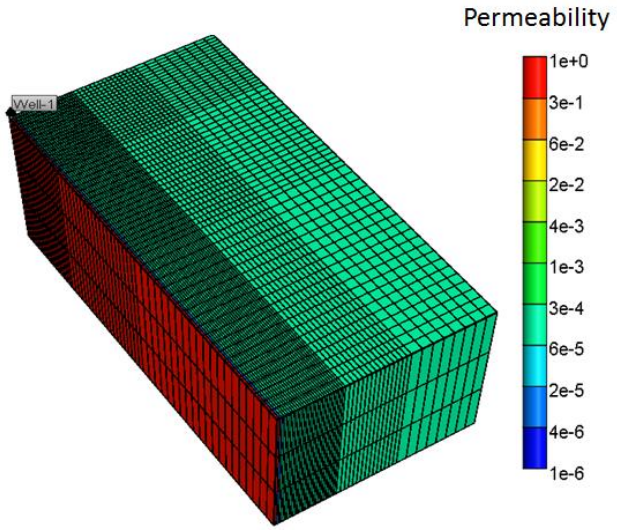

Figure 28. 3D numerical simulation model of Scenario 3

As Figure 29 and Figure 30 show, when the capillary pressure of invasion zone is low, permeability of invasion zone, relative permeability or height does not impact load recovery obviously.

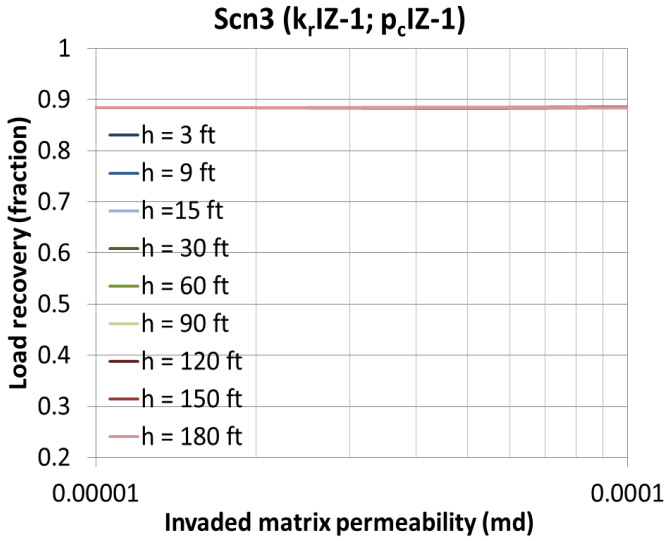

Figure 29. Impacts of invasion zone properties on load recovery: Scenario 3, LR vs. k-IZ sensing h (Fixing k_r-IZ1, p_c-IZ1)

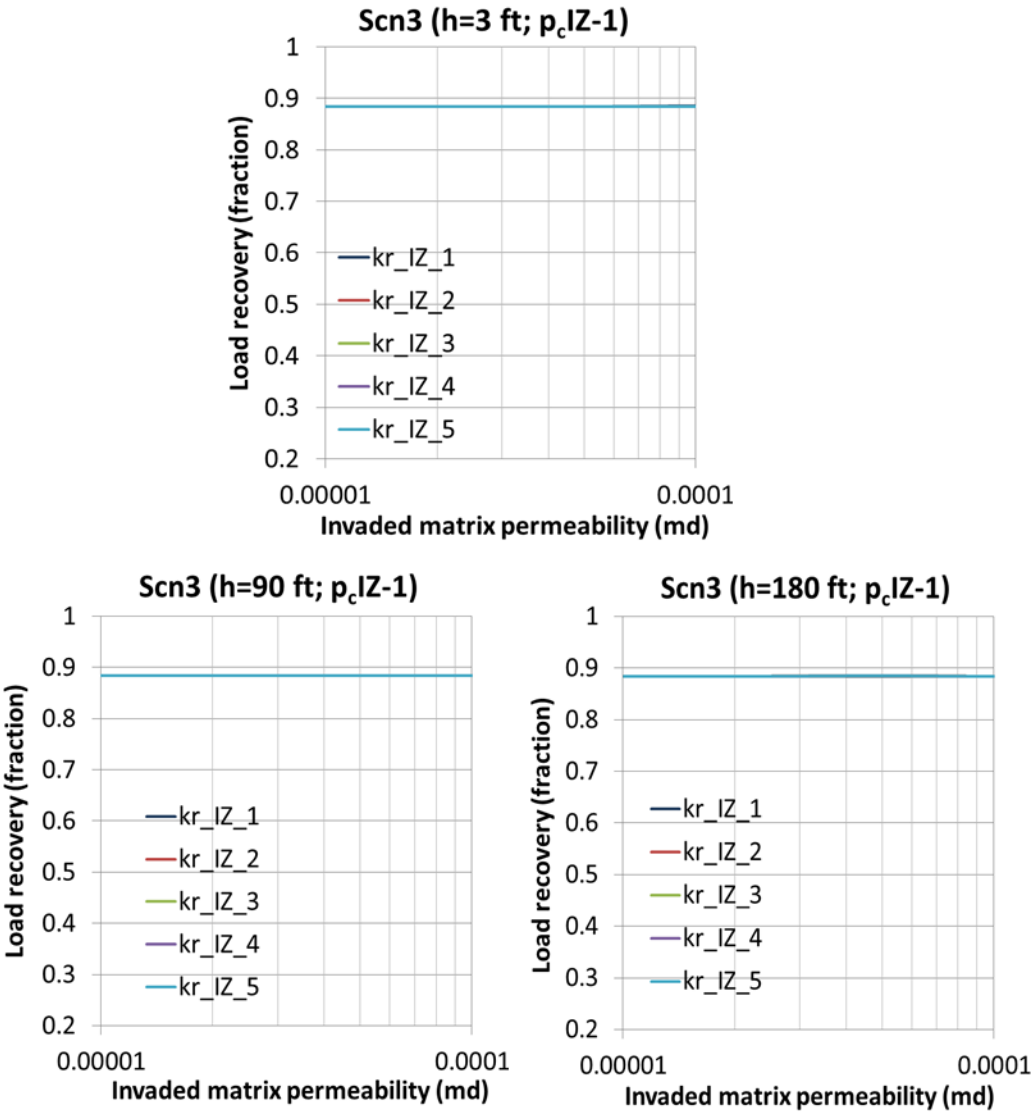

Figure 30. Impacts of invasion zone properties on load recovery: Scenario 3, LR vs. k_r-IZ sensing k-IZ (Varying h, fixing p_c-IZ1)

To interpret the observation, we examined the water production profile of a case in Scenario 3, and the key inputs are listed in Table 7. The rationale of this selection includes two aspects: first, we want to eliminate any potential of injected fracturing fluid retention in primary fracture space due to the properties of primary fracture, therefore we

applied the inputs of base model in Scenario 1; second, since we want to validate whether any of the properties of invasion zone may impact load recovery so we use extreme value of all the properties, including the minimum permeability of invasion zone, the lowest relative permeability and largest height. We do not consider capillary pressure here because we haven't studied the impact of invasion zone capillary pressure at this time.

Table 7. Key inputs of the models in Scenario 1 and Scenario 3 for comparison

Primary fracture	Value	Unit	Note
Conductivity	1	md-ft	Base model
Height	180	ft	Max. value
Relative permeability	k_r-PF1		Base model
Invasion zone	Value	Unit	Note
Permeability	1.00E-05	md-ft	Min. value
Height	180	ft	Max. value
Relative permeability	k_r-IZ5		Min. value
Capillary pressure	p_c-IZ1		Min. value

Figure 31 compares the cumulative water production profile between the case of Scenario 1 and the case of Scenario 3. Basically most of injected fluid in the primary fracture can be flowed back due to the high conductivity of primary fracture in both cases. However, the extra injection volume located in the invasion zone cannot be flowed back at all.

The strength of gas influx from invasion zone into the fracture space in the case of Scenario 3 is weaker than that in the case of Scenario 1 because the reduction in matrix permeability, and this will slow down the flowback of injected fracturing fluid from primary fracture because less gas inflow induces smaller gas expansion volume for

displacing the injected fracturing fluid. However, the long term cumulative water production volume is almost the same in the two cases. This indicates that the invasion zone just delays the flowback from the primary fracture but does not affect the load recovery because primary fracture conductivity is sufficiently high to provide enough draining force to clean up primary fracture space.

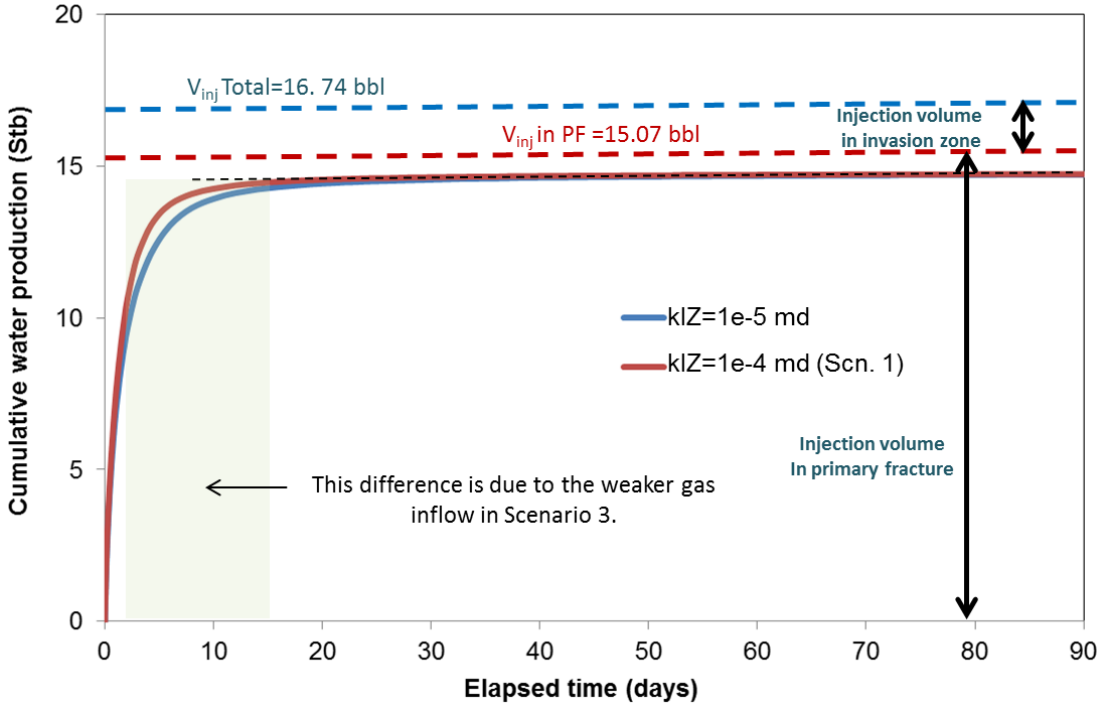

Figure 31. Cumulative water production comparison: Scenario 1 vs. Scenario 3, h = 180 ft, F_c-PF = 1 md-ft, k_r-PF1, kIZ=1e-5 md, k_r-IZ5, p_c-IZ1

Figure 32 and Figure 33 show the impact of the capillary pressure of the invasion zone on the load recovery of Scenario 3 system. As we figured out before, without capillary pressure all properties of invasion zone don't affect load recovery. However, with high capillary pressure, the impacts of height (as Figure 32) and invasion zone

permeability (as Figure 33) induce very obvious effect on load recovery while relative permeability of invasion zone does not. Larger height and higher invasion zone permeability yield reduction in load recovery according to the observation.

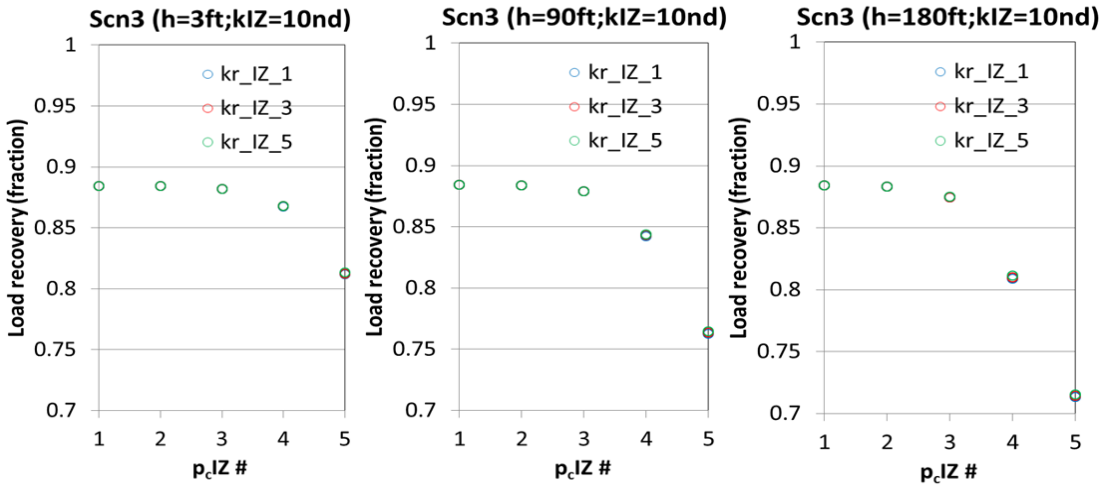

Figure 32. Impacts of invasion zone properties in Scenario 3 on load recovery study: LR vs. k_r-IZ sensing p_c-IZ (Varying h, fixing kIZ=1e-5 md)

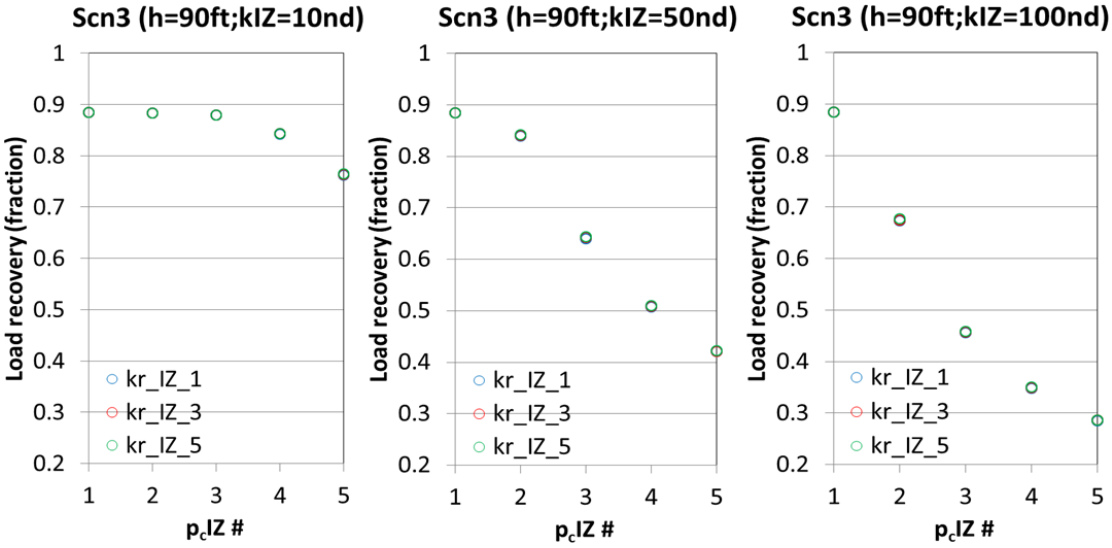

Figure 33. Impacts of invasion zone properties in Scenario 3 on load recovery study: LR vs. k_r-IZ sensing p_c-IZ (Varying k_{IZ}, fixing h=90 ft)

Capillary pressure is both the resistance for the water in the invasion zone to be drained out to the primary fracture space and the imbibing force to the injected fracturing fluid from the primary fracturing space into the matrix. With high capillary pressure, it is more difficult for gas to flow and displace the injected fracturing fluid which has invaded into the shale matrix, but it does not draw much attention because even without high capillary pressure the injected fracturing fluid located in the invasion zone can hardly be flowed back due to the extremely low permeability. However, it is possible that the injected fracturing fluid in primary fracture is imbibed into the matrix if the pressure difference for the injected fracturing fluid to flowback to the well cannot overcome the high capillary pressure. Figure 34 shows the comparison on cumulative production profile between high invasion zone capillary pressure and no invasion zone capillary pressure cases. The total injection volume is about 8.37 bbl. Without capillary pressure the flowed back volume is 7.40 bbl, which is about 88% of the total injection volume and 98% of the injection volume in primary fracture. While with high capillary pressure profile the flowed back volume is only 28.5% of the total injection volume and 31.6% of the injection volume in primary fracture.

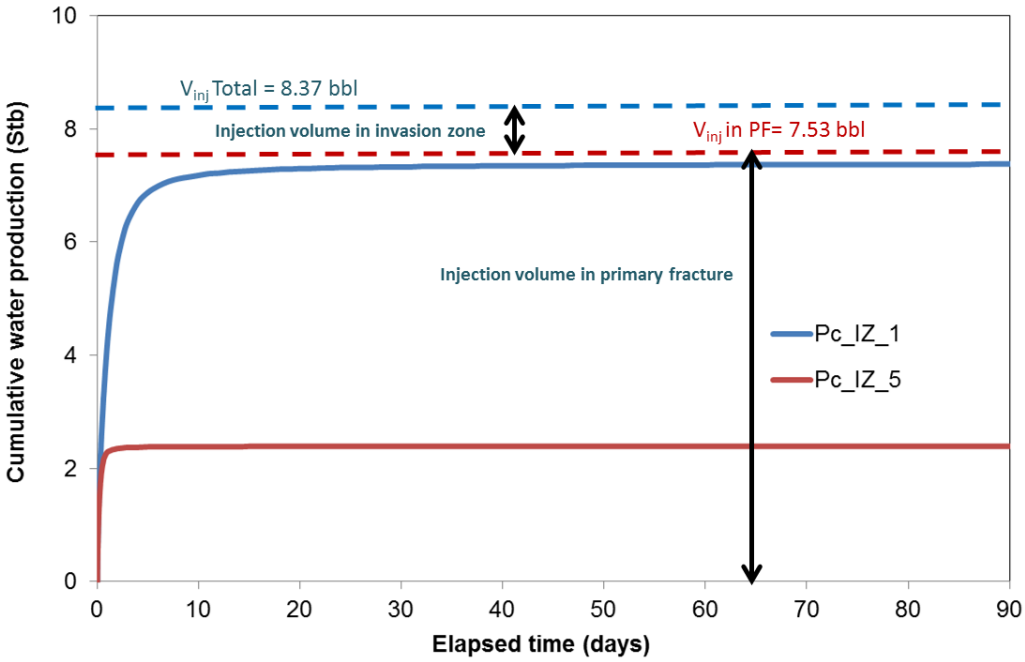

Figure 34. Cumulative water production comparison: Scenario 3, h = 90 ft, k_{IZ}=1e-4 md, k_r-IZ-1, p_c-IZ-1 vs. p_c-IZ-5

A more detailed examination on the water saturation profile sheds light on the final location of the unrecovered injected fracturing fluid. Figure 35 compares the water saturation distribution in both primary fracture space and in the invasion zone between the case of high capillary pressure in invasion zone and the case of no capillary pressure in invasion zone. According to Figure 35 in both cases the water saturation in primary fracture is almost down to 0 and that means no retained injected fracturing fluid is in primary fracture space after a period of flowback. While in the invasion zone, the case of no capillary pressure shows the water saturation in invasion zone is round 0.25, which is the irreducible water saturation set in the relative permeability profile for invasion zone In the case of high capillary pressure the water saturation in the invasion zone is obviously higher, around 0.28. Since the initial water saturation of the invasion zone is

only 0.253 and that of un-invaded matrix is set as 0.25 which is the irreducible water saturation, this increment is sourced from liquid in the primary fracture. Therefore, the capillary pressure in invasion zone is imbibing the liquid in the primary fracture.

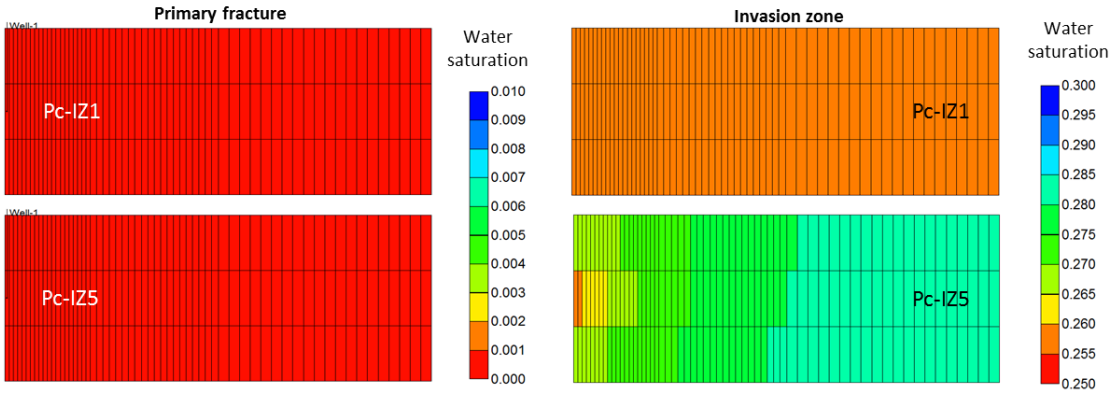

Figure 35. Water saturation distribution comparison: Scenario 3, k_{IZ} = 1e-4 md, h = 90 ft, k_r-IZ-1, p_c-IZ-5 vs. p_c-IZ-1

Larger height induces more injected fracturing fluid retention when the capillary pressure of the invasion zone is high. Larger height may yield the liquid loading effect. However, in all Scenario 3 cases the primary fracture properties are set to provide the highest cleaning up efficiency therefore liquid loading is unlikely to appear in primary fracture. The flow velocity in the primary fracture is rational to the effective pressure gradient which is calculated by subtracting gravity and capillary pressure form the difference between local pressure and well flowing pressure at a certain time. Therefore larger height allows longer time for imbibition to play its role.

Figure 36 compares the water saturation distribution in primary fracture and invasion zone after 1 day flowing between the cases of large and small heights. Though

it is hard to evaluate the difference in the decrement in average water saturation of primary fracture between the two cases, the comparison on the water saturation in the invasion zone displays a general larger increment in water saturation in the case of large height.

Figure 37 shows the same comparison as Figure 36, but it is after 15 years flow. The primary fracture has been almost cleaned up but the obvious water saturation difference between the two cases of different height clearly illustrates the effect of the high capillary pressure. Another feature of this retention is that more retained injected fluid is accumulated at the location which is far from the wellbore along the fracture direction and the lower the position is the more injected fracturing fluid is retained.

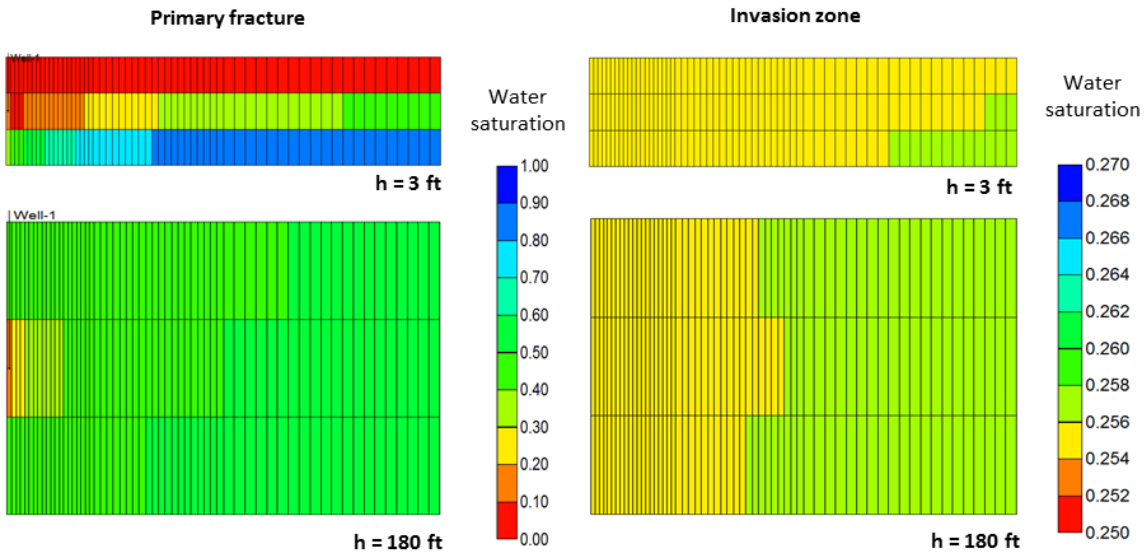

Figure 36. Water saturation distribution comparison after 1 day flowing: Scenario 3, k_{IZ} = 1e-5 md, k_r-IZ-1, p_c-IZ-5, h = 3 ft vs. h = 180 ft

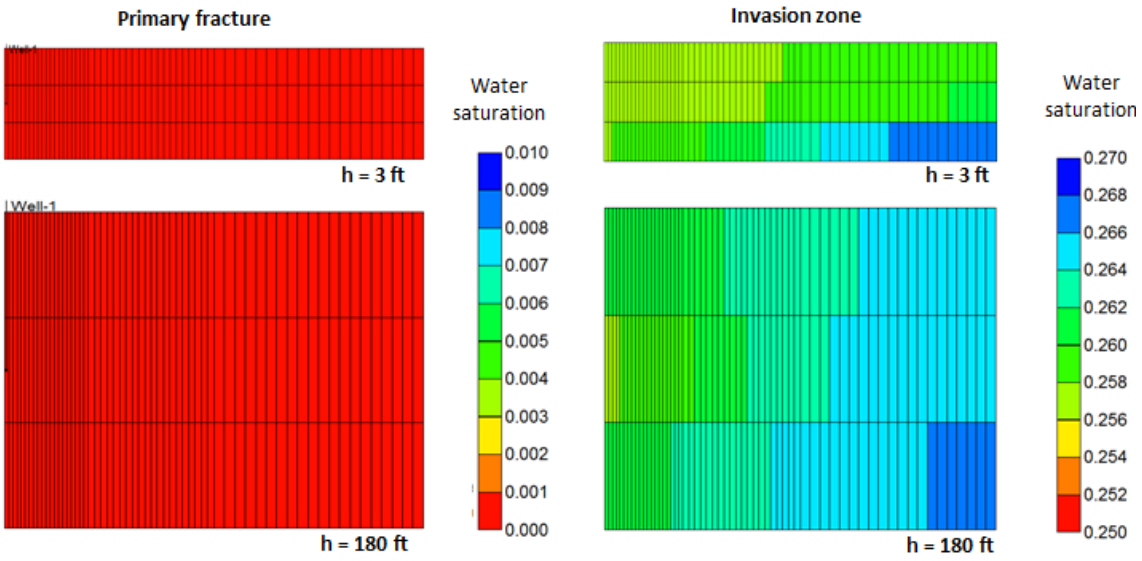

Figure 37. Water saturation distribution comparison after 15 years flowing: Scenario 3, k_{IZ} = 1e-5 md, k_r-IZ-1, p_c-IZ-5, h = 3 ft vs. h = 180 ft

Less permeability damage in the invasion zone yields more injected fracturing fluid retention. As we discovered before without capillary pressure in the invasion zone the flowback of the injected fracturing fluid from primary fracture is not affected by the permeability of the invasion zone very much. That means gas inflow into the primary fracture, whose strength depends on the invasion zone permeability a lot, does not contribute much to cleaning up the injected fracturing fluid in primary fracture. However, larger invasion permeability induces a smaller pressure gradient as Figure 38 illustrates. Therefore it is more difficult to overcome the capillary pressure so that more imbibition is likely to occur.

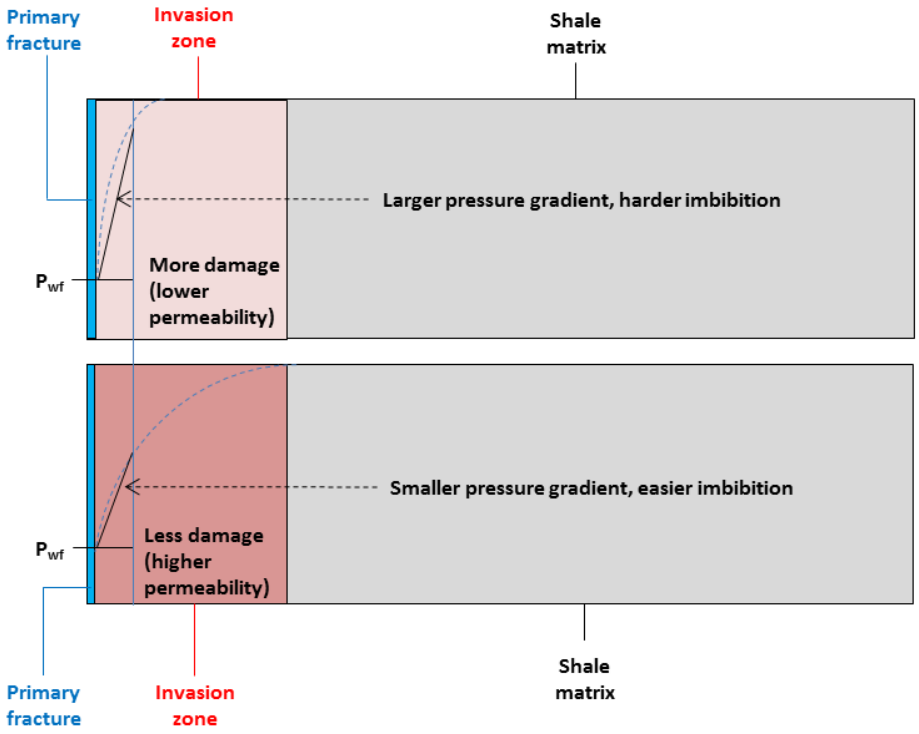

Figure 38. Illustration of that higher invasion zone permeability induces more imbibition from primary fracture into matrix by capillary pressure in Scenario 3

Figure 39 shows the comparison on the pressure profile in the direction normal to the primary fracture face between the case of no permeability damage in the invasion zone (100 nd) and the case of serious permeability damage in the invasion zone (10 md). After 1 day flow, the pressure disturbance penetrates more deeply since the permeability of the invasion zone is higher in the case of no permeability damage, so the current pressure in invasion zone is lower. Figure 40 compares the water saturation distribution in primary fracture and invasion zone after 1 day flowing between the cases of large damage and small damage to invasion zone permeability.

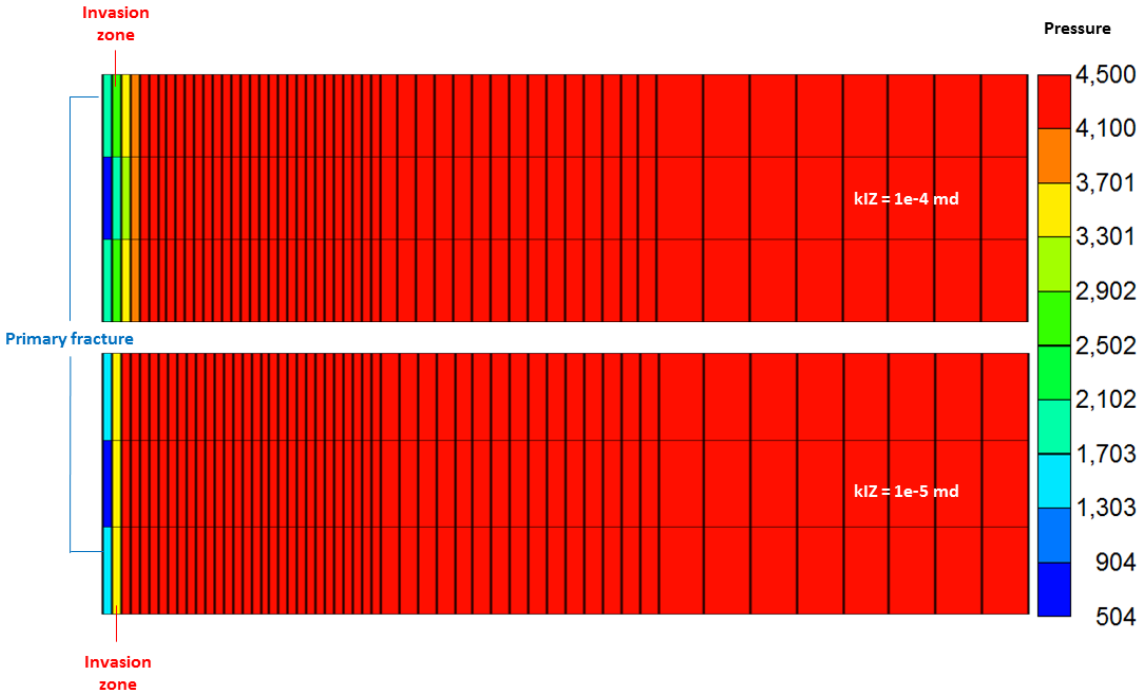

Figure 39. Pressure profile normal to primary fracture face comparison after 1 day flow: Scenario 3, k_{IZ}=1e-4 md vs. k_{IZ}=1e-5 md

Figure 40 compares the water saturation distribution in primary fracture and invasion zone after 1 day flowing between the cases of large and small invasion zone permeability. In the case of high invasion zone permeability the primary fracture is quickly cleaned up because: the higher invasion zone permeability provides stronger gas inflow to displace the injected fracturing fluid in the primary fracture; more gas flow provides larger void pore space for capillary pressure to imbibe more injected fracturing fluid in the primary fracture into the matrix before the injected fracturing fluid is flowed back to the well by the flowing pressure gradient.

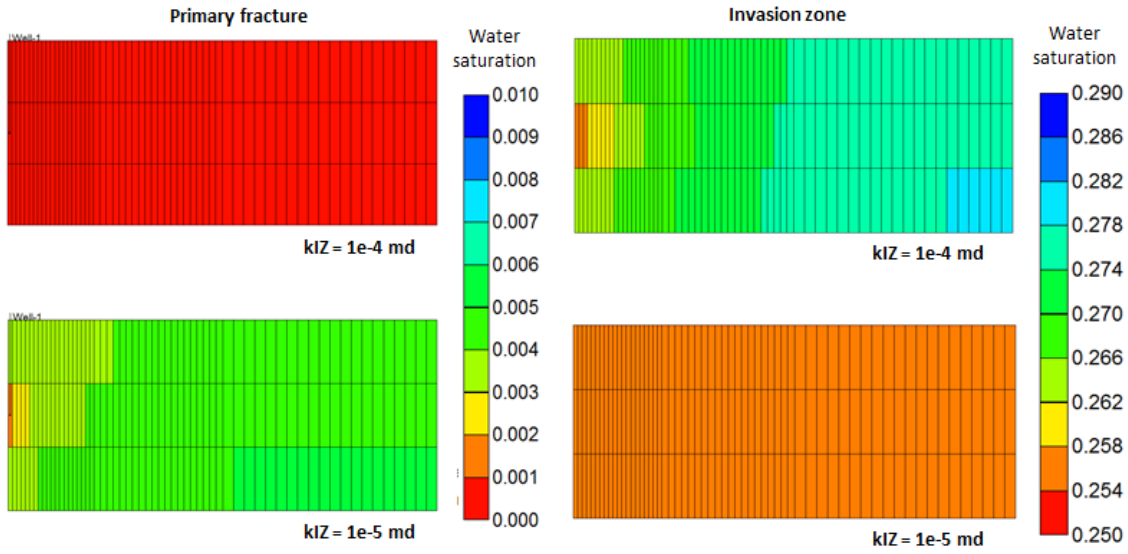

Figure 40. Water saturation distribution comparison after 1 day flowing: Scenario 3, h = 90 ft, k_r-IZ-1, p_c-IZ-5, k_{IZ} = 1e-4 md and k_{IZ} = 1e-5 md

Figure 41 compares the water saturation distribution in primary fracture and invasion zone after 15 years flowing between the cases of large and small invasion zone permeability. At that moment, primary fracture has been almost 100% cleaned up and the water saturation is significantly higher in the case of high invasion zone permeability.

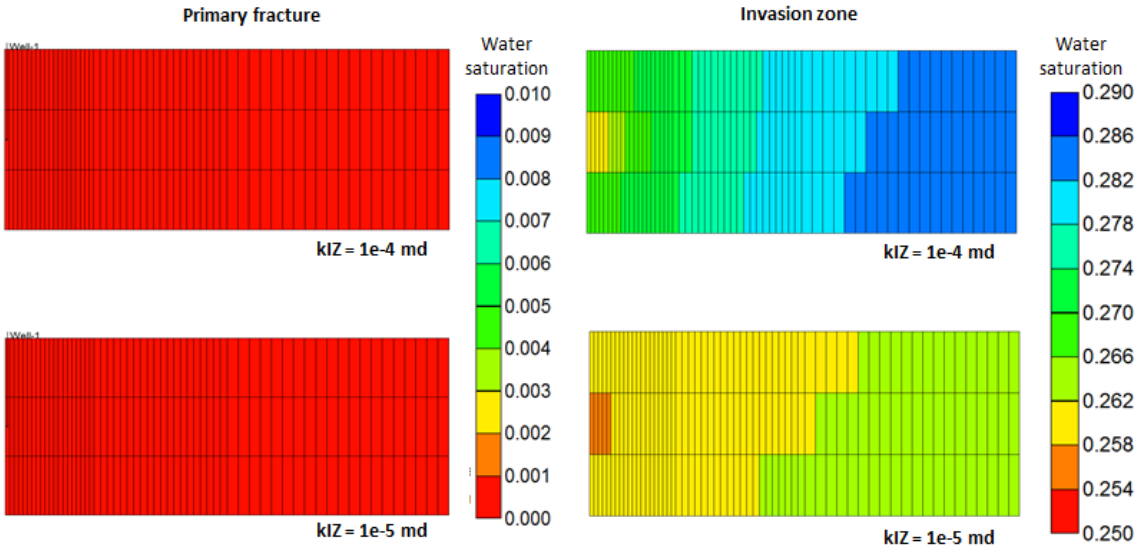

Figure 41. Water saturation distribution comparison after 15 years flowing: Scenario 3, h = 90 ft, k_r-IZ-1, p_c-IZ-5, k_{IZ} = 1e-4 md and k_{IZ} = 1e-5 md

Based on the study on Scenario 3, we understand the following points:

- Capillary pressure of the invasion zone is much more dominating than any other properties of invasion zone in Scenario 3.
- When invasion zone capillary pressure is low, permeability of invasion zone，relative permeability of invasion zone or height will not affect the load recovery because high conductivity primary fracture can flow most of the injected fluid in the fracture space.
- When invasion zone capillary pressure is high, larger height and higher invasion zone permeability result in reduction in load recovery: the former is mainly because larger height allows more time for capillary pressure to induce imbibition; the latter is because the higher permeability induces smaller pressure

gradient so it is easy for capillary pressure to overcome it and result in imbibition.

- The load recovery in Scenario 3 is a linear function of the portion of injected fluid volume in invasion to the total. If the injection volume in invasion zone is fixed, how it is distributed doesn't matter to the load recovery. That basically indicates that the injected fluid in invasion zone cannot be flowed back.

3.3.4 Scenario 4: Primary Fracture, Secondary Fracture and Invasion Zone

Scenario 4 considers primary fracture, secondary fractures and invasion zone surrounding the whole fracture system, as Figure 42 illustrates.

In the study on this scenario, we separately investigated the impact of the properties of each medium on load recovery to see whether the properties are affecting injected fracturing fluid flowback in different ways from in the previous three scenarios.

Generally, the properties of primary fracture, secondary fracture and invasion zone affect the load recovery in Scenario 4 in the same way with that in the first three scenarios, as Figure 43, Figure 44 and Figure 45 indicate. The only difference is that the overall load recovery of Scenario 4 is lower than those of the other scenarios because compared to the first three scenarios there always be a portion of total injected fluid volume is stored in a medium or media which have relatively lower flow capacity for injected fluid, especially for the scenarios in which invasion zone is included.

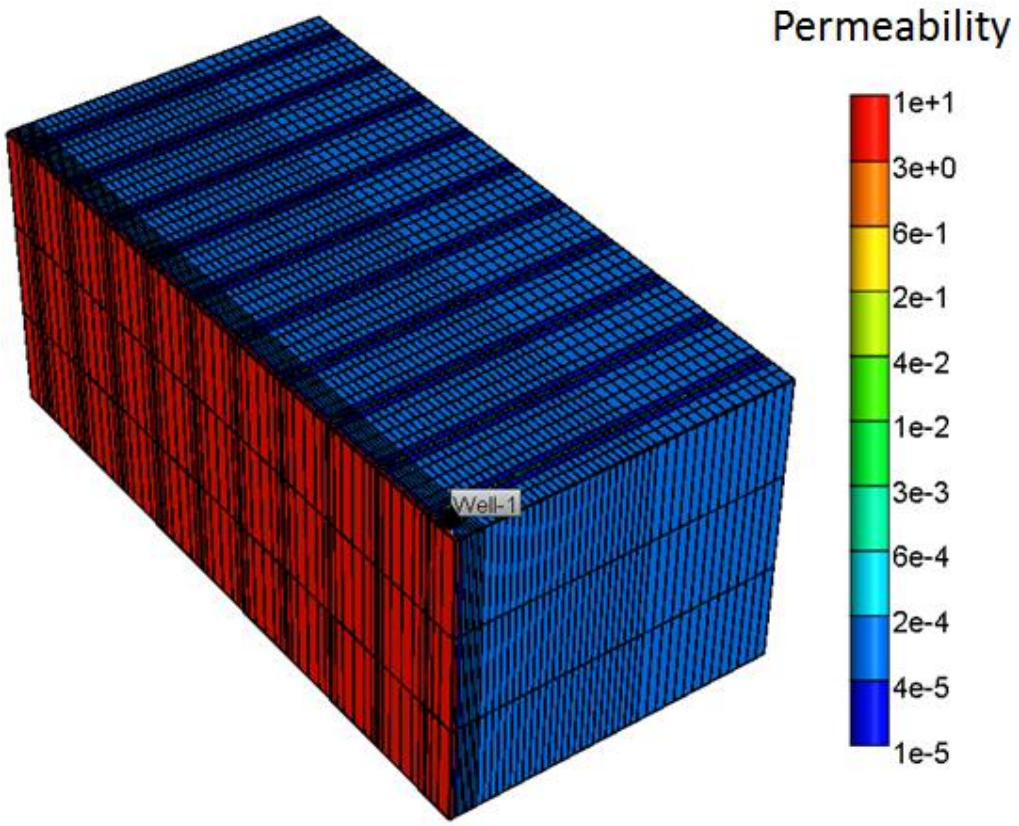

Figure 42. 3D numerical simulation model of Scenario 4

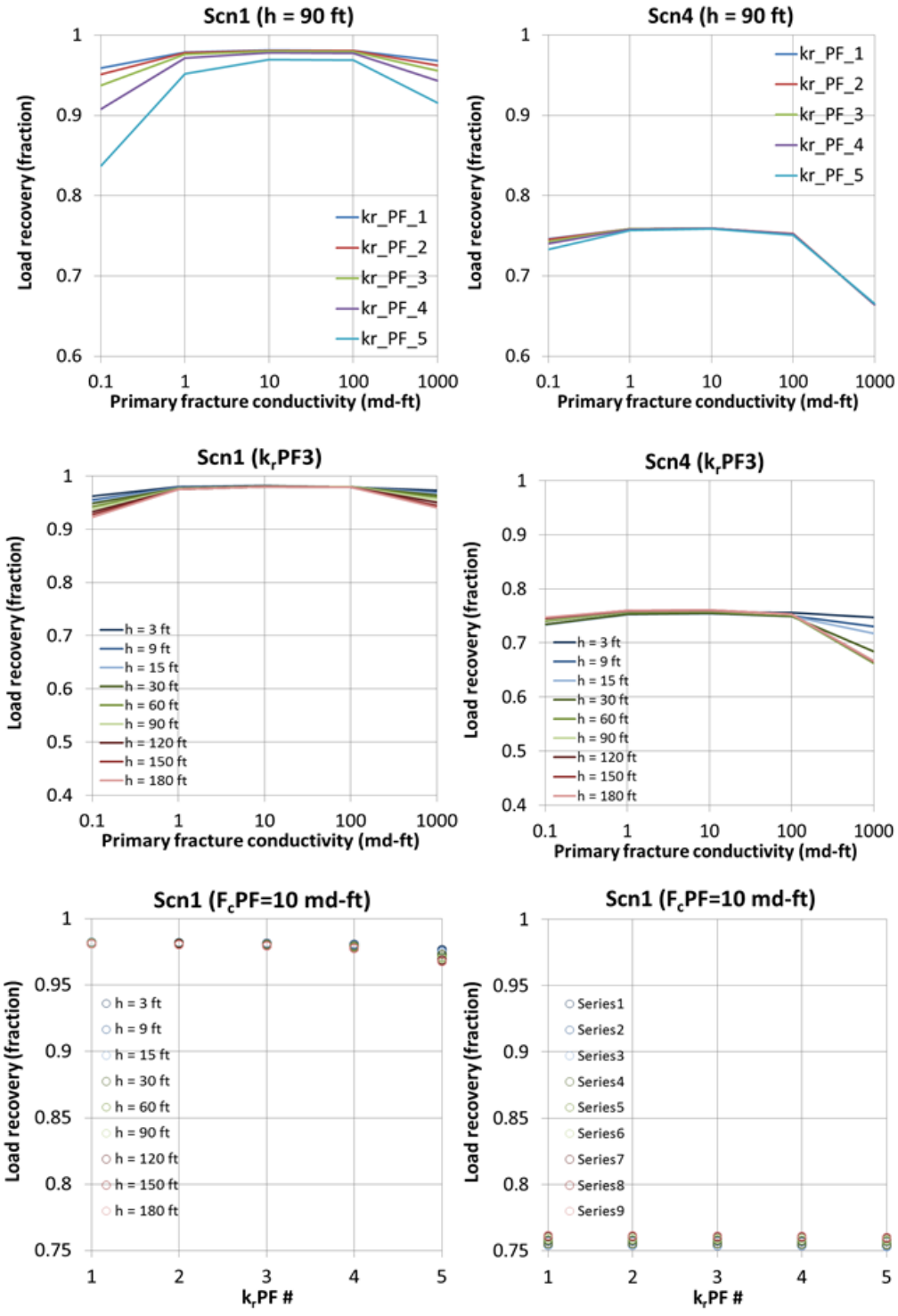

Figure 43. Primary fracture's impacts on load recovery comparison between Scenario 1 and Scenario 4

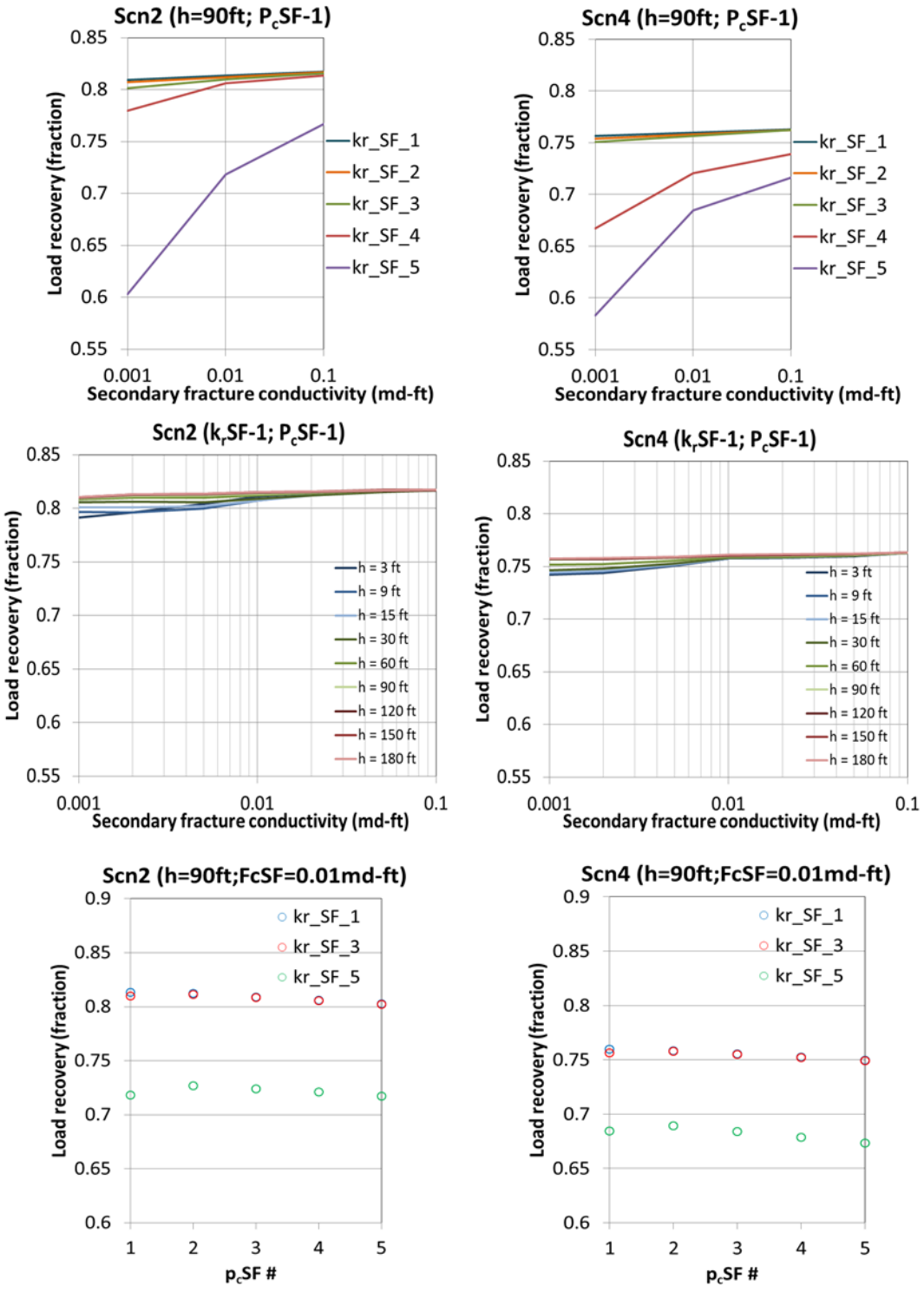

Figure 44. Secondary fracture's impacts on load recovery comparison between Scenario 2 and Scenario 4

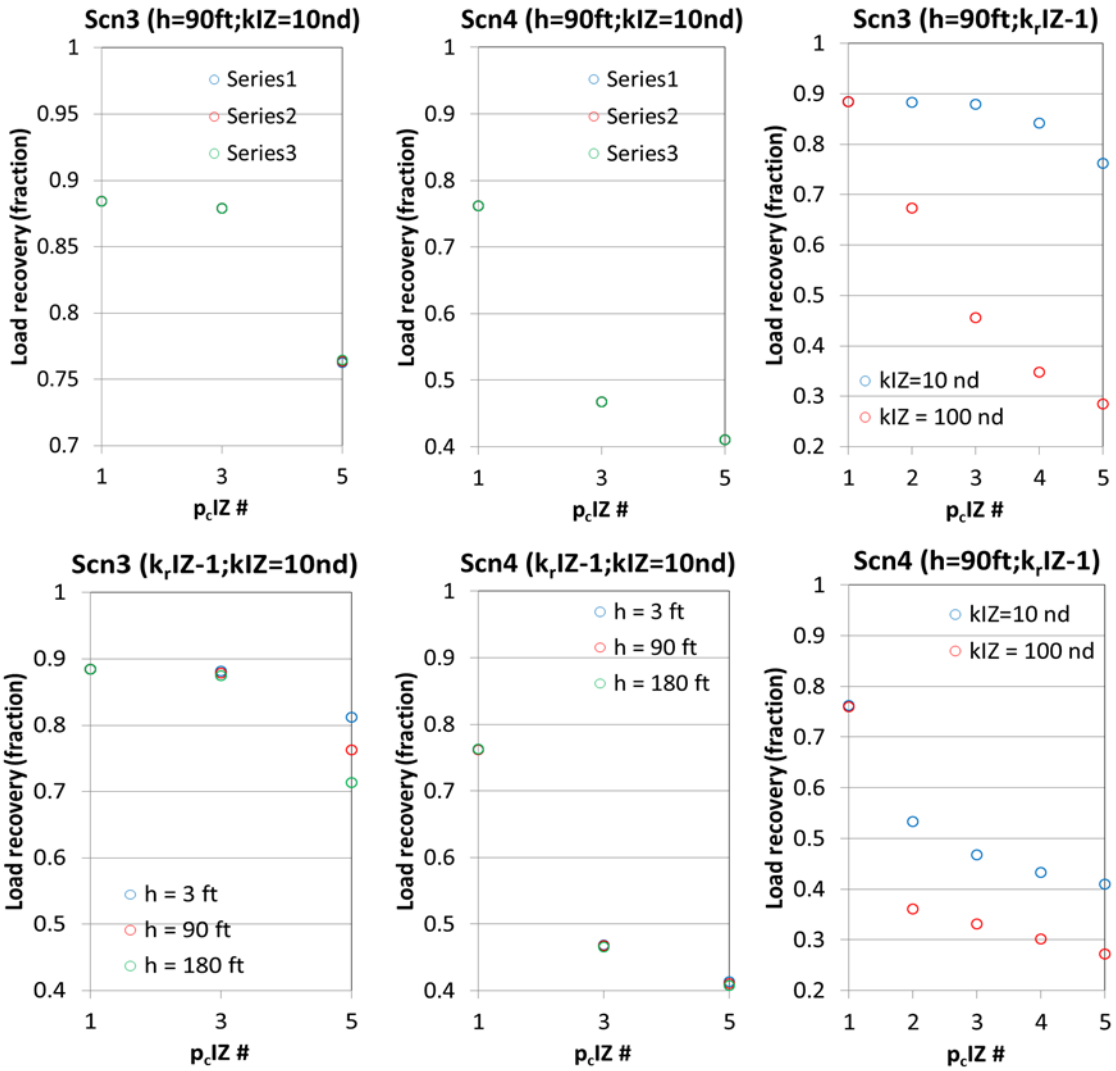

Figure 45. Invasion zone's impacts on load recovery comparison between Scenario 3 and Scenario 4

3.4 Evaluation of the Impacts of Factors on Load Recovery

Based on the studies of the properties in each medium for injected fluid storage in four scenarios we concluded the impact of each factor on load recovery in Table 8. It specifies how each factor impacts on load recovery and how the impact varies with other factors and evaluates the significance of each factor to flow back performance.

Table 8. Summary of the impacts of medium properties on load recovery

Scenario	1			2			3		
Location(s).	Primary fracture			Primary fracture + Secondary fracture			Primary fracture + Invaded zone		
medium	Primary fracture			Secondary fracture			Invaded zone		
Evaluation / Property	Impact format	impact intensification	Significance	Impact format	impact intensification	Significance	Impact format	impact intensification	Significance
Cond. (F_c)/Perm.(k)	Extreme F_c → LR ↓	lower k_r large h	Large	F_c ↓ → LR ↓	lower k_r smaller h	Large	k ↓ → LR ↑	high p_c	large
Rela. Perm. (k_r)	k_r ↓ → LR ↓	larger h extreme F_c	Large	k_r ↓ → LR ↓	lower F_c	Large	LR →	None	very small
Height (h)	h ↑ → LR ↓	lower kr; extreme F_c	Medium	h ↓ → LR ↓	lower F_c	small	h ↑ → LR ↓	high p_c	large
Capi. Pressure (P_c)	Not assumed			P_c ↑ → LR ↓	lower k_r lower F_c	small	P_c ↑ → LR ↓	Always	Very large
Scenario	4								
Location(s).	Primary fracture + Secondary fracture + Invaded zone								
medium	Primary fracture			Secondary fracture			Invaded zone		
Evaluation / Property	Impact format	impact intensification	Significance	Impact format	impact intensification	Significance	Impact format	impact intensification	Significance
Cond. (F_c)/Perm.(k)	Extreme F_c → LR ↓	lower k_r; large h	Large	F_c ↓ → LR ↓	lower k_r smaller h	Large	k ↓ → LR ↑	Larger p_c	large
Rela. Perm. (k_r)	k_r ↓ → LR ↓	extreme F_c	Small	k_r ↓ → LR ↓	lower F_c	Large	LR →	None	very small
Height (h)	h (small) ↑ → LR ↓ h (large) ↑ → LR ↗	extreme F_c	small to medium	h ↓ → LR ↓	lower F_c	small	h ↑ → LR ↓	high p_c	small
Capi. Pressure (P_c)	Not assumed			P_c ↑ → LR ↓	lower k_r lower F_c	small	P_c ↑ → LR ↓	Always	Large

Base on the studies we carried out above, we can conclude the following understanding of the impacts of the factors which affect flowback on the load recovery of injected fracturing fluid in shale gas wells.

- The key mechanism controlling flowback is a competition between gas and liquid flow. Essentially, the load recovery is determined by how much water can be flowed back before the gas saturation is high enough to induce gas blocking.
- Generally, conductivity and relative permeability are the dominating fracture properties to flowback while capillary pressure is the dominating matrix property affecting load recovery.

- Liquid loading should be only considered in primary fracture but not in other media.
- The observed low load recovery might be induced by the combination of low conductivity and low relative permeability of fracture system and high capiillary pressure of the invaded matrix.

In this chapter we studied the mechanisms of injected fracturing fluid retention through simulation modeling. For each storage medium we indicated the corresponding dominant retention mechanism and evaluated how the storage medium properties induce injected fracturing fluid retention and their impacts on load recovery. The simulation models constructed in this chapter are also applicable for the study on the mechaisms and characteristics of flowback.

CHAPTER IV

MECHANISMS AND CHARACTERISTICS OF FLOWBACK

The four flowback model scenarios provide a basis for study of flowback mechanisms and characteristics. In this chapter we create a new Water/Gas two-phase flow simulation model integrating both displacement and vaporization mechanisms and considering the scenarios we built up in the previous chapter. We focus on simulation of Scenarios 1 and 2 defined in the previous chapter to investigate and analyze which flowback mechanisms control the flowback dynamics and what behavior characterize them.

4.1 Mechanisms Controlling Injected Fracturing Fluid Flowback

As Mahadevan et al (2007) indicated the flowback of injected fluid in gas wells can be divided into "displacement" and "vaporization" regimes in sequence. The displacement is commonly comprehended as the process of gas expansion compelling injected fracturing fluid to flow. Vaporization means the solution of water in gas, and that basically indicates that gas flow can carry some vapor in gaseous phase when it flows to the well. As pressure decreases gas becomes more under-saturated so more water can be "vaporized" in the gas.

Some researchers studied the flowback mechanisms of displacement from the perspectives of both modeling and statistics. Clarkson (2012) modeled the early flowback data as displacement behavior and used the model match, seen as a 1/2 slope

trend of GWR vs. Cumulative gas production plot on Log-Log coordinate in Figure 46, to estimate the fracture half-length. Ilk et al (2010) also observed a ½ slope trend in several production long term data sets from shale gas wells, as seen in Figure 47, but he did not provide a model for the behavior.

Zhang (2013) observed -1/2 slope trend of GWR vs. Cumulative gas production plot on log-log coordinate from both Horn River Shale and Barnett gas (Figure 48). Considering the work Mahadevan et al (2007), she hypothesized that the -1/2 slope represented displacement; and that the -1 slope trend following -1/2 slope trend observed from Horn River shale gas wells could represent vaporization.

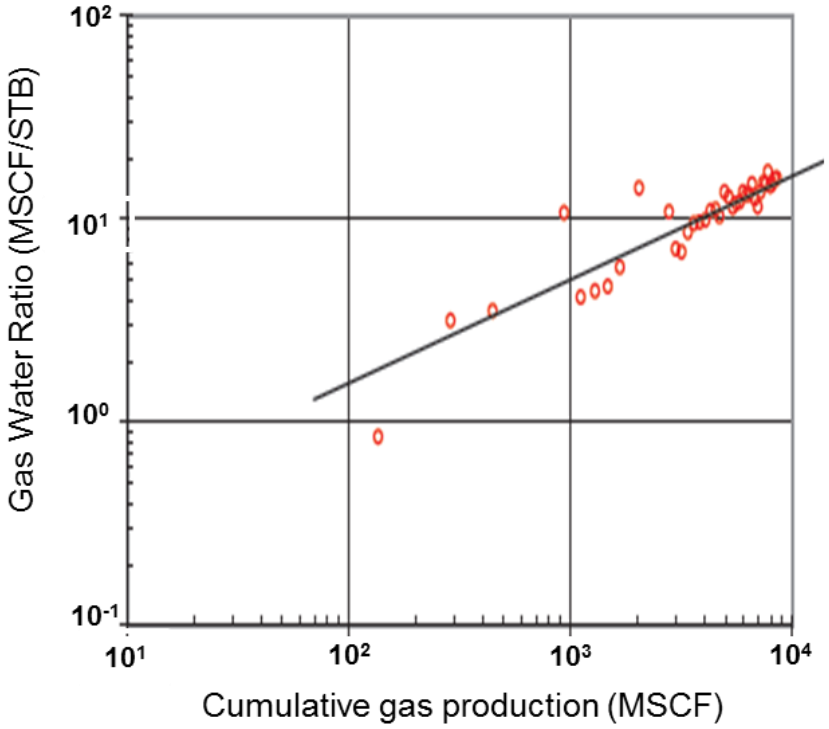

Figure 46. Gas-water ratio vs. Cumulative gas production plot (Clarkson 2012)

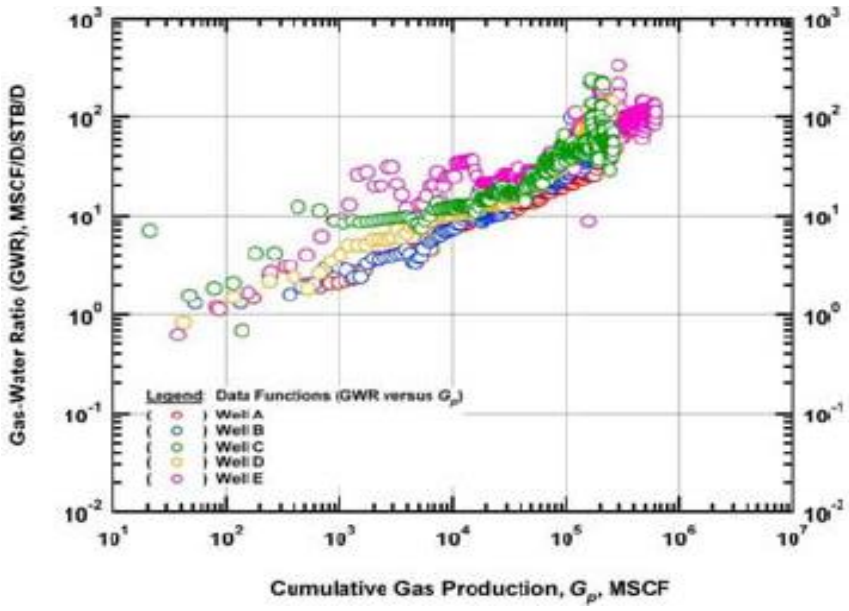

Figure 47. Gas-water ratio vs. Cumulative gas production plot for shale gas wells (Ilk et al. 2010)

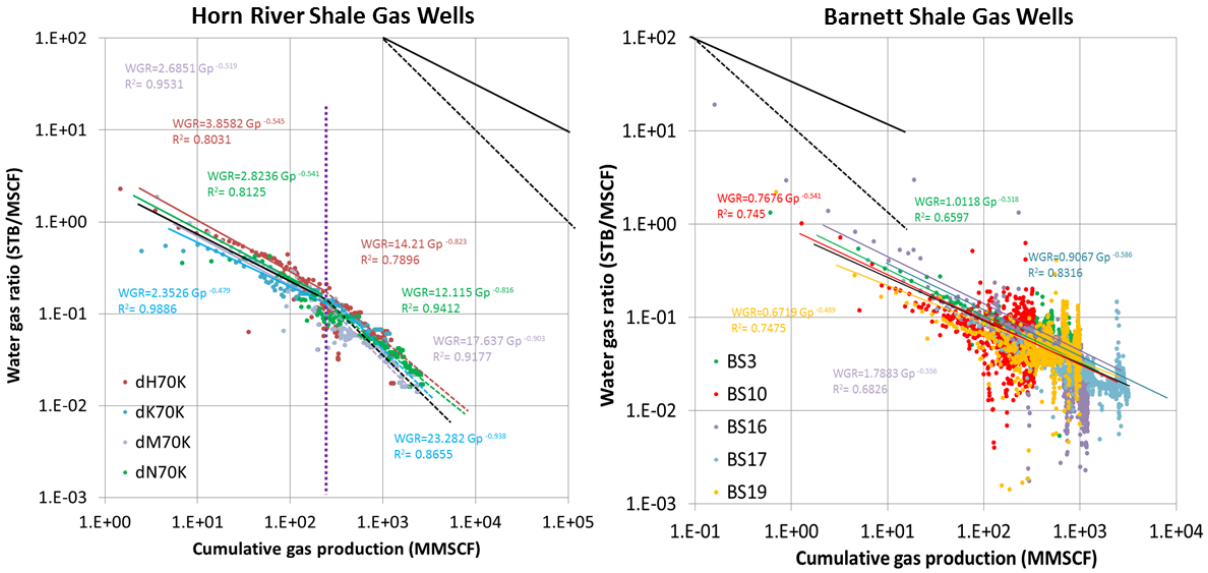

Figure 48. Gas-water ratio vs. Cumulative gas production plot for Horn River and Barnett shale gas wells (Adopted from Zhang 2013)

4.2 Flowback Behavior Study Using CMG Simulation

As a starting point, we use the commercial simulator CMG to study characteristic flowback behavior. As in previous chapters, Scenarios 1 and 2 are modeled, with production to a propped hydraulic fracture, in Scenario 1 from a homogeneous shale matrix, and in Scenario 2 from unpropped secondary fractures in the shale matrix. Figure 49 shows the diagnostic plots of flowback (Water gas ratio vs. Cumulative gas production on Log-Log plot) for Scenario 1 and Scenario 2. Because CMG does not include water vaporization in gas, these models cannot characterize this behavior.

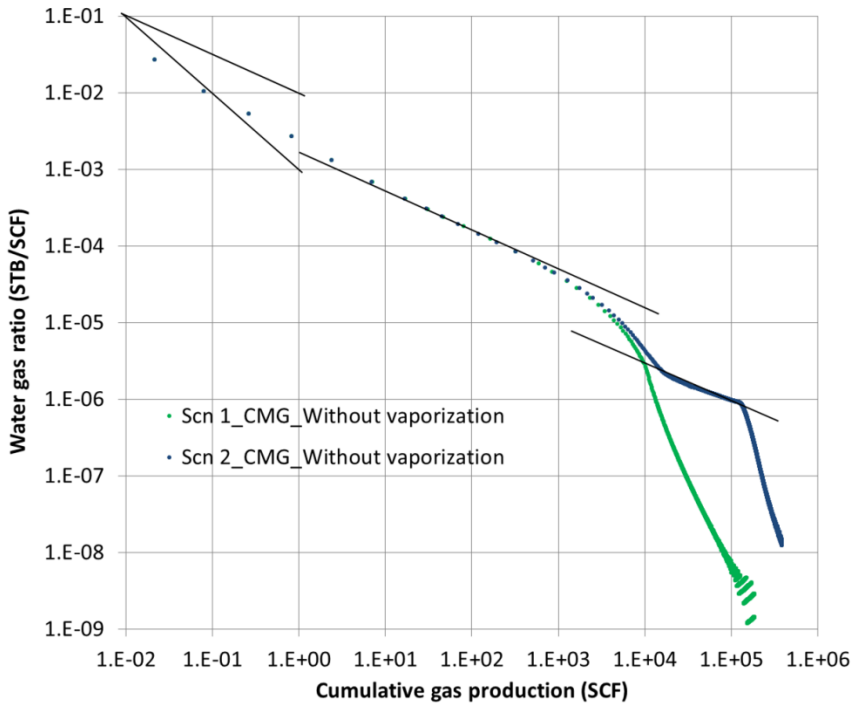

Figure 49. Flowback characteristic diagnostic plot: Water-gas ratio vs. Cumulative gas production for two scenarios

From the diagnostic plots -1/2 slope trend is displayed, followed by a sharply downward dipping trend. As seen in Figure 49, there is a -1/2 slope trend that can only represent the displacement mechanism. The steep downward trend occurs as the existing water is depleted down to the immobile water saturation.

To couple the vaporization mechanism into the flowback model, we first devise an empirical relationship based on the measured behavior of vaporized water mole fraction in total gaseous phase fluid versus pressure found from literature (Sage and Lacey, 1955; Rushing et al 2008; Donson and Standing, 1944; Epaminondas C. Voutsas et al., 2000). Figure 50 shows the vaporization behavior.

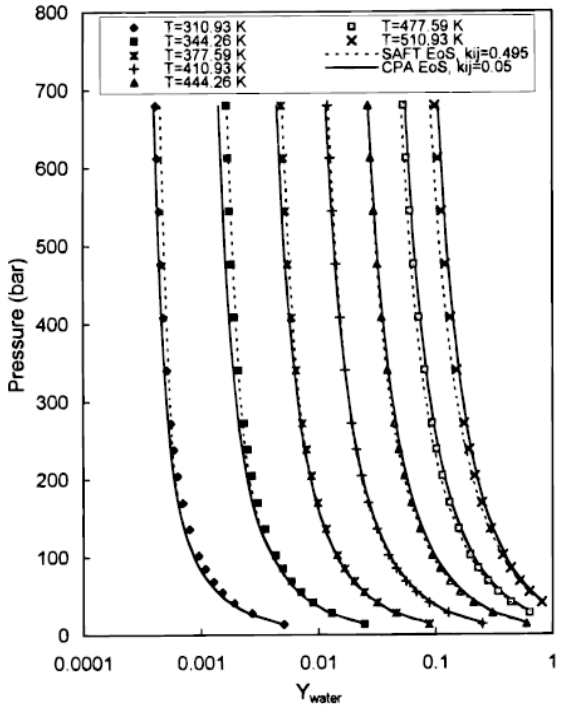

Figure 50: Laboratory measurements of water vapor content from Sage and Lacey compared to CPA and SAFT correlations (Epaminondas C. Voutsas et al., 2000)

The laboratory experiments concluded the equation format as:

$$y_w = ap^b \tag{2}$$

Where a and b are empirically regressed coefficients depending on fluid composites and temperature. For pure methane gas at temperature of 344 K (160 degree Fahrenheit), a fit with laboratory data shown in Figure 51 yields a = 0.6126 and b = -0.67 for the pressure unit of psi.

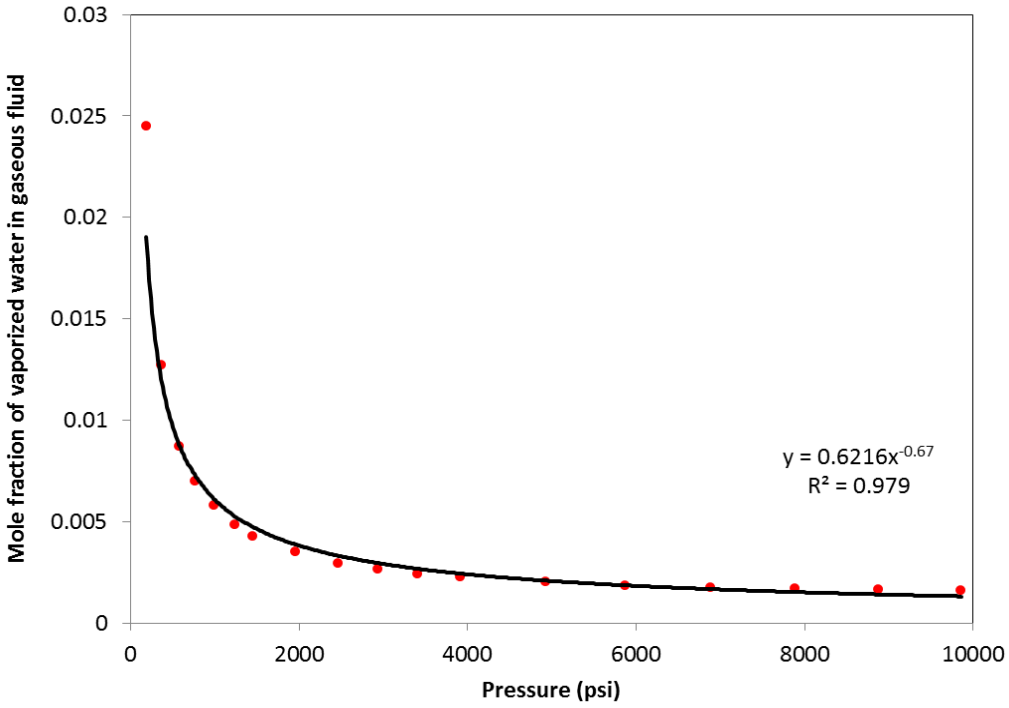

Figure 51. Empirical regression for mole fraction solubility of water in methane versus pressure (344K or 160 F)

To approximate the vaporization behavior we add vaporization to the CMG simulation results. Figure 52 illustrates the workflow of the approximated approach. The mole fraction of vaporized water can be computed using the average drainage volume pressure for each time step. Then the extracted gas production rate is used to compute the vaporized water production rate for the computed mole fraction of vaporized water in gas. Therefore, water gas ratio is update by dividing the sum of the vaporized displaced water production rates

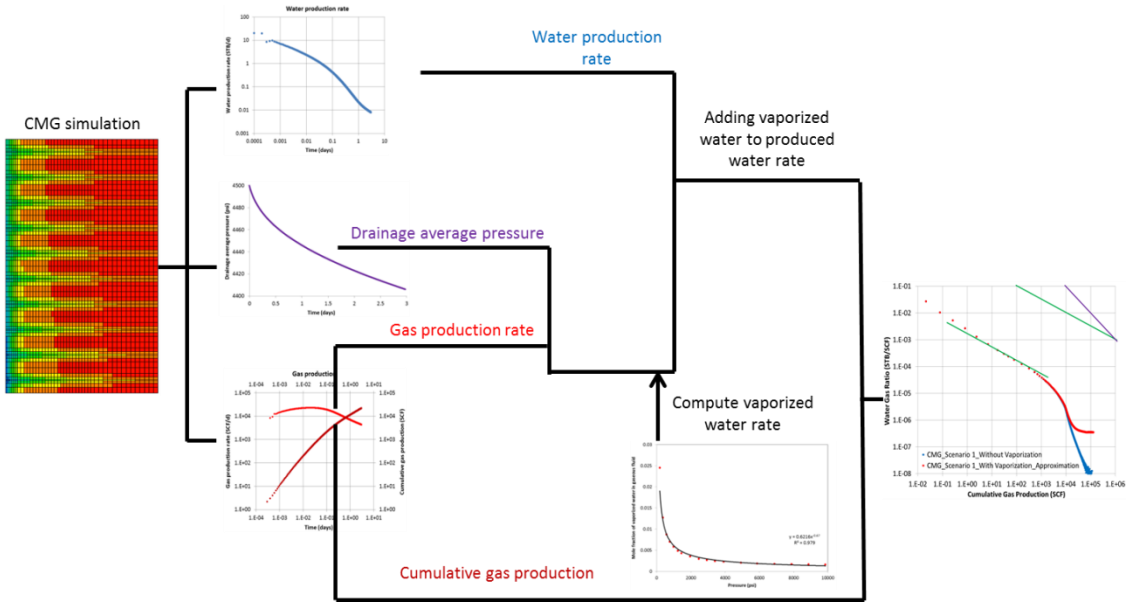

Figure 52. Workflow of approximated computation of vaporized water production by CMG

We applied this approximated approach to model the vaporization impact on flowback diagnostic plot. Interestingly, in order to observe produced vaporized water it was necessary to increase the irreducible water saturation of the relative permeability profile for the primary fractures to 0.25 in order to provide sufficient source of water in

place for vaporization to take effect. Moreover, temperature is adjusted to 160 F˚ (344K) in order to apply the empirically regressed correlation coefficient a=0.6126 and b=-0.67. Figure 53 and Figure 54 separately show the comparison between CMG simulation results without vaporization and with vaporization modeled by the approximated approach for Scenario 1 and Scenario 2 model.

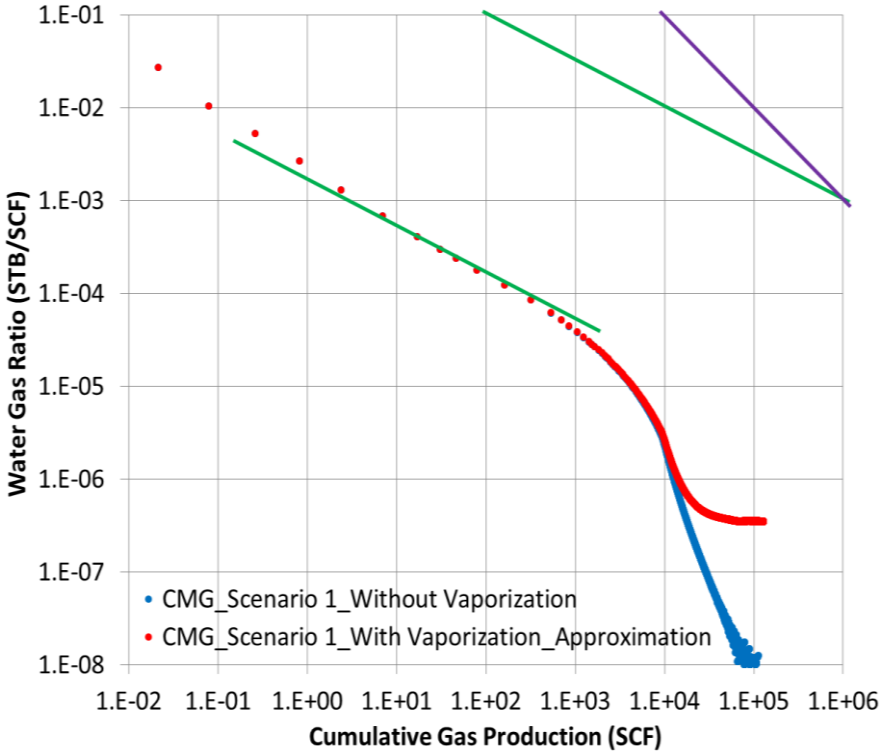

Figure 53. WGR vs. Cumulative gas production plot comparison between without vaporization and with vaporization for Scenario 1 by CMG approximation approach

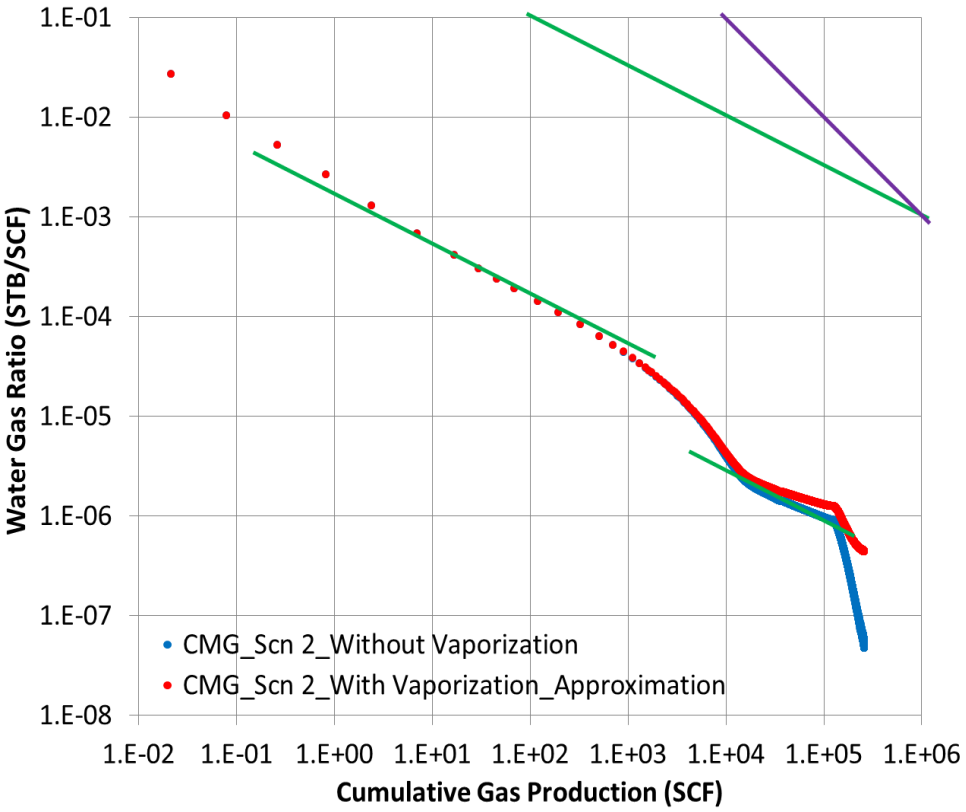

Figure 54. WGR vs. Cumulative gas production plot comparison between without vaporization and with vaporization for Scenario 2 by CMG approximation approach

If vaporization mechanism is taken into account WGR curve is lifted up at certain cumulative gas production in both scenarios. During the early time the impact of the vaporization mechanism on injected fracturing fluid flowback is not significant, and it becomes apparent only when the water-gas ratio declines to a sufficiently low level and the impact of the vaporization mechanism becomes more and more apparent.

This approximated approach by CMG helps to illustrate the difference brought by vaporization mechanism compared to pure displacement flow, however, the flaws in this method may significantly mislead. First, this approach doesn't model the vaporization mechanism in a direct dynamic way. For each time step the impact of

vaporization mechanism is approximated as a function of instantaneous average pressure of current drainage volume while it doesn't account for the unevenly distributed gas flux and pressure field in reality. Second, this model conflicts the material balance for water. The water production provided by vaporization mechanism only depends on the corresponding gas flow rate and the mole fraction at the corresponding pressure condition, but the water left in place is not considered. From this perspective the approximated approach overestimates water production at late time.

4.3 Simulation Model Including Water Vaporization

Since the approximated approach on CMG simulation for vaporization coupling study contains conflict against physical and cannot describe the transient dynamic coupled with vaporization, we formulated and a modified water/gas two-phase flowback simulation model implemented with MATLAB code.

We started with the fundamental two phase flow and integrated vaporization mechanism into the flow equation. Figure 55 shows the illustration of the two phase flow including vaporized water in gaseous phase through a volume element.

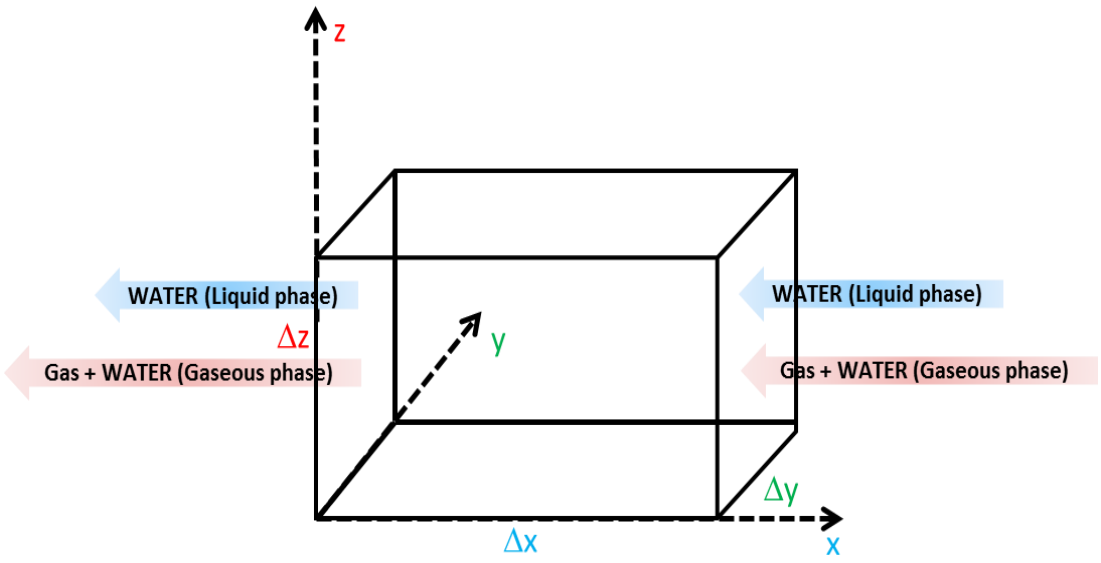

Figure 55. Illustration of two phase flow model including vaporization mechanism

Here we have liquid phase and gaseous phase. The gaseous phase contains both gas composite and water composite while the liquid phase only contains water composite. To make the phase and composite definition clear in the model, we emphasize the subscripts: *l* represents water in liquid phase; *w* represents water composite; *g* represents gaseous phase; *wg* represents the vaporized water in gaseous phase; *gg* represents gas in gaseous phase.

The saturation conservation equation is shown as Equation 3. Within the gaseous phase we note y_{wg} as the mole fraction of vaporized water composite in gaseous phase and y_{gg} as the mole fraction of natural gas composite in gaseous phase. Therefore, the mole fraction conservation equation for gaseous phase is shown as Equation 4.

$$S_l + S_g = 1 \tag{3}$$

$$y_{wg} + y_{gg} = 1 \tag{4}$$

The molecular weight of the gaseous phase is shown as Equation 5. It is a mole based average of water molecular weight and gas molecular weight.

$$M_g = M_w y_{wg} + M_{gg} y_{gg} \tag{5}$$

The gaseous phase density is:

$$\rho_g = \frac{M_g}{V} = \frac{y_{wg} M_w + M_{gg} y_{gg}}{V} = y_{wg} \frac{M_w}{V} \frac{M_{gg}}{M_{gg}} + y_{gg} \frac{M_{gg}}{V} = \left(y_{wg} \frac{M_w}{M_{gg}} + y_{gg} \right) \rho_{gg} \tag{6}$$

For water composite which refers both liquid phase water and vaporized water, we have the conservation equation:

$$\frac{\partial}{\partial t}\left(\frac{\emptyset S_l}{B_l}\right) + \frac{\partial}{\partial t}\left(\frac{\rho_g \emptyset S_g}{\rho_{w,sc}} \frac{y_{wg} M_w}{M_g}\right)$$

$$= \nabla\left[\frac{k k_{rl}}{B_l \mu_l}(\nabla p_l - \gamma_l \nabla \mathrm{z})\right] + \nabla\left[\frac{\rho_g k k_{rg}}{\rho_{w,sc} \mu_g} \frac{y_{wg} M_w}{M_g}(\nabla p_g - \gamma_g \nabla \mathrm{z})\right] - q_w \tag{7}$$

We treat the formation volume factor of the vaporized water as:

$$\frac{1}{B_{wg}} = \frac{V_{w,sc}}{V_{wg}} = \frac{\rho_{wg}}{\rho_{w,sc}} = \frac{\rho_g}{\rho_{w,sc}} \frac{y_{wg} M_w}{M_g} \tag{8}$$

Here the density of the vaporized gas is sourced from the relationship:

$$y_{wg} = \frac{\rho_{wg}}{\rho_g} \frac{M_g}{M_w} \tag{9}$$

For gas composite we have the conservation equation:

$$\frac{\partial}{\partial t}\left(\frac{\rho_g \emptyset S_g}{\rho_{gg,sc}} \frac{y_{gg} M_{gg}}{M_g}\right) = \nabla\left[\frac{\rho_g k k_{rg}}{\rho_{gg,sc} \mu_g} \frac{y_{gg} M_{gg}}{M_g}\left(\nabla p_g - \gamma_g \nabla \mathrm{z}\right)\right] - q_{gg} \tag{10}$$

Similarly, we treat the formation volume factor of the gas composite as:

$$\frac{1}{B_{gg}} = \frac{V_{gg,sc}}{V_{gg}} = \frac{\rho_{gg}}{\rho_{gg,sc}} = \frac{\rho_g}{\rho_{g,sc}} \frac{y_{gg} M_{gg}}{M_g} \tag{11}$$

The density of the gas composite is sourced from the relationship:

$$y_{gg} = \frac{\rho_{gg}}{\rho_g} \frac{M_g}{M_{gg}} \tag{12}$$

Take Equation 6 into Equation 7 and Equation 10, we can get:

$$\frac{\partial}{\partial t}\left(\frac{\emptyset S_l}{B_l}\right)+\frac{\partial}{\partial t}\left(\frac{\left(y_{wg}\frac{M_w}{M_{gg}}+y_{gg}\right)\rho_{gg}\emptyset S_g}{\rho_{w,sc}}\frac{y_{wg}M_w}{M_g}\right)$$

$$=\nabla\left[\frac{kk_{rl}}{B_l\mu_l}(\nabla p_l-\gamma_l\nabla \mathrm{z})\right]$$

$$+\nabla\left[\frac{\left(y_{wg}\frac{M_w}{M_{gg}}+y_{gg}\right)\rho_{gg}kk_{rg}}{\rho_{w,sc}\mu_g}\frac{y_{wg}M_w}{M_g}\left(\nabla p_g-\gamma_g\nabla \mathrm{z}\right)\right]-q_w \qquad (13)$$

$$\frac{\partial}{\partial t}\left(\frac{\left(y_{wg}\frac{M_w}{M_{gg}}+y_{gg}\right)\rho_{gg}\emptyset S_g}{\rho_{gg,sc}}\frac{y_{gg}M_{gg}}{M_g}\right)$$

$$=\nabla\left[\frac{\left(y_{wg}\frac{M_w}{M_{gg}}+y_{gg}\right)\rho_{gg}kk_{rg}}{\rho_{gg,sc}\mu_g}\frac{y_{gg}M_{gg}}{M_g}\left(\nabla p_g-\gamma_g\nabla \mathrm{z}\right)\right]-q_{gg} \qquad (14)$$

Because,

$$\frac{\rho_{gg}}{\rho_{w,sc}}=\frac{\rho_{gg}}{\rho_{gg,sc}}\frac{\rho_{gg,sc}}{\rho_{w,sc}}=\frac{1}{B_{gg}}\frac{\rho_{gg,sc}}{\rho_{w,sc}} \qquad (15)$$

Therefore, we will have the mass balance equations as:

$$\frac{\partial}{\partial t}\left(\frac{\emptyset S_l}{B_l}\right)+\frac{\partial}{\partial t}\left(\frac{\emptyset S_g}{B_{gg}}\left(y_{wg}\frac{M_w}{M_{gg}}+y_{gg}\right)\frac{\rho_{gg,sc}}{\rho_{w,sc}}\frac{y_{wg}M_w}{M_g}\right)$$

$$=\nabla\left[\frac{kk_{rl}}{B_l\mu_l}(\nabla p_l-\gamma_l\nabla \mathrm{z})\right]$$

$$+\nabla\left[\frac{\rho_{gg}kk_{rg}}{B_{gg}\mu_g}\left(y_{wg}\frac{M_w}{M_{gg}}+y_{gg}\right)\frac{\rho_{gg,sc}}{\rho_{w,sc}}\frac{y_{wg}M_w}{M_g}\left(\nabla p_g-\gamma_g\nabla \mathrm{z}\right)\right]-q_w \quad (16)$$

$$\frac{\partial}{\partial t}\left(\frac{\rho_{gg}\emptyset S_g}{B_{gg}}\left(y_{wg}\frac{M_w}{M_{gg}}+y_{gg}\right)\frac{y_{gg}M_{gg}}{M_g}\right)$$

$$=\nabla\left[\frac{\rho_{gg}kk_{rg}}{B_{gg}\mu_g}\left(y_{wg}\frac{M_w}{M_{gg}}+y_{gg}\right)\frac{y_{gg}M_{gg}}{M_g}\left(\nabla p_g-\gamma_g\nabla \mathrm{z}\right)\right]-q_{gg} \quad (17)$$

If we define the following functions:

$$f\left(y_{wg}\right)=\left(y_{wg}\frac{M_w}{M_{gg}}+y_{gg}\right)\frac{\rho_{gg,sc}}{\rho_{w,sc}}\frac{y_{wg}M_w}{M_g} \quad (18)$$

And according to Equation 5 we have:

$$\frac{\left(y_{wg}\frac{M_w}{M_{gg}}+y_{gg}\right)}{M_g}=\frac{1}{M_{gg}} \quad (19)$$

The function $f\,(y_{wg})$ can be expressed by:

$$f(y_{wg}) = \frac{\rho_{gg,sc}}{\rho_{w,sc}} \frac{y_{wg} M_w}{M_{gg}} \tag{20}$$

Similarly, we can define the function of g (y_{gg}) as:

$$g(y_{gg}) = \left(y_{wg} \frac{M_w}{M_{gg}} + y_{gg} \right) \frac{y_{gg} M_{gg}}{M_g} \tag{21}$$

And it can be expressed as Equation 22 if we introduce Equation 19 into Equation 21:

$$g(y_{gg}) = y_{gg} \tag{22}$$

Finally, we can get the final format of the conservation equations:

$$\frac{\partial}{\partial t}\left(\frac{\emptyset S_l}{B_l}\right) + \frac{\partial}{\partial t}\left(\frac{\emptyset S_g}{B_{gg}} f(y_{wg})\right) = \nabla\left[\frac{k k_{rl}}{B_l \mu_l}(\nabla p_l - \gamma_l \nabla \mathrm{z})\right] + \nabla\left[\frac{k k_{rg}}{B_{gg} \mu_g} f(y_w)(\nabla p_g - \gamma_g \nabla \mathrm{z})\right] - q_w \tag{23}$$

$$\frac{\partial}{\partial t}\left(\frac{\emptyset S_g}{B_{gg}} g(y_{gg})\right) = \nabla\left[\frac{k k_{rg}}{B_{gg} \mu_g} g(y_{gg})(\nabla p_g - \gamma_g \nabla \mathrm{z})\right] - q_{gg} \tag{24}$$

According to Equation 2 which is empirically expressed from the experiment data, we can define the function for the mole fraction of vaporized water in gaseous phase fluid:

$$y_{wg} = h(p_g) = a(p_g)^b \tag{25}$$

Correspondingly, the function for y_{gg} can be expressed as:

$$y_{gg} = 1 - h(p_g) = 1 - a(p_g)^b \tag{26}$$

Plus the capillary pressure equation (Eq. 27) the derivation of the model is accomplished.

$$p_c = p_g - p_l \tag{27}$$

The discretization of this flow model is shown in Appendix A. Appendix B shows validation of the numerical model against CMG simulations and specifies the model we use for validation and vaporization effect study.

The flowback diagnostic plot of WGR vs. cumulative gas production for Scenario 1 is shown as Figure. 56. On Log-Log plot a -1/2 slope trend is displayed followed by a sharp decline.

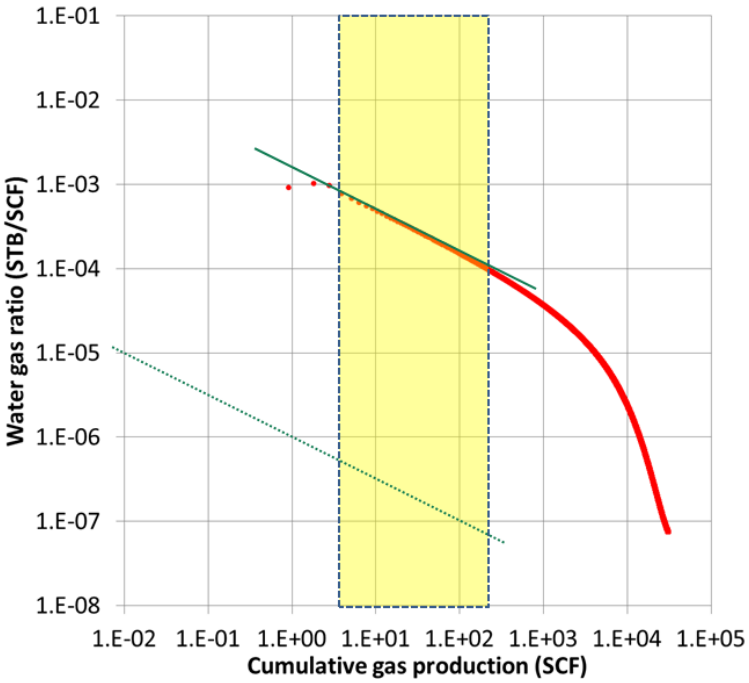

Figure 56. WGR vs. cumulative gas production plot - Scenario 1

From the simulated data we tracked the time period in which the -1/2 slope trend on the flowback diagnostic plot appear and the gas and production rates during the very time period. The corresponding time range of this -1/2 slope trend is between 0.0006 days to 0.0082 days. According to the Figure 57 during that time period WGR is a linear function of time to -2/3 power since the plot of WGR vs. time has a -2/3 slope trend on Log-Log coordinate. Data from Barnett Shale gas wells which only show -1/2 slope trend on the plot of WGR vs. cumulative gas production also confirm this feature as Figure 58 shows.

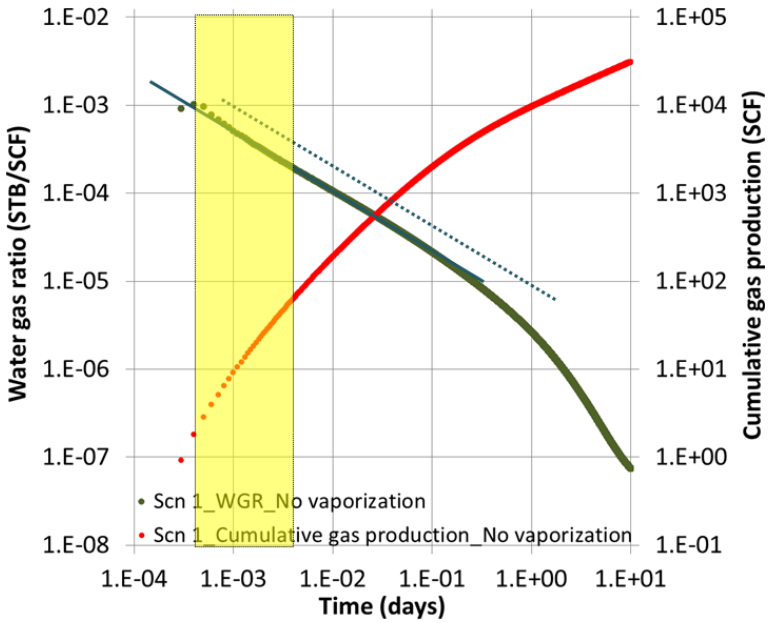

Figure 57. WGR and cumulative gas production vs. time on Log-Log plot-Scenario 1

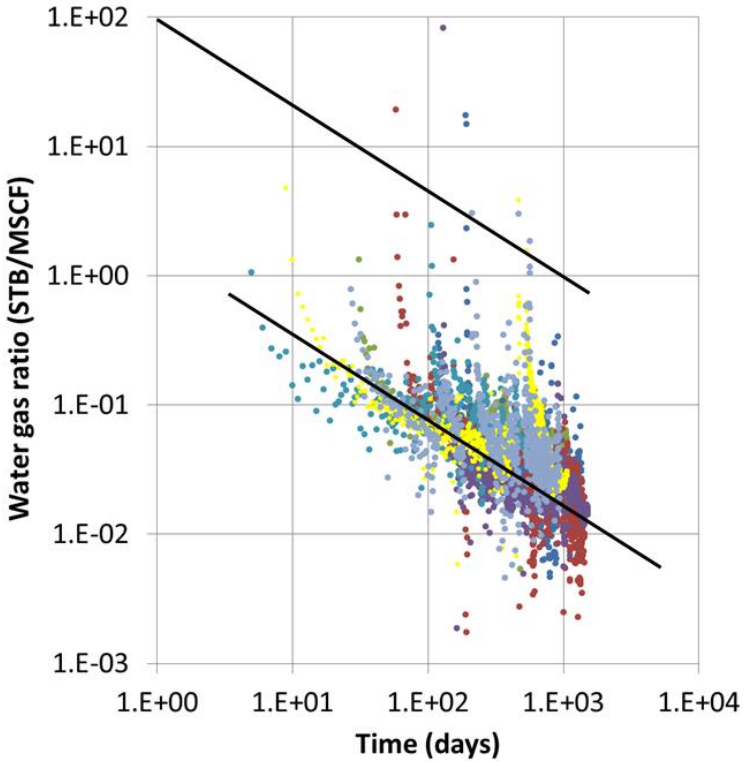

Figure 58. WGR vs. time on Log-Log plot for Barnett shale gas wells

In Scenario 2, the characteristics of the plot of WGR vs. cumulative gas production on Log-Log coordinate include two -1/2 slope trends as Figure 59 shows. The first -1/2 slope is identical to that in the case of Scenario 1. As the water in the primary fracture is displaced gas inflow from matrix to the primary fracture space dominates more and more and water production from primary fracture is reduced. As time goes water in the secondary fracture space flows toward well perforation through the primary fracture and that will supply water production so that the water production decline rate is lowered. The second -1/2 slope trend of the plot of WGR vs. cumulative gas production represents the water displacement from the secondary fracture, and the -1/2 slope trend lasts till the water left behind in secondary fracture cannot be effectively flowed back due to the high gas saturation building up caused by gas flow from matrix.

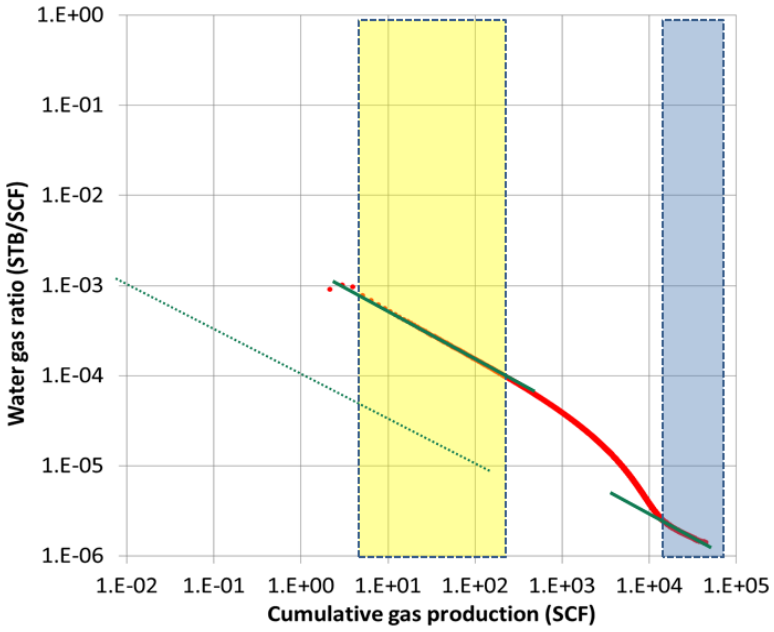

Figure 59. WGR vs. cumulative gas production plot - Scenario 2

The cumulative gas production:

$$Q_g = \int_0^t q_g dt \propto t^{\frac{1}{2}} \tag{28}$$

According to the definition of water-gas ration:

$$WGR = \frac{q_w}{q_g} \propto t^{-\frac{1}{4}} \tag{29}$$

Therefore we have:

$$WGR \propto t^{-\frac{1}{4}} = \left(t^{\frac{1}{2}}\right)^{-\frac{1}{2}} \propto Q_g^{-1/2} \tag{30}$$

Figure 60 confirms the relationship between WGR and time and that between cumulative gas production and time for the displacement of secondary fracture by showing the corresponding slope trend on Log-Log coordinate.

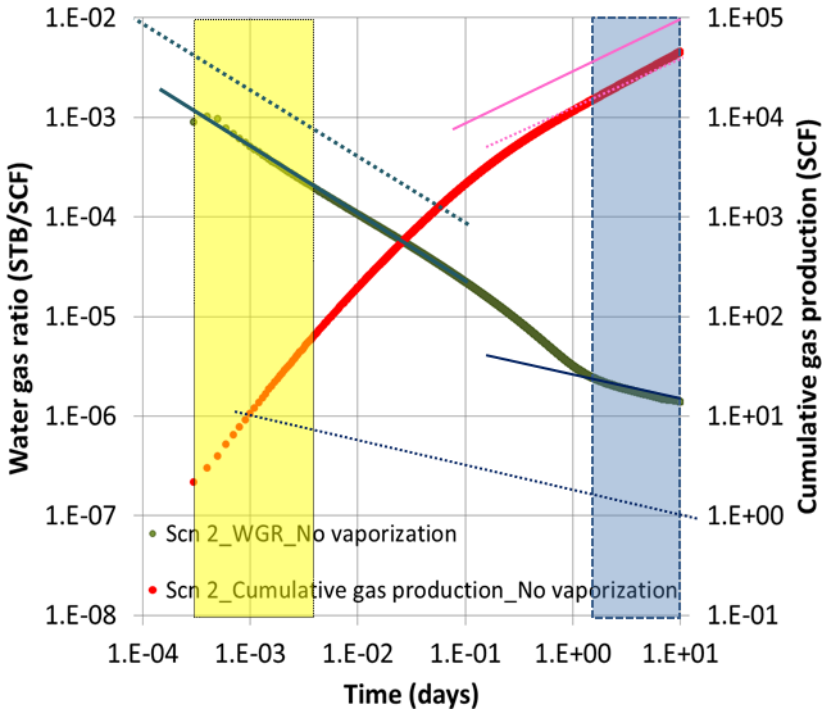

Figure 60. WGR and cumulative gas production vs. time on Log-Log plot-Scenario 2

Considering the vaporization mechanism we applied the water vaporization mole fraction correlation Figure 51 shows. Figure 61 shows comparison of the plot of WGR vs. cumulative gas production on Log-Log plot between with and without vaporization for Scenario 1. The overall impact of vaporization on flowback is increasing the water production. According to the plot as production goes the impact of vaporization becomes more and more dramatic since the gap between the WGR curve without vaporization and that with vaporization is enlarged. At initial water is mainly produced by displacement since the high water saturation guarantees an effectively high relative permeability to water for water to be flowed by the pressure gradient. Meanwhile since the pressure is relatively high the vaporization of water in gaseous phase is not too much. As production goes on the water displacement is gradually weakened because the decrement in water

saturation due to gas invasion lowers the mobility of water because of the lower relative permeability due to water and the pressure drop increases the vaporized water mole fraction solved in the gaseous phase. Therefore, when water displacement flow driven by the pressure gradient is sufficiently reduced vaporization will dominate the flowback of injected fracturing fluid.

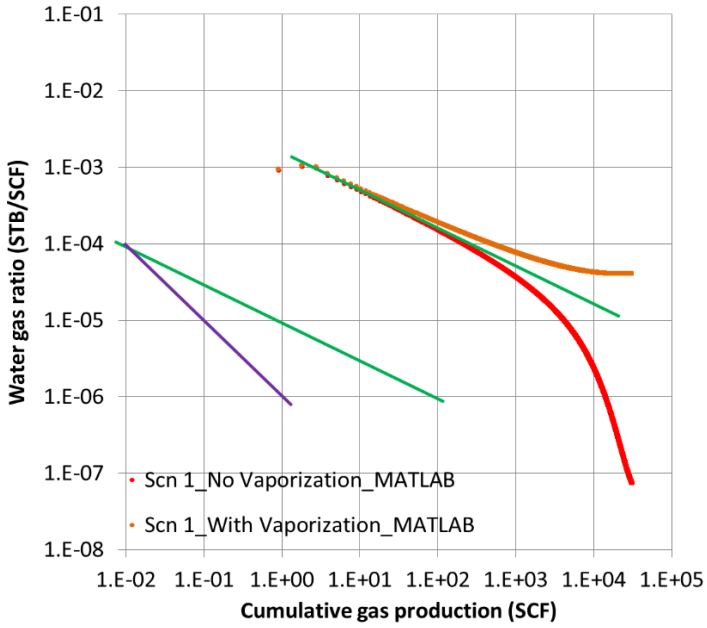

Figure 61. WGR vs. cumulative gas production comparison between with and without vaporization - Scenario 1

Figure 62 shows the comparison of production rates between with and without vaporization cases. Gas production is not significantly affected by vaporization since the gas production rates of both cases almost overlap each other. While water production rate is obviously enhanced when vaporization effect is integrated in the simulation model. Again, the later the time is the more obvious vaporization effect will be.

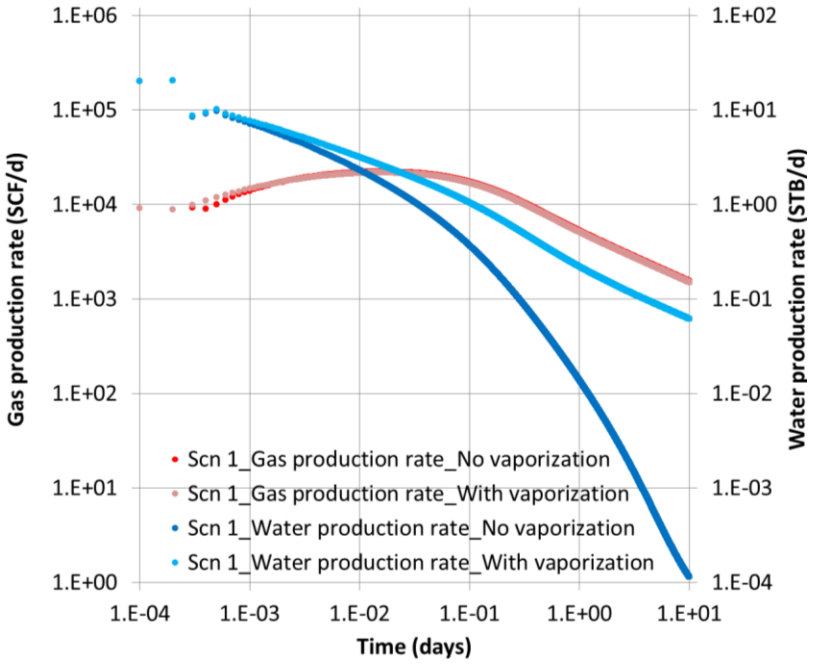

Figure 62. Production rate comparison between with and without vaporization - Scenario 1

Figure 63 shows the comparison of the cumulative gas and water production on between with and without vaporization of Scenario 1. A more accurate examination on the cumulative production indicates that the cumulative gas production by 10 days is lowered by 1.9% while the cumulative water production is increased by 6.5 times. 10 days flowback without vaporization almost clears up all the injected fracturing fluid volume in primary fracture and the load recovery is about 75%, which equals to the saturation of all mobile water in the whole system.

The cumulative water production provided by both displacement and vaporization is way higher than that driven by only displacement. The increment brought by integrating vaporization mechanism obviously exceeds the irreducible water volume

defined by the relative permeability to water for primary fracture and it indicates that vaporization doesn't not only help clean up the injected fracturing fluid in primary fracture space but also dries out the water in the matrix since 0.25 initial water saturation is defined in the simulation model of Scenario 1.

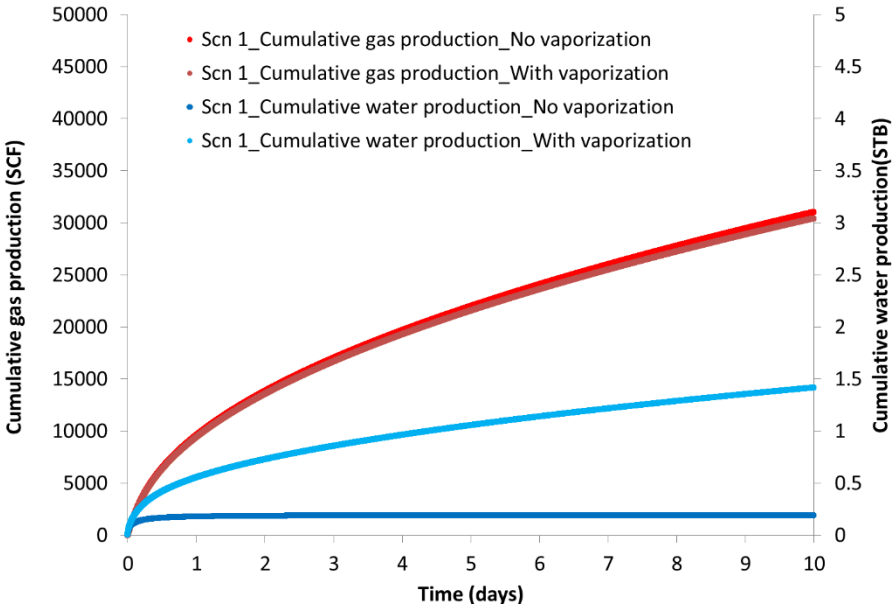

Figure 63. Cumulative production comparison between with and without vaporization - Scenario 1

Figure 64 shows the comparison of the plot of WGR vs. cumulative gas production between with and without vaporization for Scenario 2. As we analyzed before, without vaporization the first -1/2 slope trend indicates the displacement of injected fracturing fluid from primary fracture while the second -1/2 slope trend indicates the displacement from secondary fracture. When vaporization is considered its effect becomes obviously when secondary fracture is cleaned up. Similarly to Scenario 1

vaporization facilitates the water production as the WGR curve with vaporization is lifted up compared to that without vaporization.

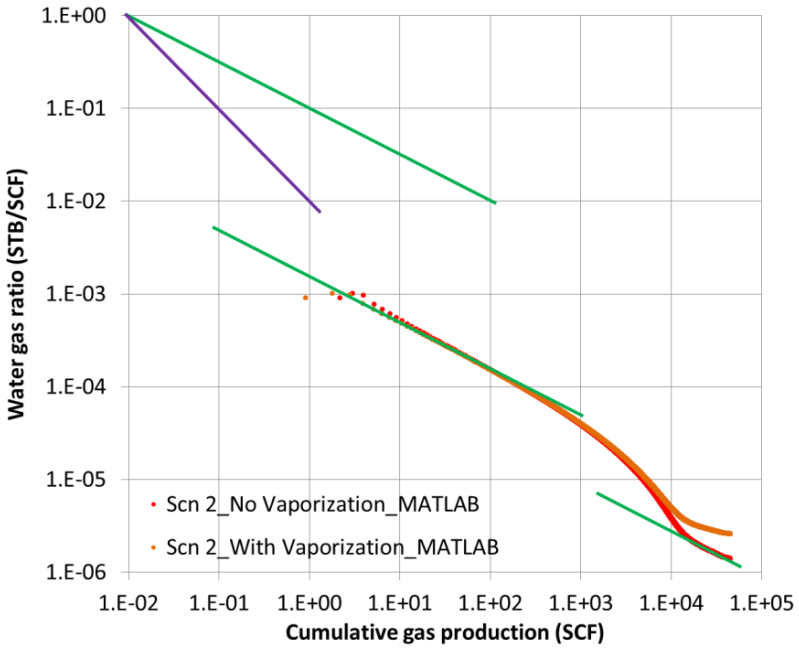

Figure 64. WGR vs. cumulative gas production comparison between with and without vaporization - Scenario 2

Figure 65 shows the production rate comparison between with and without vaporization. An obvious water production increment induced by vaporization takes place roughly at the end of the transition between the primary fracture cleanup and the secondary fracture cleanup.

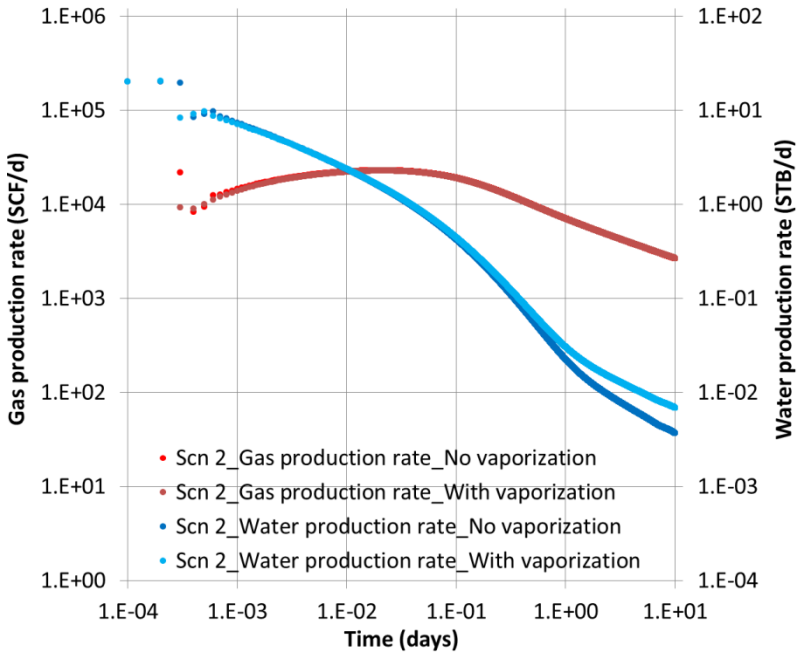

Figure 65. Production rate comparison between with and without vaporization - Scenario 2

Compared to Scenario 1 vaporization takes obvious effect later in Scenario 2. In Scenario 1 vaporization has increased water production obviously during the early displacement of primary fracture so that the plot water production rate vs. time on Log-Log coordinate loses -1/2 slope trend. However the plots with and without vaporization of Scenario 2 are almost overlapped and obviously gap doesn't appear until the late transition. A reasonable explanation to the difference in vaporization effect is that in Scenario 2 the water in secondary fracture supplies as another water source for displacement. Until the displaceable water has been almost flowed back vaporization won't take significant effect. Therefore the more water in fracture system in Scenario 2 compared to in Scenario 1 delays the vaporization effect.

Figure 66 shows the comparison of the cumulative gas and water production on between with and without vaporization for Scenario 2. Similar to Scenario 1 gas production is not significantly impacted by vaporization. Correspondingly the load recovery is increased from 51% to 61% due to vaporization.

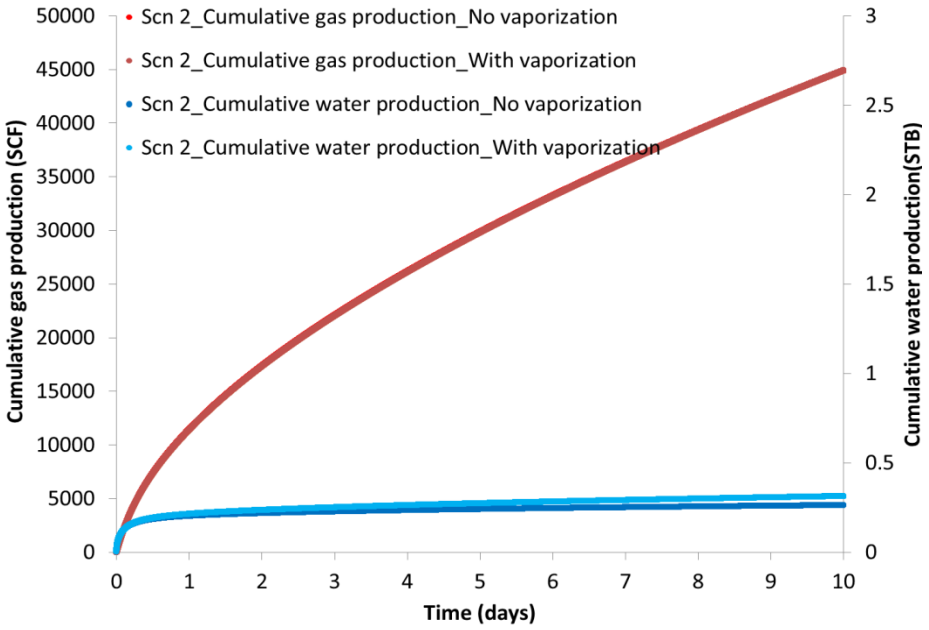

Figure 66. Cumulative production comparison between with and without vaporization - Scenario 2

Cumulative water production is increased by vaporization in Scenario 2 but the increment (19% compared to cumulative water production without vaporization by 10 days production) is not as much as in Scenario 1. Unlike in Scenario 1 in which vaporization essentially dries out the formation by 10 days production vaporization in Scenario 2 is still flowing back the water in the fracture system since the cumulative water production is smaller than the total water volume stored in the fracture system. This indicates that the total injected fracturing fluid volume in place impacts the role of

vaporization playing in water production significantly. Moreover, the capacity of water displacement also affects.

In Scenario 1 the total injected fracturing fluid volume is relatively small and high conductivity primary fracture can flow the injected fracturing fluid very fast. The water flowback rate declines very fast in the early time and that induces the obvious vaporization effect take places at very early time since quick displacement cleanup makes that remained water saturation is not high enough to provide effective relative permeability for further displacement flow.

However, in Scenario 2 secondary fracture stores an extra injected fracturing fluid volume (in the secondary fracture) and the relatively lower conductivity delays the cleanup of the whole fracture system by displacement. By a certain time point, more unrecovered injected fracturing fluid is left in Scenario 2 than in Scenario 1 and the retained water inhibits the vaporization effect because there is still enough water left behind for displacement to last for a further while. When the water saturation is down to the immobile water saturation level or the gas inflow blocks the retained injected fracturing fluid, the displacement mechanism will be almost eliminated to a very weak level and the vaporization mechanism will take the domination in flowback process. If flowback lasts for a sufficient long time vaporization may dry out the matrix.

According to the flowback modeling study we have achieved the following understanding:

- Injected fracture fluid flowback by displacement can be identified by the diagnostic plot of water gas ratio vs. cumulative gas production. Both

displacement of primary fracture and secondary fracture will display -1/2 slope trend on the diagnostic plot on Log-Log coordinate.

- Vaporization lifts the plot of WGR vs. cumulative gas production upward. It doesn't impact gas production significantly but increases water production. The vaporization mechanism does not play the dominating role of recovering the injected fracturing fluid until displacement dies down due to the smaller residual water saturation which yields a low water mobility or gas blocking effect.
- The total injected fracturing fluid volume and the flow capacity impacts the vaporization effect. Larger injected fracturing fluid volume and lower flow capacity will delay the significant vaporization effect on water production because the displacement of the injected fracturing fluid in fractures will be slowed.
- According to the simulation result vaporization does not seem to explain the -1 slope trend on the plot of WGR vs. cumulative gas production observed in Horn River shale gas well data.

In this chapter a water/gas simulation model including vaporization mechanism was built up and the flowback characteristics were modeled. Through the analysis the impact of vaporization on flowback perform has been evaluated and the relationship between the displacement and vaporization was discussed.

CHAPTER V

SUMMARY AND CONCLUSIONS

We have investigated the possible locations for injected fracturing fluid storage and studied the characteristics of storage and flow capacity for each of several possible injected fracturing fluid retention media. Four flowback simulation scenarios were constructed and through sensitivity study we concluded the impact of each possible factor on flowback performance for each scenario.

Construction of a water-gas two-phase flowback simulation model that includes both displacement and vaporization mechanisms enabled a more detailed study on injected fracturing fluid flowback behavior than can be done with commercial simulation software. We studied the characteristics of flowback and evaluated the impact of vaporization on flowback behavior and production performance.

Based on the work completed, we come to the following conclusions:

- The injected fracturing fluid can be stored in the propped hydraulic fractures, the unpropped opened natural fractures or induced micro-fractures and the invasion zone surrounding the fracture faces.
- The flowback performance from propped primary fracture mostly depends on the conductivity, but too high or too low conductivity reduces the load recovery. The impact of relative permeability and liquid loading on load recovery will be enlarged at extreme conductivity conditions. Overall the load recovery is usually

high when only propped hydraulic fractures are created due to the high conductivity.

- Conductivity and relative permeability are the dominating factors determining the flow back performance in unpropped secondary fracture system while capillary pressure is not since the conductivity of secondary fractures is still sufficiently high to overcome the capillary pressure.
- High capillary pressure of the matrix may induce strong imbibition and reduce load recovery significantly.
- The distribution of injected fracturing fluid greatly impacts load recovery. The more injected fracturing fluid stored in the media whose flow capacity is low, the lower load recovery will be.
- The simulations in this study indicated that injected fracturing fluid flowback is mainly controlled by the displacement mechanism. The displacement of injected fracturing fluid in fractures can be diagnosed by observing -1/2 slope trends of the plot of WGR vs. cumulative gas production on Log-Log coordinate.
- Simulations performed in this study reproduced the -1/2 slope trend on a diagnostic graph of water-gas ratio versus cumulative gas production, but inclusion of unpropped secondary fractures resulted in a second -1/2 slope trend.
- The vaporization mechanism doesn't impact gas production dramatically but affects water production obviously. However, vaporization will not appear as a dominating mechanism until the injected fracturing fluid has been reduced to

immobile saturation in the fracture systems or in the shale matrix where gas blocking has occurred.

- For the range of properties in the simulations performed in this study, the model including vaporization did not reproduce the -1 slope trend of the WGR vs. cumulative gas production plot observed in Horn River shale wells.

REFERENCES

Aften, C., Paktinat, J., and O'neil, B. 2011. Critical Evaluation of Biocide-Friction Reducers Interactions Used in Shale Flowback Slickwater Fracs. Paper SPE-141358 presented at SPE International Symposium on Oilfield Chemistry, The Woodlands, Texas, USA, 11-13 April. http://dx.doi.org/10.2118/141358-MS.

Ahmed, A, A., and Ehlig-Economides, C, A. 2013. Investigation of Created Fracture Geometry through Hydraulic Fracture Treatment Analysis. Paper SPE 168699 presented at Unconventional Resources Technology Conference, Denver, Colorado, USA, 12-14 August. http://dx.doi.org/10.2118/168699-MS.

Alkouh, A. B., and Wattenbarger, R. A. 2013. New Advances in Shale Reservoir Analysis Using Flowback Data. Paper SPE 165721 presented at 2013 SPE Eastern Regional Meeting, Pittsburgh, Pennsylvania, USA, 20 - 22, August. http://dx.doi.org/10.2118/165721-MS.

Apiwathanasorn, S., and Ehlig-Economides, C. A. 2012. Evidence of Reopened Microfractures in Production Data Analysis of Hydraulically Fractured Shale Gas Wells. Paper SPE 162842 presented at SPE Canadian Unconventional Resources Conference, Calgary, Alberta, Canada, 30 October-1 November. http://dx.doi.org/10.2118/162842-MS.

Blasingame, T.A. 2008. The Characteristic Flow Behavior of Low-Permeability Reservoir Systems. Paper SPE 114168 presented at SPE Unconventional Reservoirs Conference, Keystone, Colorado, USA, 10-12 February. http://dx.doi.org/10.2118/114168-MS.

Chekani, M., Bagherpour, M. H., Alavi, M., and Kharrat, R. 2010. Novel approach to mitigate gas production in a high GOR carbonate reservoir with drilled wells - Case study. Paper SPE 135875 presented at SPE Production and Operations Conference and Exhibition, Tunis, Tunisia, 8-10 June. http://dx.doi.org/10.2118/135875-MS.

Cheng, Y. 2010. Impact of Water Dynamics in Fractures on the Performance of Hydraulically Fractured Wells in Gas Shale Reservoirs. Paper SPE 127863 presented at SPE International Symposium and Exhibition on Formation Damage Control, Lafayette, Louisiana, USA, 10-12 February. http://dx.doi.org/10.2118/127863-MS.

Cipolla, C. L., Warpinski, N. R., Mayerhofer, M. J., Lolon, E. P., and Vincent, M. C. 2008. The Relationship between Fracture Complexity, Reservoir Properties, and Fracture Treatment Design. Paper SPE 115769 presented at SPE Annual Technical Conference and Exhibition, Denver, Colorado, USA, 21-24 September. http://dx.doi.org/10.2118/115769-MS.

Clarkson, C.R. 2012. Modeling 2-Phase Flowback of Multi-Fractured Horizontal Wells Completed in Shale. Paper SPE 162593 presented at SPE Canadian Unconventional Resources Conference, Calgary, Alberta, Canada, 30 October-1 November. http://dx.doi.org/10.2118/162593-MS.

Crafton, J. W. 2008. Modeling Flowback Behavior or Flowback Equals "Slowback". Paper SPE 119894 presented at SPE Shale Gas Production Conference, Fort Worth, Texas, USA, 16-18 November. http://dx.doi.org/10.2118/119894-MS.

Crafton, J. W. 2010. Flowback Performance in Intensely Naturally Fractured Shale Gas Reservoirs. Paper SPE 131785 presented at SPE Unconventional Gas Conference, Pittsburgh, Pennsylvania, USA, 23-25 February. http://dx.doi.org/10.2118/131785-MS.

Crafton, J. W., and Gunderson, D. 2007. Stimulation Flowback Management--Keeping a Good Completion Good. Paper. Paper SPE 110851 presented at SPE Annual Technical Conference and Exhibition, Anaheim, California, U.S.A, 11-14 November. http://dx.doi.org/10.2118/110851-MS.

Das, P., and Achalpurkar, M. 2013. Impact of Rock Mechanics and Formation Softening Analysis in Shale Fracturing Fluid Design. Paper SPE 137336 presented at the 2013 SPE Kuwait Oil and Gas Show and Conference, Kuwait International Fair, Kuwait City, Kuwait, 7-10 October. http://dx.doi.org/10.2118/137336-MS.

Dayan, A., Stracener, S. M., and Clark, P. E. 2009. Proppant Transport in Slickwater Fracturing of Shale Gas Formations. Paper SPE 125058 presented at SPE Annual Technical Conference and Exhibition, New Orleans, Louisiana, 4-7 October. http://dx.doi.org/10.2118/125058-MS.

Donson, C. R. and Standing, M. B.; "Pressure-Volume-Temperature and Solubility Relations for Natural-Gas-Water Mixtures," Drilling and Production Practice, American Petroleum Institute (1944) 173-179.

Dutta, R., Lee, C. H., Odumabo, S., Ye, P., Walker, S.C., Karpyn, Z.T., and Ayala, L.F. 2012. Quantification of Fracturing Fluid Migration due to Spontaneous Imbibition in Fractured Tight Formations. Paper SPE 154939 presented at SPE Americas Unconventional Resources Conference, Pittsburgh, Pennsylvania USA, 5-7 June. http://dx.doi.org/10.2118/154939-MS.

Ehlig-Economides, C. A., Ahmed, I., Apiwathanasorn, S., Lightner, J., Song, B., Vera, F., Xue, H., and Zhang, Y. 2012. Stimulated Shale Volume Characterization: Multiwell Case Study from the Horn River Shale: 2. Flow Perspective. Paper SPE 159546 presented at SPE Annual Technical Conference and Exhibition, San Antonio, Texas, USA, 8-10 October. http://dx.doi.org/10.2118/159546 -MS.

Ehlig-Economides, C. A., Economides, M. J. 2011. Water as Proppant. Paper SPE 147603 presented at SPE Annual Technical Conference and Exhibition, Denver, Colorado, USA, 30 October-2 November. http://dx.doi.org/10.2118/127863-MS.

Ezulike, D. O., Dehghanpour, H., and Hawkes, R. T. 2013. Understanding Flowback as a Transient 2-Phase Displacement Process: An Extension of the Linear Dual-Porosity Model. Paper SPE 167164 presented at SPE Unconventional Resources Conference - Canada, Calgary, Alberta, Canada, 05 – 07 November. http://dx.doi.org/10.2118/167164-MS.

Fan, L., Thompson, J. W., and Robinson, J. R. 2010. Understanding Gas Production Mechanism and Effectiveness of Well Stimulation in the Haynesville Shale Through Reservoir Simulation. Paper SPE 136696 presented at Canadian Unconventional Resources and International Petroleum Conference, Calgary, Alberta, Canada, 19-21 October. http://dx.doi.org/10.2118/136696-MS.

Hill, A. D., Zhang, J., Kamerov, A., and Zhu, D. 2013. Laboratory Measurement of Hydraulic-Fracture Conductivities in the Barnett Shale. Paper IPTC-16444-MS presented at International Petroleum Technology Conference, Beijing, China, 26-28 March. http://dx.doi.org/10.2523/16444-MS.

Holditch, S.A. 1979. Factors Affecting Water Blocking and Gas Flow From Hydraulically Fractured Gas Wells. *J Pet Technol* 31(12):1515-1524. SPE-7561-PA. http://dx.doi.org/10.2118/7561-PA .

Ilk, D., Currie, S.M., Symmons, D., Rushing, J. A., Broussard, N J., and Blasingame, T.A. 2010. A Comprehensive Workflow for Early Analysis and Interpretation of Flowback Data from Wells in Tight Gas/Shale Reservoir Systems. Paper SPE 135607 presented at SPE Annual Technical Conference and Exhibition, Florence, Italy, 19-22 September. http://dx.doi.org/10.2118/135607-MS.

King, G.E. 2010. Thirty Years of Gas Shale Fracturing: What Have We Learned? Paper SPE 133456 presented at SPE Annual Technical Conference and Exhibition, Florence, Italy, 19-22 September. http://dx.doi.org/10.2118/133456-MS.

Mahadevan, J., and Sharma, M. M. 2003. Clean-up of Water Blocks in Low Permeability Formations. Paper SPE 84216 presented at SPE Annual Technical Conference and Exhibition, Denver, Colorado, 5-8 October. http://dx.doi.org/10.2118/84216-MS.

Mahadevan, J., Sharma, M. M., and Yortsos, Y. C. 2007. Evaporative Cleanup of Water Blocks in Gas Wells. *SPE J* 12(02):209-216. SPE-94215-PA. http://dx.doi.org/10.2118/94215-PA .

Makhanov, K., Dehghanpour, H., and Kuru, E. 2012. An Experimental Study of Spontaneous Imbibition in Horn River Shales. Paper SPE 162650 presented at SPE Canadian Unconventional Resources Conference, Calgary, Alberta, Canada, 30 October-1 November. http://dx.doi.org/10.2118/162650-MS.

Munoz, A. V., Asadi, M., Woodroof, R. A., and Morales, R. 2009. Long-Term Post-Frac Performance Analysis Based on Flowback Analysis Using Chemical Frac-Tracers. Paper SPE 121380 presented at Latin American and Caribbean Petroleum Engineering Conference, Cartagena de Indias, Colombia, 31 May-3 June. http://dx.doi.org/10.2118/121380-MS.

Newsham, K. E., Rushing, J. A., and Lasswell, P M. 2003. Use of Vapor Desorption Data to Characterize High Capillary Pressures in a Basin-Centered Gas Accumulation with Ultra-Low Connate Water Saturations. Paper SPE 84596 presented at SPE Annual Technical Conference and Exhibition, Denver, Colorado, 5-8 October. http://dx.doi.org/10.2118/84596-MS.

Odusina, E., Sondergeld, C., and Rai, Chandra. 2011. NMR Study of Shale Wettability. Paper SPE 147371 presented at Canadian Unconventional Resources Conference, Alberta, Canada, 15-17 November. http://dx.doi.org/10.2118/147371-MS.

Palisch, T. T., Vincent, M. C., and Handren. P. J. 2008. Slickwater Fracturing: Food for Thought. Paper SPE 115766 presented at the SPE Annual Technical Conference and Exhibition, Denver, Colorado, USA, 21-24 September. http://dx.doi.org/10.2118/115766-MS.

Panga, M. K. R., Ismail, S., Cheneviere, P., and Samuel, M. 2007. Preventive Treatment for Enhancing Water Removal from Gas Reservoirs by Wettability Alteration. Paper SPE 105367 presented at SPE Middle East Oil & Gas Show and Conference, Kingdom of Bahrain, 11–14 March. http://dx.doi.org/10.2118/105367-MS.

Parmar, J. S., Dehghanpour, H., and Kuru, E. 2013. Drainage Against Gravity: Factors Impacting the Load Recovery In Fractures. Paper SPE 164530 presented at SPE Unconventional Resources Conference - USA, The Woodlands, TX, USA, Apr 10 - 12, 2013. http://dx.doi.org/10.2118/164530-MS.

Pegals, M., Hinkel, J, J., and Willberg, D. M. 2012. Measuring Capillary Pressure Tells More Than Pretty Pictures. Paper SPE 151729 presented at SPE International Symposium and Exhibition on Formation Damage Control, Lafayette, Louisiana, USA, 15-17 Febuary. http://dx.doi.org/10.2118/151729-MS.

Penny, G. S., Pursley, J. T., and Clawson, T. D. 2006. Field Study of Completion Fluids to Enhance Gas Production in the Barnett Shale. Paper SPE 100434 presented at the SPE Gas Technology Symposium, Calgary, Alberta, Canada, 15-17 May. http://dx.doi.org/10.2118/100434-MS.

Roychaudhuri, B., Tsotsis, T., and Jessen, K. 2011. An Experimental and Numerical Investigation of Spontaneous Imbibition in Gas Shales. Paper SPE 147652 presented at SPE Annual Technical Conference and Exhibition, Denver, Colorado, USA, 30 October-2 November 2011. http://dx.doi.org/10.2118/147652-MS.

Rushing, J. A., Newsham, K. E., Van Fraassen, K. C., Mehta, S. A., and Moore, G.R. 2008. The Catalytic Effects of Nonhydrocarbon Contaminants on Equilibrium Water Vapor Content for a Dry Gas at HP/HT Reservoir Conditions. Paper SPE 114517 presented at CIPC/SPE Gas Technology Symposium 2008 Joint Conference, Calgary, Alberta, Canada, 16-19 June. http://dx.doi.org/10.2118/114517-MS.

Sage, B.H. and Lacey, W.N. 1955. Some Properties of the Lighter Hydrocarbons, Hydrogen Sulfide, and Carbon Dioxide: Monograph on Api Research Project 37: American Petroleum Institute.

Shanley, K. W., Cluff, R. M., and Robinson, J. W. 2004. Factors Controlling Prolific Gas Production from Low-Permeability Sandstone Reservoir: Implications for Resource Assessment, Prospect Development, and Risk Analysis. AAPG Bul. 88, 8(8):1083-1121. DOI: 10.1306/03250403051.

Turner, R. G., Hubbard, M.G., and Dukler, A.E. 1969. Analysis and Prediction of Minimum Flow Rate for the Continuous Removal of Liquids from Gas Wells. JPT 21(11):1475-1482. http://dx.doi.org/10.2118/2198-PA.

Wang, D., Butler, R., Liu, H., and Ahmed, S. 2010. Flow Rate Behavior in Shale Rock. Paper SPE 138521 presented at SPE Eastern Regional Meeting, Morgantown, West Virginia, USA, 12-1 October. http://dx.doi.org/10.2118/138521-MS.

Wang, D., Butler, R., Zhang, J., and Seright, R. 2012. Wettability Survey in Bakken Shale Using Surfactant Formulation Imbibition. Paper SPE 153853 presented at SPE Improved Oil Recovery Symposium, Tulsa, Oklahoma, USA, 14-18 April. http://dx.doi.org/10.2118/153853-MS.

Warpinski, N. R., Mayerhofer, M. J., Vincent, M. C., Cipolla, C. L., and Lolon, E. P. 2008. Stimulating Unconventional Reservoirs: Maximizing Network Growth While Optimizing Fracture Conductivity. Paper SPE 114173 presented at SPE Unconventional Reservoirs Conference, Keystone, Colorado, USA, 10-12 February. http://dx.doi.org/10.2118/114173-MS.

Zhang, Y. 2013. Accounting for Remaining Injected Fracturing Fluid. MS Thesis, Texas A&M University, College Station, Texas (October, 2013).

Zhou, D., and Yuan, H. 2009. New Model for Gas Well Loading Prediction. Paper SPE 120580 presented at SPE Production and Operations Symposium, Oklahoma City, Oklahoma, 4-8 April 2009. http://dx.doi.org/10.2118/120580-MS.

APPENDIX A: NUMERICAL MODEL DISCRETIZATION

The final format of the conservation equations for water and gas are:

$$\frac{\partial}{\partial t}\left(\frac{\emptyset S_l}{B_l}\right)+\frac{\partial}{\partial t}\left(\frac{\emptyset S_g}{B_{gg}}f(y_{wg})\right)$$

$$=\nabla\left[\frac{kk_{rl}}{B_l\mu_l}(\nabla p_l-\gamma_l\nabla \mathrm{z})\right]+\nabla\left[\frac{kk_{rg}}{B_{gg}\mu_g}f(y_w)\left(\nabla p_g-\gamma_g\nabla \mathrm{z}\right)\right]-q_w \qquad (A1)$$

$$\frac{\partial}{\partial t}\left(\frac{\emptyset S_g}{B_{gg}}g(y_{gg})\right)=\nabla\left[\frac{kk_{rg}}{B_{gg}\mu_g}g(y_{gg})\left(\nabla p_g-\gamma_g\nabla \mathrm{z}\right)\right]-q_{gg} \qquad (A2)$$

We have the saturation conservation equation, mole fraction of gaseous phase conservation equation and capillary pressure equation:

$$S_l+S_g=1 \qquad (A3)$$

$$y_{wg}+y_{gg}=1 \qquad (A4)$$

$$p_c=p_g-p_l \qquad (A5)$$

For one cell (block-center method), we can discretize the following in x direction:

$$\frac{\partial}{\partial x}\left(\frac{kk_{rl}}{B_l\mu_l}\frac{\partial p_l}{\partial x}\right)+\frac{\partial}{\partial x}\left(\frac{kk_{rg}}{B_{gg}\mu_l}f\frac{\partial p_g}{\partial x}\right)$$

$$=\frac{\partial}{\partial x}\left(\frac{kk_{rl}}{B_l\mu_l}\frac{p_{l,i+\frac{1}{2},j,k}-p_{l,i-\frac{1}{2},j,k}}{\Delta x}\right)+\frac{\partial}{\partial x}\left(\frac{kk_{rg}}{B_{gg}\mu_g}f\frac{p_{g,i+\frac{1}{2},j,k}-p_{g,i-\frac{1}{2},j,k}}{\Delta x}\right)$$

$$=\frac{1}{\Delta x^2}\left(\frac{kk_{rl}}{B_l\mu_l}\right)_{i+\frac{1}{2},j,k}\left(p_{l,i+1,j,k}-p_{l,i,j,k}\right)$$

$$+\frac{1}{\Delta x^2}\left(\frac{kk_{rl}}{B_l\mu_l}\right)_{i-\frac{1}{2},j,k}\left(p_{l,i-1,j,k}-p_{l,i,j,k}\right)$$

$$+\frac{1}{\Delta x^2}\left(\frac{kk_{rg}}{B_{gg}\mu_g}f\right)_{i+\frac{1}{2},j,k}\left(p_{g,i+1,j,k}-p_{g,i,j,k}\right)$$

$$+\frac{1}{\Delta x^2}\left(\frac{kk_{rg}}{B_{gg}\mu_g}f\right)_{i-\frac{1}{2},j,k}\left(p_{g,i-1,j,k}-p_{g,i,j,k}\right) \qquad (A6)$$

The y direction term is discretized in the same way, but in z direction we taken gravity into account, and the discretization is:

$$\frac{\partial}{\partial z}\left(\frac{kk_{rl}}{B_l\mu_l}\left(\frac{\partial p_l}{\partial z}-\gamma_l\nabla z\right)\right)+\frac{\partial}{\partial z}\left(\frac{kk_{rg}}{B_{gg}\mu_l}f\left(\frac{\partial p_g}{\partial z}-\gamma_g\nabla z\right)\right)$$

$$=\frac{\partial}{\partial z}\left(\frac{kk_{rl}}{B_l\mu_l}\left(\frac{p_{l,i,j,k+\frac{1}{2}}-p_{l,i,j,k-\frac{1}{2}}}{\Delta z}-\gamma_l sin\theta\right)\right)$$

$$+\frac{\partial}{\partial z}\left(\frac{kk_{rg}}{B_{gg}\mu_g}f\left(\frac{p_{g,i,j,k+\frac{1}{2}}-p_{g,i,j,k-\frac{1}{2}}}{\Delta z}-\gamma_g sin\theta\right)\right)$$

$$=\frac{1}{\Delta z^2}\left(\frac{kk_{rl}}{B_l\mu_l}\right)_{i,j,k+\frac{1}{2}}\left(p_{l,i,j,k+1}-p_{l,i,j,k}\right)$$

$$+\frac{1}{\Delta z^2}\left(\frac{kk_{rl}}{B_l\mu_l}\right)_{i,j,k-\frac{1}{2}}\left(p_{l,i,j,k-1}-p_{l,i,j,k}\right)$$

$$+\frac{1}{\Delta z^2}\left(\frac{kk_{rg}}{B_{gg}\mu_g}f\right)_{i,j,k+\frac{1}{2}}\left(p_{g,i,j,k+1}-p_{g,i,j,k}\right)$$

$$+\frac{1}{\Delta z^2}\left(\frac{kk_{rg}}{B_{gg}\mu_g}f\right)_{i,j,k-\frac{1}{2}}\left(p_{g,i,j,k-1}-p_{g,i,j,k}\right)$$

$$-\frac{\gamma_l sin\theta}{\Delta z}\left(\left(\frac{kk_{rl}}{B_l\mu_l}\right)_{i,j,k+\frac{1}{2}}-\left(\frac{kk_{rl}}{B_l\mu_l}\right)_{i,j,k-\frac{1}{2}}\right)$$

$$-\frac{\gamma_g sin\theta}{\Delta z}\left(\left(\frac{kk_{rg}}{B_{gg}\mu_g}f\right)_{i,j,k+\frac{1}{2}}-\left(\frac{kk_{rg}}{B_{gg}\mu_g}f\right)_{i,j,k-\frac{1}{2}}\right) \qquad (A7)$$

Similarly, for one cell (center-block method) in gas equation, we have the discretization in x direction as follows:

$$\frac{\partial}{\partial x}\left(\frac{kk_{rg}}{B_{gg}\mu_g}g\frac{\partial p_g}{\partial x}\right)=\frac{\partial}{\partial x}\left(\frac{kk_{rg}}{B_{gg}\mu_g}g\frac{p_{g,i+\frac{1}{2},j,k}-p_{g,i-\frac{1}{2},j,k}}{\Delta x}\right)$$

$$=\frac{1}{\Delta x^2}\left(\frac{kk_{rg}}{B_{gg}\mu_g}g\right)_{i+\frac{1}{2},j,k}\left(p_{g,i+1,j,k}-p_{g,i,j,k}\right)$$

$$+\frac{1}{\Delta x^2}\left(\frac{kk_{rg}}{B_{gg}\mu_g}g\right)_{i-\frac{1}{2},j,k}\left(p_{g,i-1,j,k}-p_{g,i,j,k}\right) \qquad (A8)$$

The discretization in y direction is similar to that in x direction. For z-direction, we take into gravity into account:

$$\frac{\partial}{\partial z}\left(\frac{kk_{rg}}{B_{gg}\mu_g}g\left(\frac{\partial p_g}{\partial z}-\gamma_g\nabla z\right)\right)=\frac{\partial}{\partial z}\left(\frac{kk_{rg}}{B_{gg}\mu_g}g\left(\frac{p_{g,i,j,k+\frac{1}{2}}-p_{g,i,j,k-\frac{1}{2}}}{\Delta z}-\gamma_g sin\theta\right)\right)$$

$$=\frac{1}{\Delta z^2}\left(\frac{kk_{rg}}{B_{gg}\mu_g}g\right)_{i,j,k+\frac{1}{2}}\left(p_{g,i,j,k+1}-p_{g,i,j,k}\right)$$

$$+\frac{1}{\Delta z^2}\left(\frac{kk_{rg}}{B_{gg}\mu_g}g\right)_{i,j,k-\frac{1}{2}}\left(p_{g,i,j,k-1}-p_{g,i,j,k}\right)$$

$$-\frac{\gamma_g sin\theta}{\Delta z}\left(\left(\frac{kk_{rg}}{B_{gg}\mu_g}g\right)_{i,j,k+\frac{1}{2}}\right.$$

$$\left.-\left(\frac{kk_{rg}}{B_{gg}\mu_g}g\right)_{i,j,k-\frac{1}{2}}\right) \qquad (A9)$$

For the accumulation terms of water conservation equation:

$$\frac{\partial}{\partial t}\left(\frac{\emptyset S_l}{B_l}\right)+\frac{\partial}{\partial t}\left(\frac{\emptyset S_g}{B_{gg}}f(y_{wg})\right)$$

$$=\frac{S_l}{B_l}\frac{\partial \emptyset}{\partial t}+\frac{\emptyset}{B_l}\frac{\partial S_l}{\partial t}+\emptyset S_l\frac{\partial}{\partial t}\left(\frac{1}{B_l}\right)+\frac{\emptyset S_g}{B_{gg}}\frac{\partial f}{\partial t}+\frac{\emptyset f}{B_{gg}}\frac{\partial S_g}{\partial t}+\frac{S_g f}{B_{gg}}\frac{\partial \emptyset}{\partial t}$$

$$+\emptyset S_g f\frac{\partial}{\partial t}\left(\frac{1}{B_l}\right)$$

$$=\frac{\emptyset S_l}{B_l}\frac{1}{\emptyset}\frac{\partial \emptyset}{\partial p_l}\frac{\partial p_l}{\partial t}+\frac{\emptyset S_l}{B_l}B_l\frac{\partial}{\partial p_l}\left(\frac{1}{B_l}\right)\frac{\partial p_l}{\partial t}+\frac{\emptyset}{B_l}\frac{\partial S_l}{\partial t}+\frac{\emptyset S_g f}{B_{gg}}\frac{1}{f}\frac{\partial f}{\partial p_g}\frac{\partial p_g}{\partial t}$$

$$+\frac{\emptyset S_g f}{B_{gg}}\frac{1}{\emptyset}\frac{\partial \emptyset}{\partial p_g}\frac{\partial p_g}{\partial t}+\frac{\emptyset S_g f}{B_{gg}}B_{gg}\frac{\partial}{\partial p_g}\left(\frac{1}{B_{gg}}\right)\frac{\partial p_g}{\partial t}+\frac{\emptyset f}{B_{gg}}\frac{\partial S_g}{\partial t}$$

$$=\frac{\emptyset S_l}{B_l}c_f\frac{\partial p_l}{\partial t}+\frac{\emptyset S_l}{B_l}c_l\frac{\partial p_l}{\partial t}+\frac{\emptyset}{B_l}\frac{\partial S_l}{\partial t}+\frac{\emptyset S_g f}{B_{gg}}\frac{1}{f}\frac{\partial f}{\partial p_g}\frac{\partial p_g}{\partial t}+\frac{\emptyset S_g f}{B_{gg}}c_f\frac{\partial p_g}{\partial t}$$

$$+\frac{\emptyset S_g f}{B_{gg}}c_g\frac{\partial p_g}{\partial t}+\frac{\emptyset f}{B_{gg}}\frac{\partial S_g}{\partial t}$$

$$=\frac{\emptyset S_l}{B_l}(c_f+c_l)\frac{\partial p_l}{\partial t}+\frac{\emptyset}{B_l}\frac{\partial S_l}{\partial t}+\frac{\emptyset S_g f}{B_{gg}}\left(c_f+c_l+\frac{1}{f}\frac{\partial f}{\partial p_g}\right)\frac{\partial p_g}{\partial t}$$

$$+\frac{\emptyset f}{B_{gg}}\frac{\partial S_g}{\partial t} \qquad (A10)$$

The accumulation terms of gas conservation equation:

$$\frac{\partial}{\partial t}\left(\frac{\emptyset S_g}{B_{gg}} g(y_{gg})\right) = \frac{\emptyset S_g}{B_{gg}}\frac{\partial g}{\partial t} + \frac{\emptyset g}{B_{gg}}\frac{\partial S_g}{\partial t} + \frac{S_g g}{B_{gg}}\frac{\partial \emptyset}{\partial t} + \emptyset S_g g \frac{\partial}{\partial t}\left(\frac{1}{B_{gg}}\right)$$

$$= \frac{\emptyset g S_g}{B_{gg}}\frac{1}{g}\frac{\partial g}{\partial p_g}\frac{\partial p_g}{\partial t} + \frac{\emptyset g}{B_{gg}}\frac{\partial S_g}{\partial t} + \frac{\emptyset S_g g}{B_{gg}}\frac{1}{\emptyset}\frac{\partial \emptyset}{\partial p_g}\frac{\partial p_g}{\partial t}$$

$$+ \frac{\emptyset S_g g}{B_{gg}} B_{gg}\frac{\partial}{\partial p_g}\left(\frac{1}{B_{gg}}\right)\frac{\partial p_g}{\partial t}$$

$$= \frac{\emptyset g S_g}{B_{gg}}\frac{1}{g}\frac{\partial g}{\partial p_g}\frac{\partial p_g}{\partial t} + \frac{\emptyset g}{B_{gg}}\frac{\partial S_g}{\partial t} + \frac{\emptyset S_g g}{B_{gg}} c_f \frac{\partial p_g}{\partial t} + \frac{\emptyset S_g g}{B_{gg}}\ c_g \frac{\partial p_g}{\partial t}$$

$$= \frac{\emptyset g S_g}{B_{gg}}\left(c_f + c_g + \frac{1}{g}\frac{\partial g}{\partial p_g}\right)\frac{\partial p_g}{\partial t} + \frac{\emptyset g}{B_{gg}}\frac{\partial S_g}{\partial t} \qquad (A11)$$

Since we have the capillary pressure equation and saturation conservation equation, we will have:

$$\frac{\partial p_l}{\partial t} = \frac{\partial\left(p_g - p_c\right)}{\partial t} = \frac{\partial p_g}{\partial t} - \frac{\partial p_c}{\partial t} = \frac{\partial p_g}{\partial t} - \frac{\partial p_c}{\partial S_l}\frac{\partial S_l}{\partial t} \qquad (A12)$$

$$\frac{\partial S_g}{\partial t} = \frac{\partial(1 - S_l)}{\partial t} = -\frac{\partial S_l}{\partial t} \qquad (A13)$$

Therefore, we will have:

$$\frac{\partial}{\partial t}\left(\frac{\emptyset S_l}{B_l}\right)+\frac{\partial}{\partial t}\left(\frac{\emptyset S_g}{B_{gg}}f(y_{wg})\right)$$

$$=\frac{\emptyset S_l}{B_l}(c_f+c_l)\left(\frac{\partial p_g}{\partial t}-\frac{\partial p_c}{\partial S_l}\frac{\partial S_l}{\partial t}\right)+\frac{\emptyset}{B_l}\frac{\partial S_l}{\partial t}$$

$$+\frac{\emptyset S_g f}{B_{gg}}\left(c_f+c_l+\frac{1}{f}\frac{\partial f}{\partial p_g}\right)\frac{\partial p_g}{\partial t}+\frac{\emptyset f}{B_{gg}}\frac{\partial(1-S_l)}{\partial t}$$

$$=\left[\frac{\emptyset S_l}{B_l}(c_f+c_l)+\frac{\emptyset S_g f}{B_{gg}}\left(c_f+c_l+\frac{1}{f}\frac{\partial f}{\partial p_g}\right)\right]\frac{\partial p_g}{\partial t}$$

$$+\left[\frac{\emptyset}{B_l}-\frac{\emptyset f}{B_{gg}}-\frac{\emptyset S_l}{B_l}(c_f+c_l)\frac{\partial p_c}{\partial S_l}\right]\frac{\partial S_l}{\partial t}$$

$$=\left[\frac{\emptyset S_l}{B_l}(c_f+c_l)+\frac{\emptyset S_g f}{B_{gg}}\left(c_f+c_l+\frac{1}{f}\frac{\partial f}{\partial p_g}\right)\right]\frac{p_{g,i,j,k}^{n+1}-p_{g,i,j,k}^{n}}{\Delta t}$$

$$+\left[\frac{\emptyset}{B_l}-\frac{\emptyset f}{B_{gg}}-\frac{\emptyset S_l}{B_l}(c_f+c_l)\frac{\partial p_c}{\partial S_l}\right]\frac{S_{l,i,j,k}^{n+1}-S_{l,i,j,k}^{n}}{\Delta t} \qquad (A14)$$

$$\frac{\partial}{\partial t}\left(\frac{\emptyset S_g}{B_{gg}}g(y_{gg})\right)=\frac{\emptyset g S_g}{B_{gg}}\left(c_f+c_g+\frac{1}{g}\frac{\partial g}{\partial p_g}\right)\frac{\partial p_g}{\partial t}+\frac{\emptyset g}{B_{gg}}\frac{\partial S_g}{\partial t}$$

$$=\frac{\emptyset g(1-S_l)}{B_{gg}}\left(c_f+c_g+\frac{1}{g}\frac{\partial g}{\partial p_g}\right)\frac{\partial p_g}{\partial t}-\frac{\emptyset g}{B_{gg}}\frac{\partial S_l}{\partial t}$$

$$=\frac{\emptyset g(1-S_l)}{B_{gg}}\left(c_f+c_g+\frac{1}{g}\frac{\partial g}{\partial p_g}\right)\frac{p_{g,i,j,k}^{n+1}-p_{g,i,j,k}^{n}}{\Delta t}$$

$$-\frac{\emptyset g}{B_{gg}}\frac{S_{l,i,j,k}^{n+1}-S_{l,i,j,k}^{n}}{\Delta t} \qquad (A15)$$

We integrate the difference equation within the cell volume $\Delta V=\Delta x\,\Delta y\,\Delta z$, we can get:

$$\Delta V\left[\frac{\emptyset S_l}{B_l}(c_f+c_l)+\frac{\emptyset S_g f}{B_{gg}}\left(c_f+c_l+\frac{1}{f}\frac{\partial f}{\partial p_g}\right)\right]\frac{p_{g,i,j,k}^{n+1}-p_{g,i,j,k}^{n}}{\Delta t}$$

$$+\Delta V\left[\frac{\emptyset}{B_l}-\frac{\emptyset f}{B_{gg}}-\frac{\emptyset S_l}{B_l}(c_f+c_l)\frac{\partial p_c}{\partial S_l}\right]\frac{S_{l,i,j,k}^{n+1}-S_{l,i,j,k}^{n}}{\Delta t}$$

$$=\frac{\Delta y\Delta z}{\Delta x}\left(\frac{kk_{rl}}{B_l\mu_l}\right)_{i+\frac{1}{2},j,k}(p_{l,i+1,j,k}-p_{l,i,j,k})$$

$$+\frac{\Delta y\Delta z}{\Delta x}\left(\frac{kk_{rl}}{B_l\mu_l}\right)_{i-\frac{1}{2},j,k}(p_{l,i-1,j,k}-p_{l,i,j,k})$$

$$+\frac{\Delta y\Delta z}{\Delta x}\left(\frac{kk_{rg}}{B_{gg}\mu_g}f\right)_{i+\frac{1}{2},j,k}(p_{g,i+1,j,k}-p_{g,i,j,k})$$

$$+\frac{\Delta y\Delta z}{\Delta x}\left(\frac{kk_{rg}}{B_{gg}\mu_g}f\right)_{i-\frac{1}{2},j,k}(p_{g,i-1,j,k}-p_{g,i,j,k})$$

$$+\frac{\Delta x\Delta z}{\Delta y}\left(\frac{kk_{rl}}{B_l\mu_l}\right)_{i,j+\frac{1}{2},k}(p_{l,i,j+1,k}-p_{l,i,j,k})$$

$$+\frac{\Delta x\Delta z}{\Delta y}\left(\frac{kk_{rl}}{B_l\mu_l}\right)_{i,j-\frac{1}{2},k}(p_{l,i,j-1,k}-p_{l,i,j,k})$$

$$+\frac{\Delta x\Delta z}{\Delta y}\left(\frac{kk_{rg}}{B_{gg}\mu_g}f\right)_{i,j+\frac{1}{2},k}(p_{g,i,j+1,k}-p_{g,i,j,k})$$

$$+\frac{\Delta x\Delta z}{\Delta y}\left(\frac{kk_{rg}}{B_{gg}\mu_g}f\right)_{i,j-\frac{1}{2},k}(p_{g,i,j-1,k}-p_{g,i,j,k})$$

$$+\frac{\Delta x\Delta y}{\Delta z}\left(\frac{kk_{rl}}{B_l\mu_l}\right)_{i,j,k+\frac{1}{2}}(p_{l,i,j,k+1}-p_{l,i,j,k})$$

$$+\frac{\Delta x\Delta y}{\Delta z}\left(\frac{kk_{rl}}{B_l\mu_l}\right)_{i,j,k-\frac{1}{2}}(p_{l,i,j,k-1}-p_{l,i,j,k})$$

$$+\frac{\Delta x\Delta y}{\Delta z}\left(\frac{kk_{rg}}{B_{gg}\mu_g}f\right)_{i,j,k+\frac{1}{2}}\left(p_{g,i,j,k+1}-p_{g,i,j,k}\right)$$

$$+\frac{\Delta x\Delta y}{\Delta z}\left(\frac{kk_{rg}}{B_{gg}\mu_g}f\right)_{i,j,k-\frac{1}{2}}\left(p_{g,i,j,k-1}-p_{g,i,j,k}\right)$$

$$-\frac{\gamma_l sin\theta\Delta V}{\Delta z}\left(\left(\frac{kk_{rl}}{B_l\mu_l}\right)_{i,j,k+\frac{1}{2}}-\left(\frac{kk_{rl}}{B_l\mu_l}\right)_{i,j,k-\frac{1}{2}}\right)$$

$$-\frac{\gamma_g sin\theta\Delta V}{\Delta z}\left(\left(\frac{kk_{rg}}{B_{gg}\mu_g}f\right)_{i,j,k+\frac{1}{2}}-\left(\frac{kk_{rg}}{B_{gg}\mu_g}f\right)_{i,j,k-\frac{1}{2}}\right)-q_w \qquad (A16)$$

We take the capillary pressure equation into account to express the liquid phase pressure as gaseous phase pressure, and we will have the difference equation of water:

$$\Delta V\left[\frac{\emptyset S_l}{B_l}(c_f+c_l)+\frac{\emptyset S_g f}{B_{gg}}\left(c_f+c_l+\frac{1}{f}\frac{\partial f}{\partial p_g}\right)\right]\frac{p_{g,i,j,k}^{n+1}-p_{g,i,j,k}^{n}}{\Delta t}$$

$$+\Delta V\left[\frac{\emptyset}{B_l}-\frac{\emptyset f}{B_{gg}}-\frac{\emptyset S_l}{B_l}(c_f+c_l)\frac{\partial p_c}{\partial S_l}\right]\frac{S_{l,i,j,k}^{n+1}-S_{l,i,j,k}^{n}}{\Delta t}$$

$$=\left[\frac{\Delta y\Delta z}{\Delta x}\left(\frac{kk_{rl}}{B_l\mu_l}\right)_{i+\frac{1}{2},j,k}+\frac{\Delta y\Delta z}{\Delta x}\left(\frac{kk_{rg}}{B_{gg}\mu_g}f\right)_{i+\frac{1}{2},j,k}\right](p_{g,i+1,j,k}-p_{g,i,j,k})$$

$$+\left[\frac{\Delta y\Delta z}{\Delta x}\left(\frac{kk_{rl}}{B_l\mu_l}\right)_{i-\frac{1}{2},j,k}+\frac{\Delta y\Delta z}{\Delta x}\left(\frac{kk_{rg}}{B_{gg}\mu_g}f\right)_{i-\frac{1}{2},j,k}\right](p_{g,i-1,j,k}-p_{g,i,j,k})$$

$$+\left[\frac{\Delta x\Delta z}{\Delta y}\left(\frac{kk_{rl}}{B_l\mu_l}\right)_{i,j+\frac{1}{2},k}+\frac{\Delta x\Delta z}{\Delta y}\left(\frac{kk_{rg}}{B_{gg}\mu_g}f\right)_{i,j+\frac{1}{2},k}\right](p_{g,i,j+1,k}-p_{g,i,j,k})$$

$$+\left[\frac{\Delta x\Delta z}{\Delta y}\left(\frac{kk_{rl}}{B_l\mu_l}\right)_{i,j-\frac{1}{2},k}+\frac{\Delta x\Delta z}{\Delta y}\left(\frac{kk_{rg}}{B_{gg}\mu_g}f\right)_{i,j-\frac{1}{2},k}\right](p_{g,i,j-1,k}-p_{g,i,j,k})$$

$$=\left[\frac{\Delta x\Delta y}{\Delta z}\left(\frac{kk_{rl}}{B_l\mu_l}\right)_{i,j,k+\frac{1}{2}}+\frac{\Delta x\Delta y}{\Delta z}\left(\frac{kk_{rg}}{B_{gg}\mu_g}f\right)_{i,j,k+\frac{1}{2}}\right](p_{g,i,j,k+1}-p_{g,i,j,k})$$

$$+\left[\frac{\Delta x\Delta y}{\Delta z}\left(\frac{kk_{rl}}{B_l\mu_l}\right)_{i,j,k-\frac{1}{2}}+\frac{\Delta x\Delta y}{\Delta z}\left(\frac{kk_{rg}}{B_{gg}\mu_g}f\right)_{i,j,k-\frac{1}{2}}\right](p_{g,i,j,k-1}-p_{g,i,j,k})$$

$$-\frac{\Delta y\Delta z}{\Delta x}\left(\frac{kk_{rl}}{B_l\mu_l}\frac{\partial p_c}{\partial S_l}\right)_{i+\frac{1}{2},j,k}(S_{l,i+1,j,k}-S_{l,i,j,k})$$

$$-\frac{\Delta y\Delta z}{\Delta x}\left(\frac{kk_{rl}}{B_l\mu_l}\frac{\partial p_c}{\partial S_l}\right)_{i-\frac{1}{2},j,k}(S_{l,i-1,j,k}-S_{l,i,j,k})$$

$$-\frac{\Delta x\Delta z}{\Delta y}\left(\frac{kk_{rl}}{B_l\mu_l}\frac{\partial p_c}{\partial S_l}\right)_{i,j+\frac{1}{2},k}(S_{l,i,j+1,k}-S_{l,i,j,k})$$

$$-\frac{\Delta x\Delta z}{\Delta y}\left(\frac{kk_{rl}}{B_l\mu_l}\frac{\partial p_c}{\partial S_l}\right)_{i,j-\frac{1}{2},k}\left(S_{l,i,j-1,k}-S_{l,i,j,k}\right)$$

$$-\frac{\Delta x\Delta y}{\Delta z}\left(\frac{kk_{rl}}{B_l\mu_l}\frac{\partial p_c}{\partial S_l}\right)_{i,j,k+\frac{1}{2}}\left(S_{l,i,j,k+1}-S_{l,i,j,k}\right)$$

$$-\frac{\Delta x\Delta y}{\Delta z}\left(\frac{kk_{rl}}{B_l\mu_l}\frac{\partial p_c}{\partial S_l}\right)_{i,j,k-\frac{1}{2}}\left(S_{l,i,j,k-1}-S_{l,i,j,k}\right)$$

$$-\frac{\gamma_l sin\theta\Delta V}{\Delta z}\left(\left(\frac{kk_{rl}}{B_l\mu_l}\right)_{i,j,k+\frac{1}{2}}-\left(\frac{kk_{rl}}{B_l\mu_l}\right)_{i,j,k-\frac{1}{2}}\right)$$

$$-\frac{\gamma_g sin\theta\Delta V}{\Delta z}\left(\left(\frac{kk_{rg}}{B_{gg}\mu_g}f\right)_{i,j,k+\frac{1}{2}}-\left(\frac{kk_{rg}}{B_{gg}\mu_g}f\right)_{i,j,k-\frac{1}{2}}\right)-q_w \qquad (A17)$$

The difference equation for gas is:

$$\frac{\emptyset g(1-S_l)}{B_{gg}}\left(c_f+c_g+\frac{1}{g}\frac{\partial g}{\partial p_g}\right)\frac{p_{g,i,j,k}^{n+1}-p_{g,i,j,k}^{n}}{\Delta t}-\frac{\emptyset g}{B_{gg}}\frac{S_{l,i,j,k}^{n+1}-S_{l,i,j,k}^{n}}{\Delta t}$$

$$=\frac{\Delta y\Delta z}{\Delta x}\left(\frac{kk_{rg}}{B_{gg}\mu_g}g\right)_{i+\frac{1}{2},j,k}\left(p_{g,i+1,j,k}-p_{g,i,j,k}\right)$$

$$+\frac{\Delta y\Delta z}{\Delta x}\left(\frac{kk_{rg}}{B_{gg}\mu_g}g\right)_{i-\frac{1}{2},j,k}\left(p_{g,i-1,j,k}-p_{g,i,j,k}\right)$$

$$+\frac{\Delta x\Delta z}{\Delta y}\left(\frac{kk_{rg}}{B_{gg}\mu_g}g\right)_{i,j+\frac{1}{2},k}\left(p_{l,i,j+1,k}-p_{l,i,j,k}\right)$$

$$+\frac{\Delta x\Delta z}{\Delta y}\left(\frac{kk_{rg}}{B_{gg}\mu_g}g\right)_{i,j-\frac{1}{2},k}\left(p_{l,i,j-1,k}-p_{l,i,j,k}\right)$$

$$+\frac{\Delta x\Delta y}{\Delta z}\left(\frac{kk_{rg}}{B_{gg}\mu_g}g\right)_{i,j,k+\frac{1}{2}}\left(p_{g,i,j,k+1}-p_{g,i,j,k}\right)$$

$$+\frac{\Delta x\Delta y}{\Delta z}\left(\frac{kk_{rg}}{B_{gg}\mu_g}g\right)_{i,j,k-\frac{1}{2}}\left(p_{g,i,j,k-1}-p_{g,i,j,k}\right)$$

$$-\frac{\gamma_g sin\theta\Delta V}{\Delta z}\left(\left(\frac{kk_{rg}}{B_{gg}\mu_g}g\right)_{i,j,k+\frac{1}{2}}-\left(\frac{kk_{rg}}{B_{gg}\mu_g}g\right)_{i,j,k-\frac{1}{2}}\right)-q_{gg} \qquad (A18)$$

The source and sink terns can be specified as:

$$q_l=\ WI_l\left(p_{l,i,j,k}-p_{wf}\right)=\frac{2\pi kk_{rl}\Delta z}{\mu_l\left(ln\left(\frac{r_o}{r_w}\right)+s\right)}\left(p_{l,i,j,k}-p_{wf}\right)$$

$$=\frac{2\pi kk_{rl}\Delta z}{\mu_l\left(ln\left(\frac{r_o}{r_w}\right)+s\right)}\left(p_{g,i,j,k}-p_{c,i,j,k}-p_{wf}\right) \qquad (A19)$$

$$q_g = WI_g\left(p_{g,i,j,k} - p_{wf}\right) = \frac{2\pi k k_{rg} \Delta z}{\mu_l \left(ln\left(\frac{r_o}{r_w}\right) + s\right)}\left(p_{g,i,j,k} - p_{wf}\right) \qquad (A20)$$

Where the effective drainage radius in the well block is according Peaceman's equation:

$$r_o = 0.14\sqrt{\Delta x^2 + \Delta y^2} \qquad (A21)$$

The water production rate is:

$$q_w = \frac{q_l}{B_l} + \frac{q_g y_w}{B_w} \qquad (A20)$$

The natural gas production rate is:

$$q_{gg} = q_g \frac{\rho_g y_{gg}}{M_g} \frac{M_{gg}}{q_{gg}} \frac{1}{B_{gg}} = \frac{q_g(1 - y_w)}{B_{gg}} \qquad (A22)$$

APPENDIX B: NUMERICAL MODEL VALIDATION

To validate the two-phase flowback model we compare the simulated results generated by the MATLAB two-phase flowback model against those generated by CMG under non-vaporization condition. Then in the next section we will show how vaporization impacts the simulation results.

According to the symmetry in Scenario 2 a quarter of one secondary fracture spacing unit is modeled as Figure 67 illustrates. The model of Scenario 1 is almost the same with that of Scenario 2 but just without the secondary fracture.

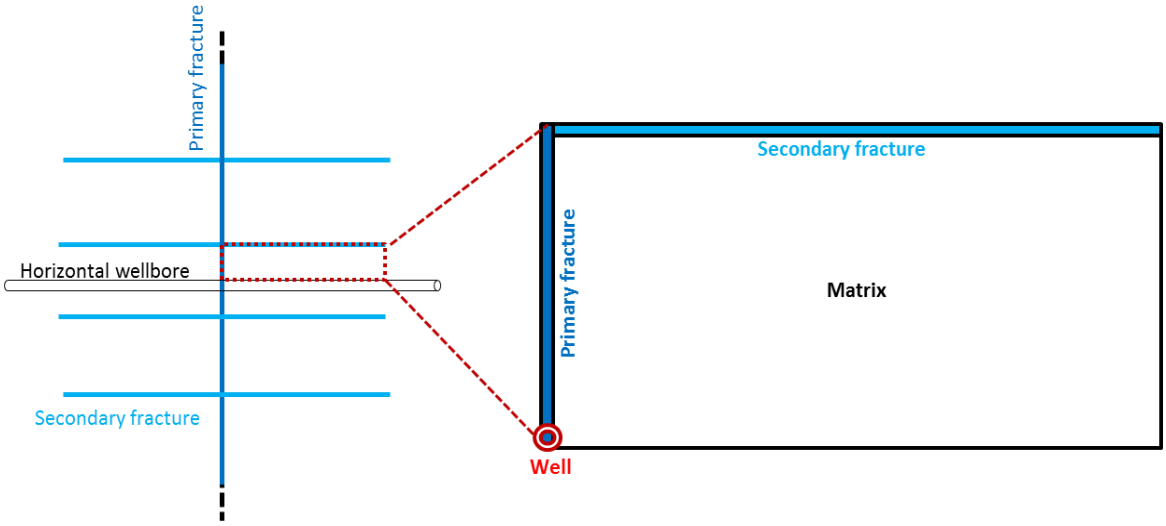

Figure 67. Map of two-phase simulation model for Scenario 2

The model size is 20 ft in X direction by 100 ft in Y direction by 30 in Z direction. Primary fracture length in this model is 20 ft, which is half of the total half-length 200 ft divided by the frequency of secondary fractures along the primary fracture

half-length. The model is an isothermal system of 160 degree Fahrenheit and initial pressure is 4500 psia.

The width of primary fracture in the simulation model is set to be 1 ft to accommodate the well diameter therefore the effective porosity is adjusted to 0.00235 according to the proppant pack porosity 0.47 and the actual width of 0.01 ft since only half width is modeled due to the symmetry. The conductivity of primary fracture is 10 md-ft

The secondary fracture length is 100 ft and the width in the simulation model is set as 1 ft, so the corresponding porosity is adjusted to 0.001 to provide the same volume as the actual porosity 1 and actual secondary fracture width 0.001 ft. All the fracture space is initially 100% water saturated and fractures fully penetrate the formation in the vertical direction. The conductivity of secondary fracture is 0.01 md-ft.

The matrix porosity is 0.08 and the permeability is 100 nd. Initial water saturation in matrix is 0.25. The gas is pure methane with specific gravity 0.65, and water is used as the injected fracturing fluid.

A vertical well is set at one corner to model one perforation cluster in the horizontal well. The perforation is right at the center in the vertical direction and it is only hydraulically connected with the primary fracture. The well is flowing with a constant bottomhole pressure of 1000 psia.

Figure 68 shows the relative permeability profiles applied to primary fracture, secondary fracture and matrix separately and Figure 69 shows the gridding strategy of the simulation model in map view.

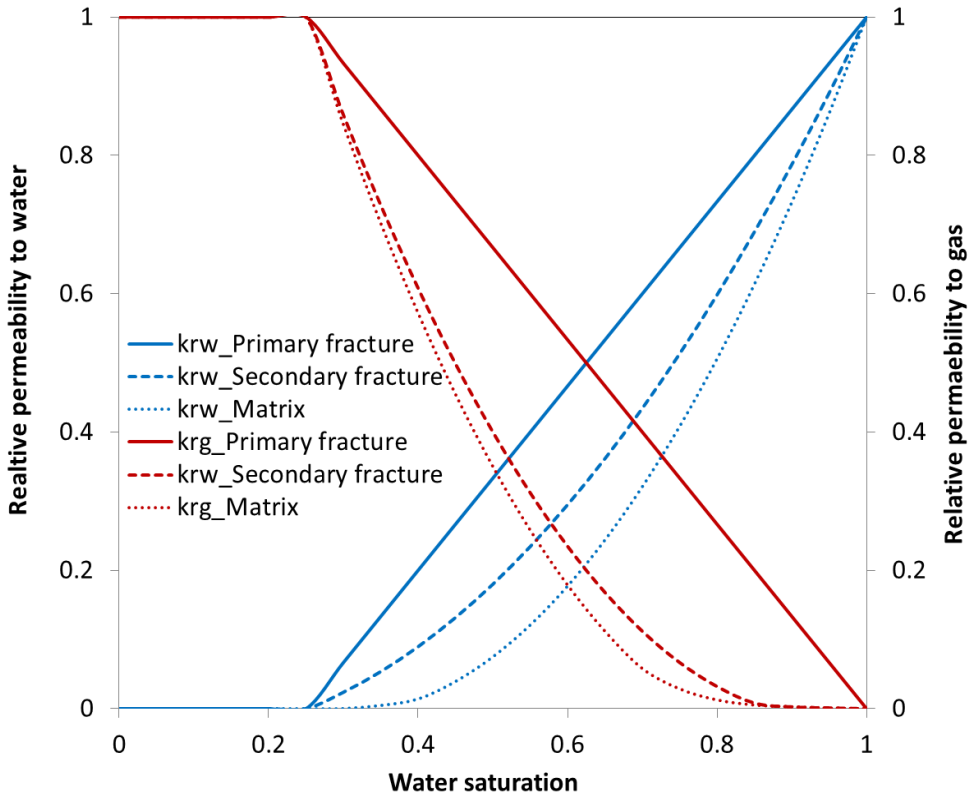

Figure 68. Relative permeability profiles used in the two-phase flow simulation

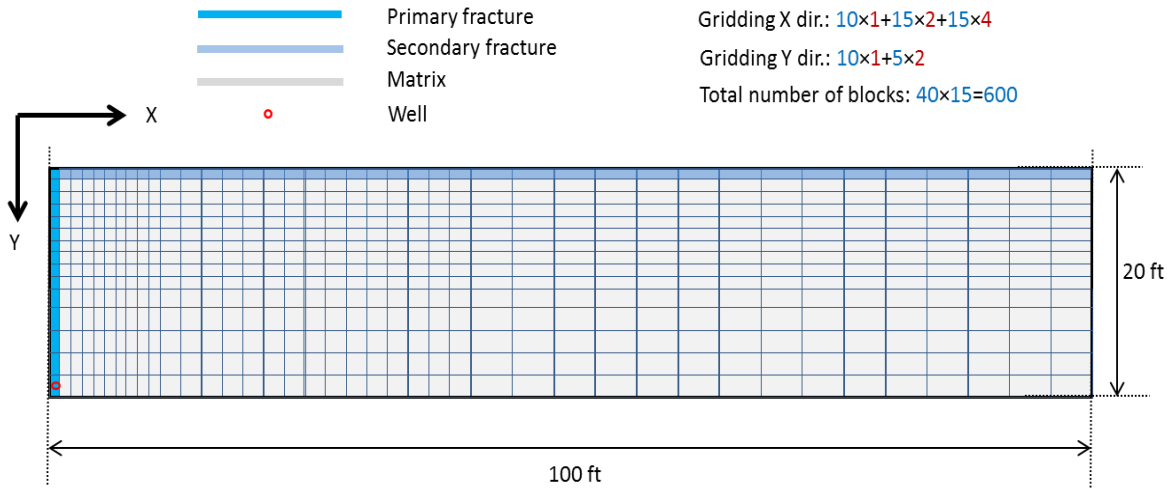

Figure 69. Gridding strategy of the simulation model in map view

Production rates of both gas and water are compared for Scenario 1 and Scenario 2 as Figure 70 and Figure 71 show. Except a few data points at very early time the simulated production data computed by MATLAB and CMG match very well and it indicates that the two-phase flowback model programmed with MATLAB is able to realize the fundamental modeling function as the commercial simulator does and demonstrates that the MATLAB coded model is a solid base for modeling the flowback behavior driven by both displacement and vaporization mechanisms.

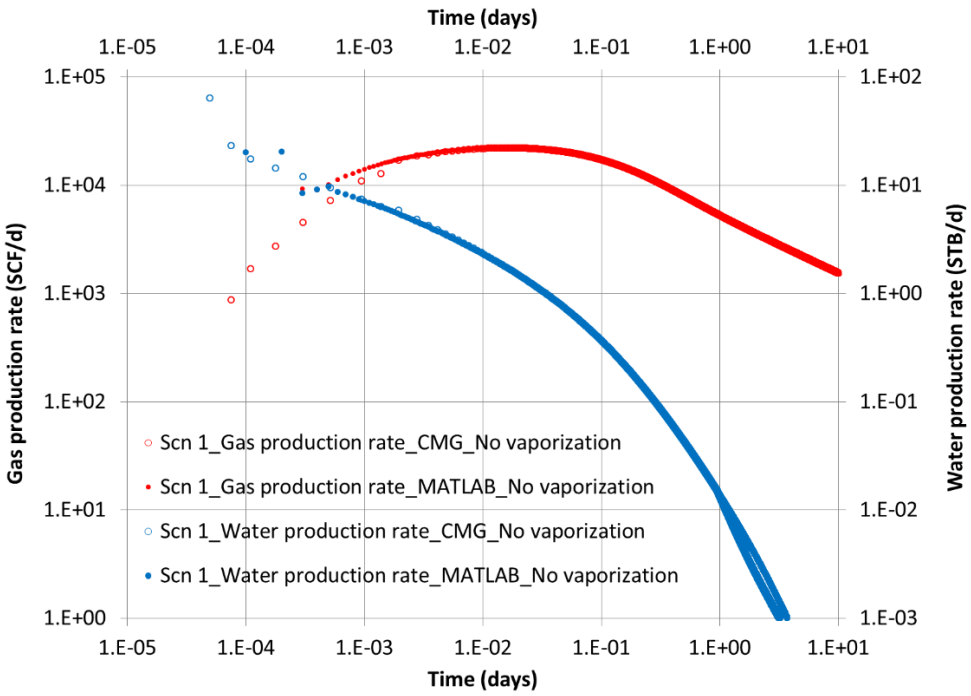

Figure 70. Production rate match between CMG and MATLAB simulation-Scenario 1

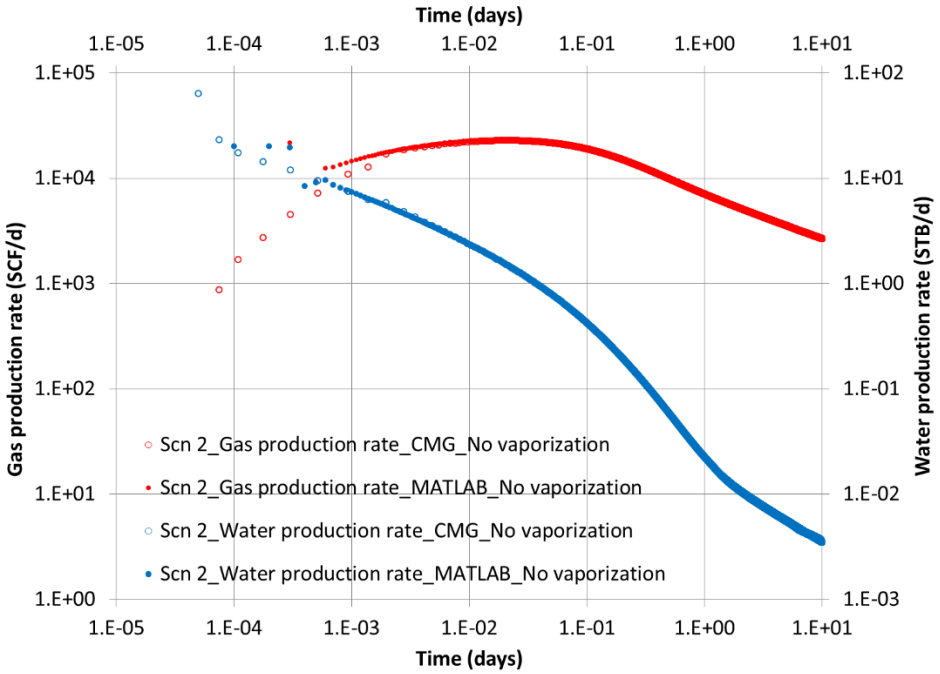

Figure 71. Production rate match between CMG and MATLAB simulation-Scenario 2

Cumulative production comparisons are shown in Figure 72 and Figure 73 for Scenario 1 and Scenario 2 separately. The comparison shows that the cumulative production simulated by the MATLAB coded simulation model matches the results simulated by CMG.

The mismatching at every early time is mainly due to the time step issue. CMG simulator is robust on time step determination for the convergence at a more harsh tolerance requirement while a fixed time step is applied in MATLAB simulation model for a relatively permissive tolerance requirement. As simulation time goes on the difference is eliminated because the same time step guarantees the convergence in both simulators.

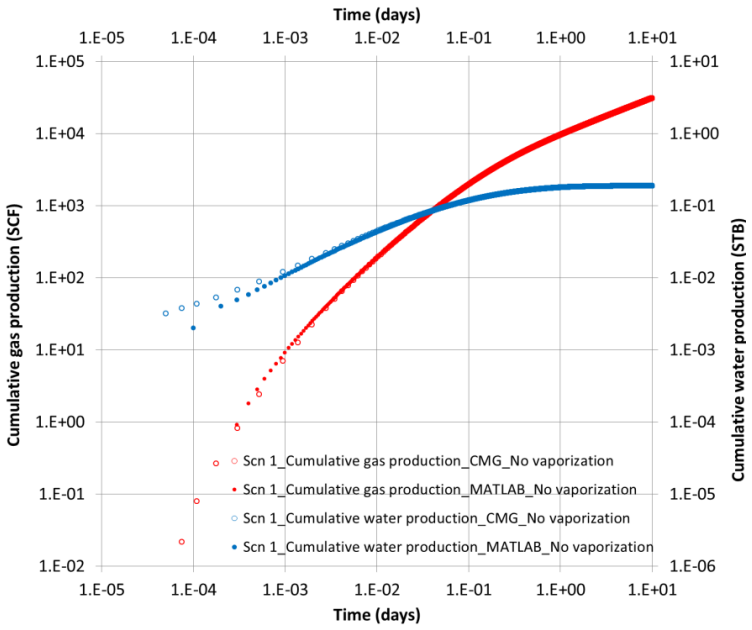

Figure 72. Cumulative production match between CMG and MATLAB simulation-Scenario 1

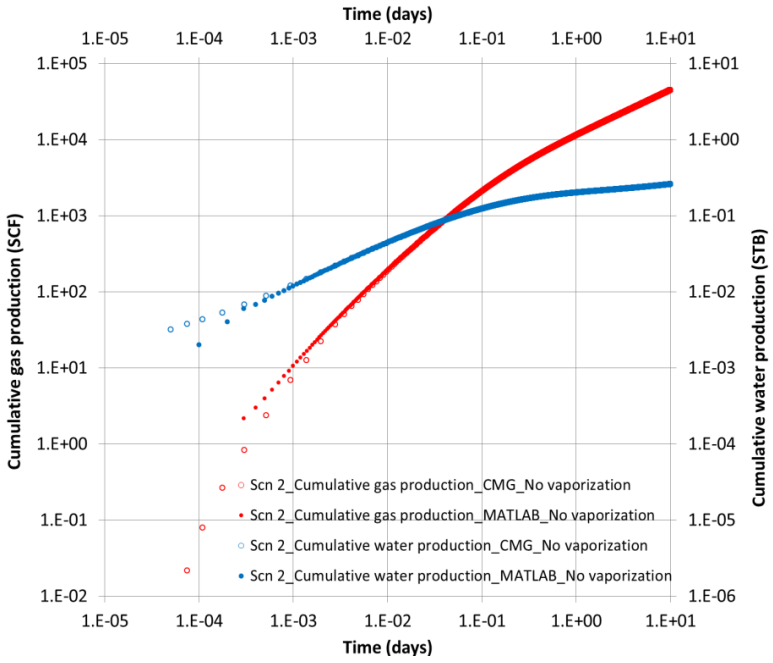

Figure 73. Cumulative production match between CMG and MATLAB simulation-Scenario 2